



**DMI**

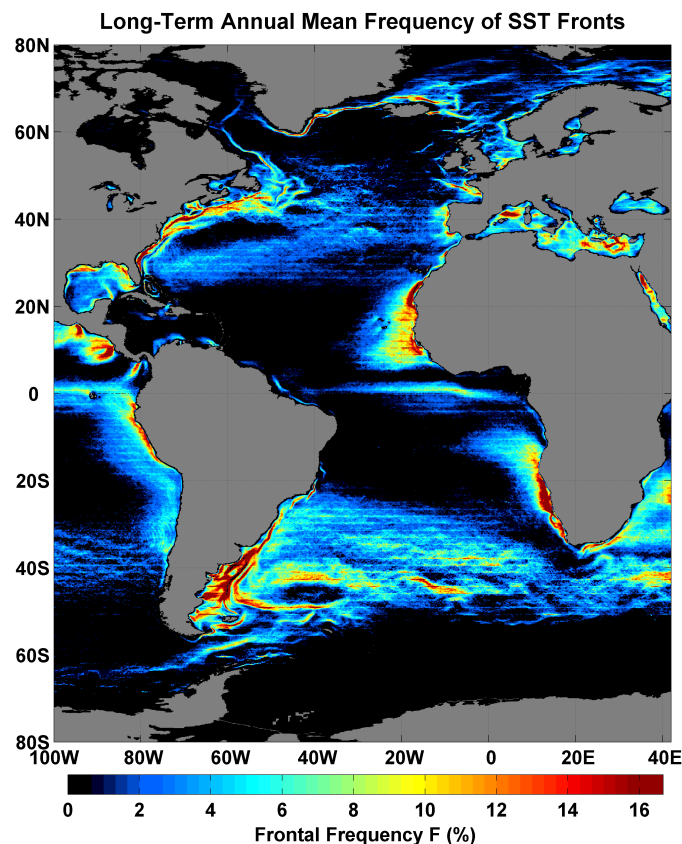
Ministry of Transport and Energy

## Technical Report 06-14

# Adaptation of global frontal climatologies for use in the OSISAF Global SST cloudmasking scheme

Søren Andersen (DMI)

Igor Belkin (University of Rhode Island)





# Colophon

**Serial title:**

Technical Report 06-14

**Title:**

Adaptation of global frontal climatologies for use in the OSISAF Global SST cloudmasking scheme

**Author(s):**

Søren Andersen (DMI), Igor Belkin (University of Rhode Island)

**Other contributors:**

**Responsible institution:**

Danish Meteorological Institute

**Language:**

English

**Url:**

[www.dmi.dk/dmi/tr06-14](http://www.dmi.dk/dmi/tr06-14)

**ISSN:**

1399-1388 (online)

**Version:**

**Website:**

[www.dmi.dk](http://www.dmi.dk)

**Copyright:**

Danish Meteorological Institute. It is allowed to copy and extract from the publication with a specification of the source material.



## Content:

Abstract .....	4
1. Introduction.....	5
2. Datasets .....	5
2.1. URI frontal climatologies.....	5
2.2. The CMS frontal climatology .....	7
2.3. Comparison of URI and CMS fields.....	8
3. Use of frontal fields in cloud detection procedure.....	10
4. Validation.....	11
5. References .....	16
Appendix 1: Comparisons between CMS and URI fields .....	17
January .....	17
February .....	19
March .....	20
April .....	22
May .....	23
June .....	25
July.....	26
August .....	28
September.....	29
October.....	31
November.....	32
December .....	34
Appendix 2: Original URI max gradient fields.....	36
Appendix 3: URI max gradient fields thresholded at 15 % frequency .....	42
Appendix 4 Original monthly gradient direction fields .....	48
Appendix 5 Gradient direction fields thresholded at 15% frequency.....	54
Appendix 6: Validation data .....	60
US East Coast.....	60
Greenland Sea/ East Greenland.....	63
Mediterranean .....	65
Polar front area.....	67
South Africa .....	68
West Africa .....	74
Previous reports.....	77



## Abstract

The derivation, adaptation and validation of global sea surface temperature front climatologies to be used as background values for adjustment of cloudmask stringency is presented. The regional Meteo-France CMS frontal climatology and data derived from the University of Rhode Island global frontal database and are compared. The global data set is applied in the cloudmasking of a set of AVHRR scenes and experiments with adjustable parameters are performed to determine optimum settings as well as to characterize and validate the effect of the frontal climatology data on the resulting cloud masks.



# 1. Introduction

It is a common problem that ocean surface temperature fronts may be misinterpreted as cloud edges during night, where visible channels are not available to make an unambiguous distinction. The nightly cloud masking procedure used in the Intermediate Operational Phase (IOP) North Atlantic Regional (NAR) SST data sets uses information on climatological sea surface temperature gradient to facilitate a more relaxed spatial inhomogeneity test in areas that are likely to be affected by ocean fronts. While during IOP, the AVHRR based SST fields have been restricted to the North Atlantic, METOP will provide global full resolution data and the OSISAF will there progress to a global scope. This means that the climatology used so far, which is based on analysis of local reception AVHRR data at Meteo-France CMS, Lannion is no longer adequate. Very few other frontal data sets exist, however a group at University of Rhode Island (URI) has a global data set based on analysis of the Pathfinder 9 km resolution global data set, which has been made available through an associated scientist arrangement with Igor Belkin. In addition to frontal gradient magnitude (K/km), fields of frontal frequency (ratio of front observations to total number of observations) and mean gradient direction are offered. The purpose of the work presented here is to:

- 1) Make a general presentation of the URI frontal climatologies.
- 2) Investigate the compatibility between the CMS and the URI climatologies for use in cloud masking.
- 3) Review and validate the cloud detection scheme using the URI climatologies on a limited set of AVHRR test data.

The report at the same time constitutes the deliverable of the associated scientist work performed by Igor Belkin. The following tasks were performed: Development and processing of monthly global frontal gradient, frequency and direction fields; removal of line artefacts from fields; identification of cloud free situations over various regions for use in validation; as well as general scientific consultancy on the use, interpretation and limitations of the frontal fields. The tasks are described in more detail in the following sections.

## 2. Datasets

### 2.1. URI frontal climatologies

The URI frontal products are based on the automated procedure by Cayula et al. (1991) and Cayula and Cornillon (1992, 1995, 1996) and developed by Ullman and Cornillon (1999, 2000, 2001), which has been applied on the entire (1985-1996) Pathfinder 9 km resolution SST dataset. The procedure detects front occurrences based on temporal persistence and shape (in particular the length of the frontal feature) and the results have been stored in a database. This is the basis for deriving long term climatological products such as the frontal frequency (ratio of front observations to total cloud free observations), frontal gradient magnitude and frontal direction, one example is given in Fig. 1. Monthly versions of these products were developed and made available through an associated scientist project with Igor Belkin of URI. Some artefacts, in the form of horizontal lines, were noted in the frontal frequency datasets that were due to subtle inconsistencies in the Pathfinder SST dataset. These were successfully removed by application of a median filter. The monthly frequency and maximum gradient climatologies were extracted over 11 areas (Fig. 2), which were subsequently assembled to form global files, shown in appendices 2 and 3.

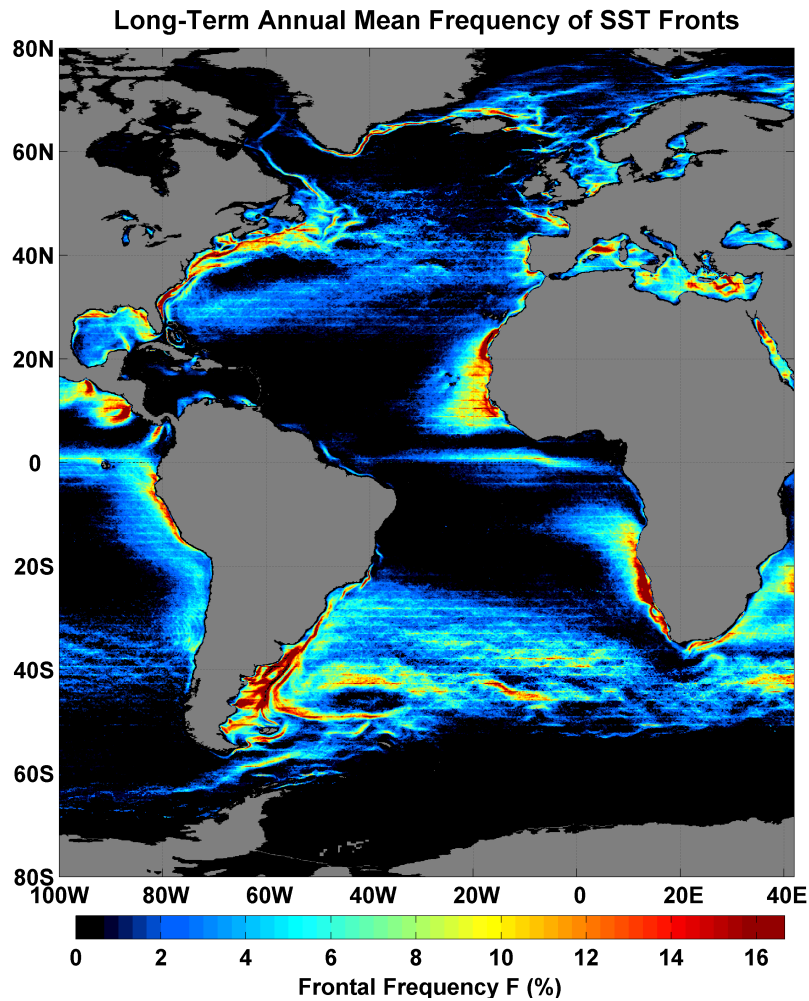


Figure 1  
Example of long term mean annual frontal frequency. Note the line artefacts that have been successfully removed in the datasets delivered to the OSISAF. After Belkin et al. (2006).

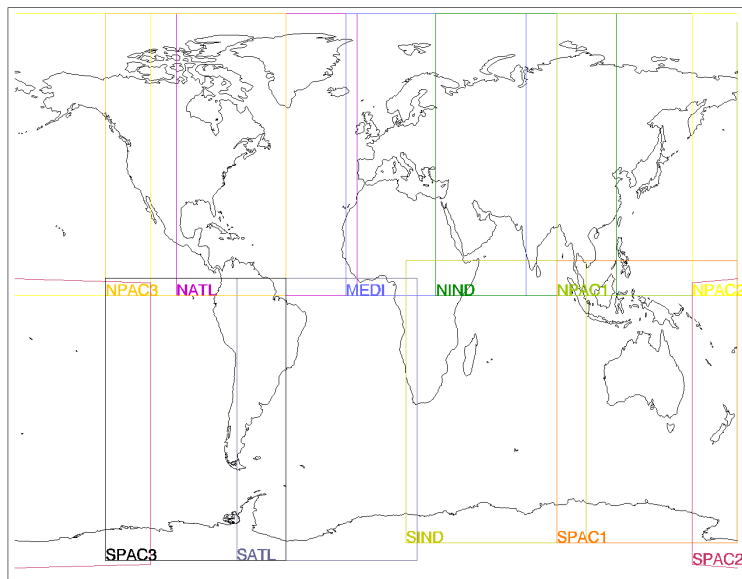


Figure 2  
Subareas for which frontal statistics were extracted from the URI data base.

Two sets of additional fields have been supplied by URI, however their use is outside the scope of the present development, but may form the basis for future improvement efforts. The data sets are:



1. Gradient direction fields have been supplied in a similar fashion and the monthly fields are shown in Appendices 4 and 5.
2. Monthly gradient cube dataset, which are per pixel histograms of frontal magnitude over the Pathfinder period. This data set is thought to be especially well suited to be used in a possible future Bayesian cloud clearing scheme.

## 2.2. The CMS frontal climatology

The CMS frontal climatology is based on manual analysis of locally received AVHRR data at Meteo-France CMS Lannion from January 1989 through September 1994. The area of coverage is the reception mask of the Lannion HRPT receiving station and all data were resampled to a 2 km resolution polar stereographic grid prior to the analysis. The following is adapted from the memo by LeBorgne (2006a).

-1,1	0,1	1,1
-1,0	0,0	1,0
-1,-1	0,-1	1,-1

Figure 3  
Definition of the 3x3 pixel box used in the following.

In a 3x3 pixel box (figure 3), the 11 micron brightness temperature gradient is determined as:

$$\text{Grad}(0,0) = 1/2 ( [(g_1)^2 + (g_2)^2]^{1/2} + 1/2^{1/2} [(g_3)^2 + (g_4)^2]^{1/2} ) \quad (1)$$

Where

- $g_1 = T(1,0) - T(-1,0)$
- $g_2 = T(0,1) - T(0,-1)$
- $g_3 = T(1,1) - T(-1,-1)$
- $g_4 = T(-1,1) - T(1,-1)$

Grad is expressed in degrees per 4 Km.

Grad is then converted in units of front intensity ( $^{\circ}/5\text{km}$ ) to insure continuity with the period when fronts were manually drawn and displayed and used on a 0-5 scale. This conversion has been made with table 1.

Values of 10 x Grad	Front intensities ( $^{\circ}/5\text{km}$ )
0-7	0
8-11	1
12-18	2
19-25	3
26-32	4
33-39	5

Table 1  
Gradient to front intensity conversion table

Daily front fields were synthesised in weekly maps recording the maximum front intensity of the week for a given pixel. These weekly maps are the raw material of the Atlas.

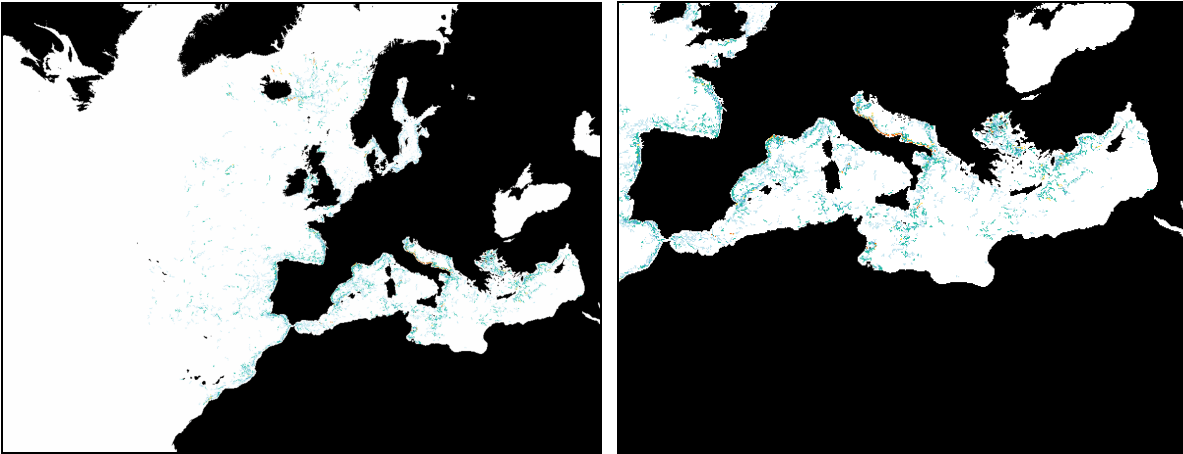


Figure 4  
Maximum front intensities in January left: the RGD area; right: zoom over the Mediterranean for  $n=2$

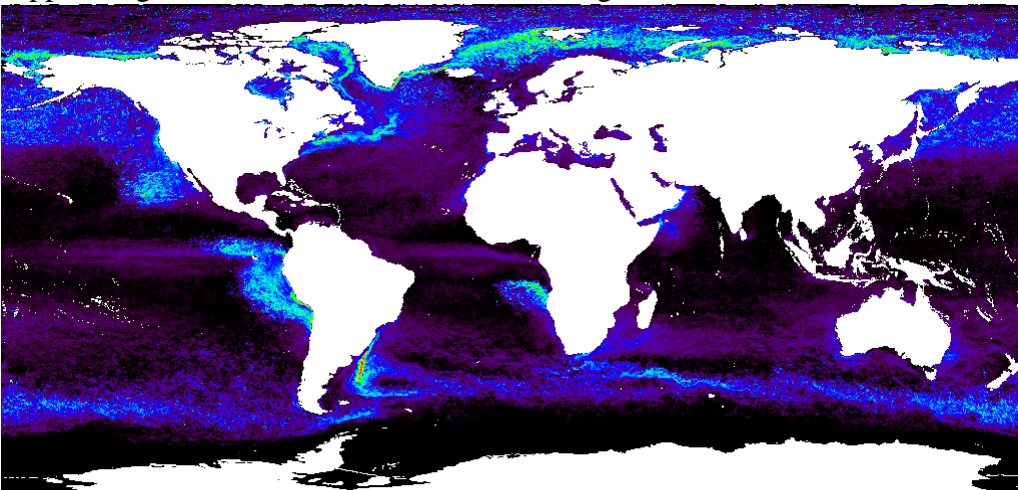
Monthly maps have been then produced by computing, within a box of  $nxn$  original pixels,:

- The mean number of pixels in  $nxn$  showing a front during the weeks within the month; this represents the spatial coverage of the front
- The maximum intensity encountered
- The mean intensity
- The frequency of the presence of the front within the box expressed in percent (100% means that the front was present for every week in the month).

Note that  $nxn$  introduces a notion of resolution, not linked to the gradient calculation, but to the statistics made on the intensities. Two resolutions have been used  $n=1$ : 2 kms and  $n=2$ : 4 kms. Here we consider only the  $2x2$  monthly maximum gradient data sets as they are the ones used in the cloud screening procedure.

### 2.3. Comparison of URI and CMS fields

The URI maximum gradient fields are derived from the URI frontal database. A number of fronts with low frequency occur, which would result in an overall reduced stringency of the cloud masking procedure at night. The effect is especially notable during summer, where the occurrence of fronts in the North Atlantic URI fields becomes very large. To mitigate this, a thresholding on frontal frequency has been developed through visual comparisons between URI and CMS fields in the Mediterranean for different values of the frontal frequency threshold, see appendix 1. It was found that a 15 % threshold gave the best correspondence between URI and CMS and was efficiently suppressing the excess front occurrences during the summer months.



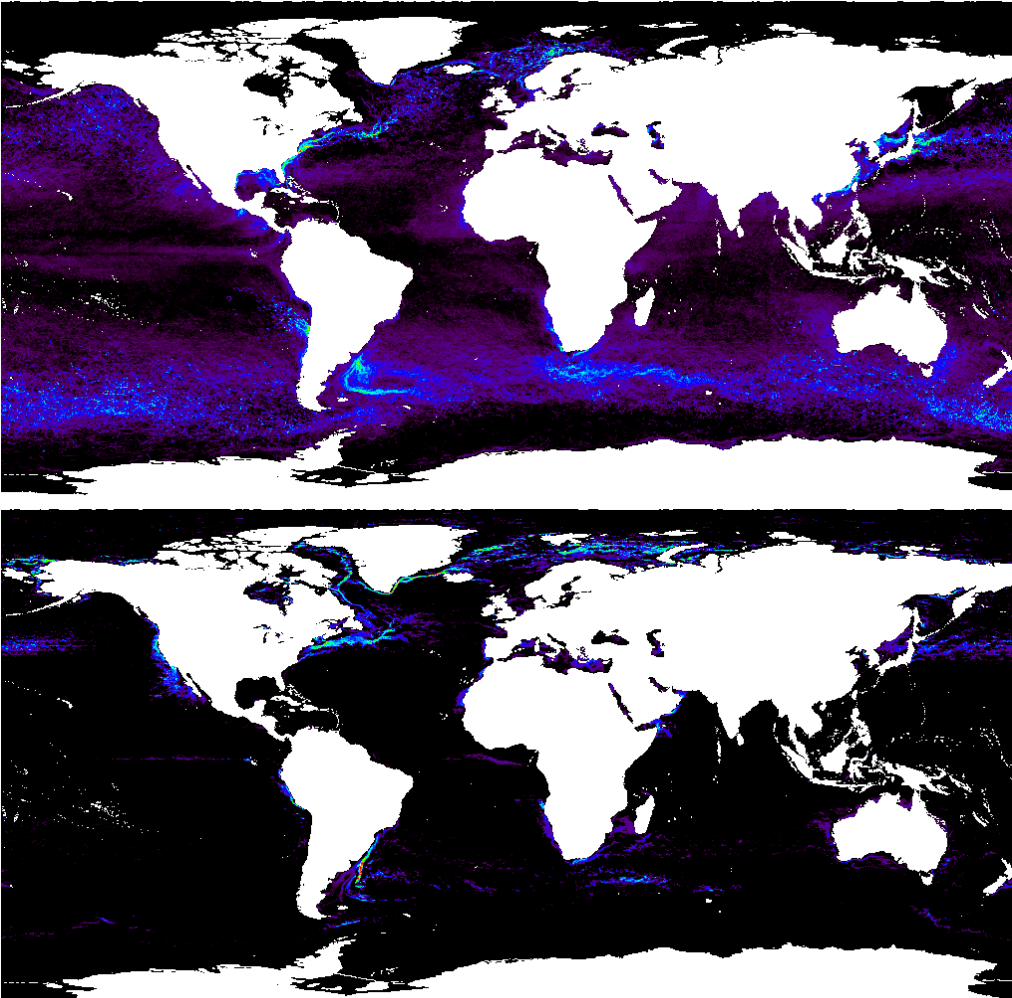


Figure 5  
Presentation of URI frontal fields for use in the OSISAF cloud screening procedure, Top: January, Middle: August, bottom: August thresholded on 15 % frontal frequency.

The CMS and URI fields are derived from data of different resolution: CMS used 2 km imagery, whereas the URI fields are derived from 9 km resolution imagery. Depending on the typical width of the fronts this may result in systematic differences between the two products. If the width of fronts is 2 km or less, the result is an underestimate of the frontal gradient in the URI fields of a factor 4.5 relative to the CMS data. If the fronts are typically close to or broader than 9 km, the two products should be similar. We make no assumption but proceed to compare the modes of the distributions of the two products, shown in appendix 1, and obtain results as in Table 2

Jan	Feb	Mar	Apr	May	Jun	Jul	Aug	Sep	Oct	Nov	Dec
4.9	5.1	5.2	4.9	4.3	4.1	4.4	4.3	4.5	4.3	4.2	4.9

Table 2

Ratio of CMS mean frontal gradient to URI median frontal gradient taken from the respective max. gradient data sets.

As the CMS data is quantized on 6 discrete values the mode of the distribution is approximated as the mean value, whereas for the URI data, the median is used. The ratio of the CMS data to the URI data varies between 4.1 and 5.2 with a seasonal dependence. In general, due to the tail of the distributions, use of the mean value will tend to overestimate the mode of the CMS data, leading to higher values of the ratio between the two modes. This may explain some of the values in table 2 that are higher than 4.5. The seasonal variation gives higher ratio values in the winter months than in summer, which is consistent with the fact that fronts are generally broader during summer. The



results would justify to apply the URI data in the present scheme after adjustment for the resolution difference, i.e. by multiplying by the factors in Table 2. However, in view of the uncertainties it is not felt that the seasonal variation is large enough to justify a non-constant factor and it is therefore recommended to use the theoretical value of 4.5, which is close to the annual average of 4.6.

### 3. Use of frontal fields in cloud detection procedure

The following is a short summary of LeBorgne (2006b). A two-step procedure is applied with 1) a run with the Maia cloudmask with liberal criteria for the spatial inhomogeneity test (the “Marine-clear” flag:  $3 \times 3$  box stdev(ch4) < 0.7) and a subsequent analysis with input from climatological maximum frontal gradients. The gradient in the scene to be processed is computed on channel 4 brightness temperatures with the same geometry as in equation 1 (from LeBorgne, 2006b):

*In a 3x3 pixel box (figure 3), the following 11 micron brightness temperature gradients are successively calculated:*

$$\text{Grad1}(0,0) = [(g_1)^2 + (g_2)^2]^{1/2} \quad (1)$$

Where

$$g_1 = [T(1,0) - T(-1,0)] / D[(1,0) - (-1,0)]$$

$$g_2 = [T(0,1) - T(0,-1)] / D[(0,1) - (0,-1)]$$

*In case one (or several) of the concerned pixels does not show a temperature then*

$$\text{Grad1}(0,0) = \text{missing}$$

$$\text{Grad2}(0,0) = [(g_3)^2 + (g_4)^2]^{1/2} \quad (1)$$

Where

$$g_3 = T(1,1) - T(-1,-1) / D[(1,1) - (-1,-1)]$$

$$g_4 = T(-1,1) - T(1,-1) / D[(-1,1) - (1,-1)]$$

*In case one (or several) of the concerned pixels does not show a temperature then*

$$\text{Grad2}(0,0) = \text{missing}$$

$$W\_grad11(0,0) = [\text{Grad1}(0,0) + \text{Grad2}(0,0)] / 2.$$

*In case one term only is missing, w\_grad takes the value of the term which is present. Note that, for a given pixel, the calculation of the distances depends only of the scan geometry and is stable whatever the line. The distances can be then pre-calculated.*

For level 1 data, distances are a constant function of the incidence angle for each scan line. In the validation study, presented in the following, we operate with resampled satellite data and distances are therefore fixed at 4 and 5.7 km for the horizontal/vertical and 45° terms, respectively.

The climatological maximum gradients, *mxgrad*, are converted to similar scales and a transmittance factor is applied to be consistent with the channel 4 gradients:

$mxgrad11 = mxgrad * TRANS11 * SCALE$ . Here *TRANS11* is set to 0.7, *SCALE* is set to 4.5 to account for the difference in URI resolution (9 km) and resampled image resolution (2 km). Furthermore, the URI gradients are given in units of K/10km, which introduces another factor of value 0.1 to be multiplied above.

An indicator is derived as:

$$\text{Grad\_indicator} = 100 \frac{\text{grad11} - mxgrad11_{lim}}{mxgrad11_{crit} - mxgrad11_{lim}}$$



where  $mxgrad11_{lim}$  is the lowest channel 4 gradient considered to be a potential problem, defined as  $mxgrad11_{lim}=mxgrad11+GRAD\_NOISE$ . The  $mxgrad11_{crit}$  is the maximum permissible gradient and is defined  $mxgrad11_{crit}=mxgrad11+D_{cloud}*GRAD\_NOISE+(1-D_{cloud})*GRAD\_MAX$ .  $D_{cloud}$  takes on values between 0 and 1 and is the normalised distance to cloudiness relative to a set maximum distance:

$$D_{cloud}=PIXNB_{cloud}/PIXNB_{max}.$$

Thus, the adjustable parameters and their standard values are:  $GRAD\_MAX=0.20$  K/km,,  $GRAD\_NOISE=0.03$  K/km and  $PIXNB_{max}=5$  pixels

Pixels with values of  $Grad\_indicator$  exceeding 100 are flagged as cloudy. It must be kept in mind that the level 1 swath data to which this method is to be applied has varying resolution between 1 and a few km. Here, the procedure is applied on data remapped to a uniform 1.5 km resolution grid. A dependence on satellite zenith angle is to be implemented in the  $SCALE$  factor above to account for the varying pixel size in level 1 AVHRR data. In comparisons of the CMS and URI frontal gradient data sets, it was found that a simple conversion factor based on the resolution scale of the data sets (2 to 9 km). We will assume that this finding holds also for resolutions between 1 and 2 km, implying that fronts are generally narrower than the AVHRR pixel size. That is to say the temperature increment is constant with length increments larger than 1 km across the front and a simple factor accounting for scale differences is applicable.

## 4. Validation

Validation has been done on a set of AVHRR images containing temperature fronts, listed in Table 3. The data set covers:

- Mediterranean (MED)
- West Africa (WAF)
- South Africa (Benguela and Agulhas currents, SAF)
- US East Coast (Western part of the Gulf Stream, US\_EC)
- Arctic and/or Iceland-Faroes Front (POLFRNT)
- East Greenland Current (EGL)

The purpose of the validation is to test the frontal climatology adjustment to the cloud detection in cloud free conditions and to assert the effect on cloud edge detection.

The validation data consisted of AVHRR scenes, of which some were locally received at DMI and the majority were LAC data retrieved from the NOAA CLASS archive. The scenes were identified with input from Igor Belkin on cloud free situations in the areas concerned. All scenes were day-time scenes to facilitate unambiguous definition of cloud free areas. The latter was done manually based on interpretation of the channel 2 and 4 images. A total of 17 images were processed and Table 3 gives details, including the regions of interest. Graphic presentations of the data can be found in appendix 6.

The data were resampled to a 2 km resolution, 1000x1000 pixel grid and subsequently MAIA was run with the following modifications:

1. Sun zenith angle set to  $180^\circ$  to force the selection of the nighttime set of tests.
2. The two tests involving channel 3 were bypassed since channel 3 temperatures, if available, are contaminated by solar radiation during daytime. This involves the test on channel 3 minus channel 4 and vice versa.

The “Marine\_Clear” field was extracted from the MAIA output and taken as input to the following



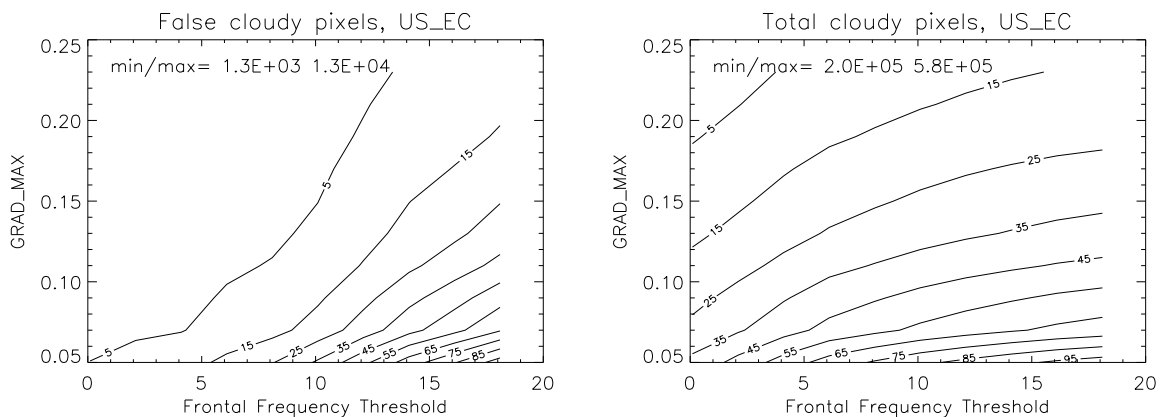
spatial inhomogeneity tests, outlined earlier. Subsequently *GRAD\_MAX*, *GRAD\_NOISE* and the frontal frequency threshold used in thinning the maximum gradient climatology were varied within the following ranges:

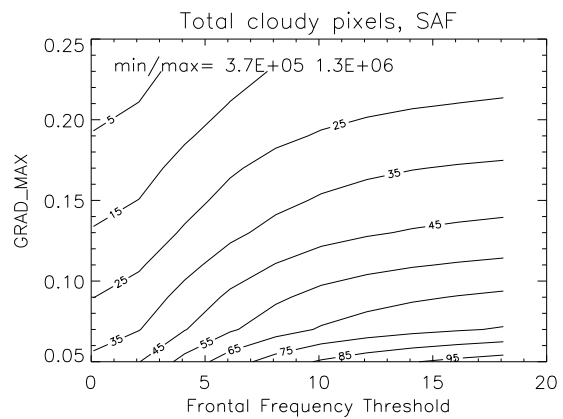
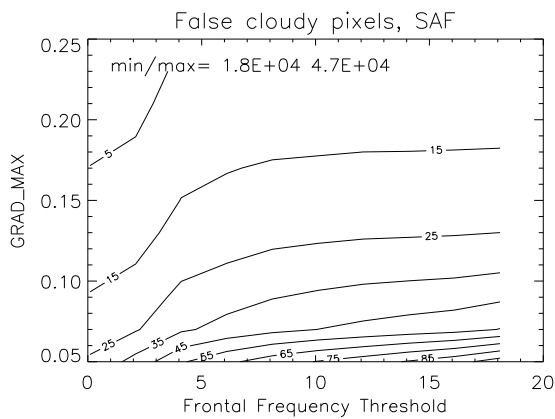
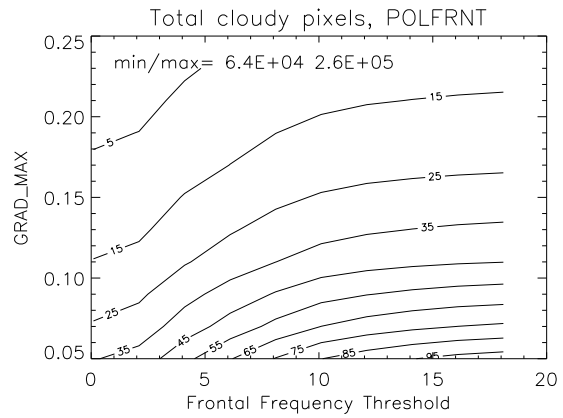
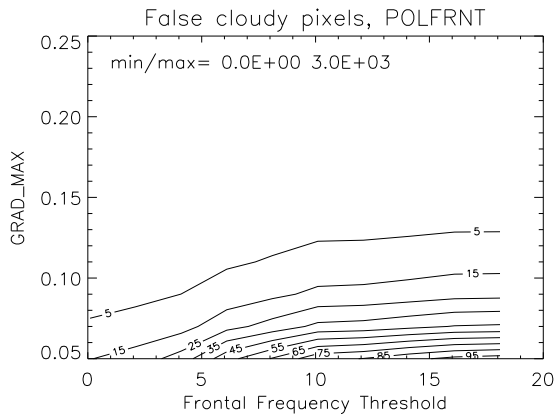
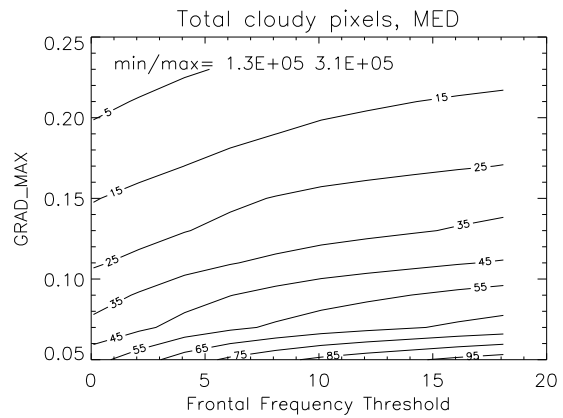
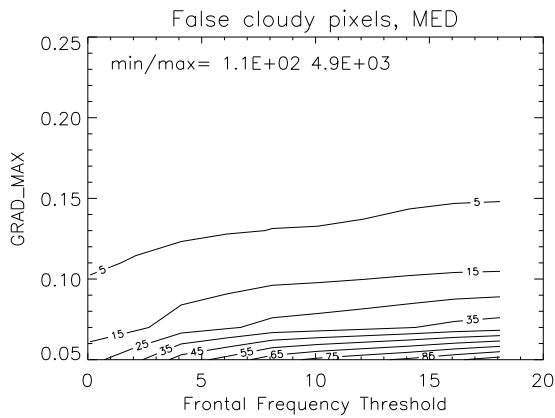
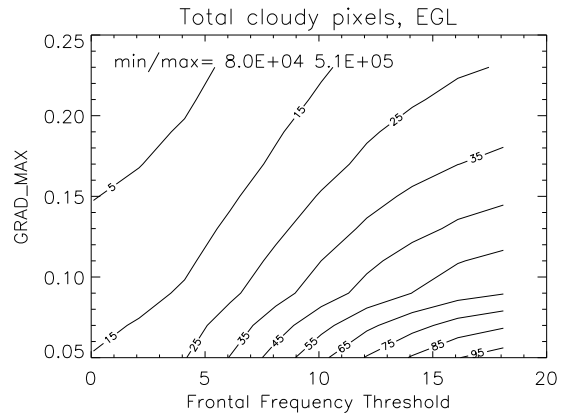
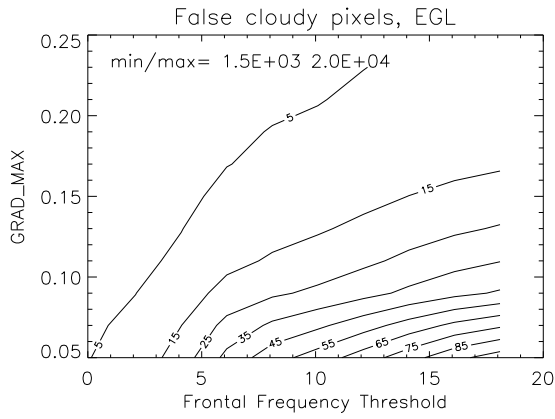
*GRAD\_MAX*: [0.05; 0.23], Freq. threshold: [0%;18%], *GRAD\_NOISE*: [0.00;0.09]

The resulting numbers of cloudy pixels were recorded over the total scene as well as in the cloud free regions of interest. In the regions of interest, the mean *Grad\_indicator* values were also recorded.

It was found that *GRAD\_NOISE* does not influence these statistics significantly. This is most probably due to 1) the lower range of the variations, and 2) that the effects of variations *GRAD\_NOISE* are mostly confined to the 5 pixel zone around clouds. In Figure 6, we therefore present the results obtained from variations of *GRAD\_MAX* and the frontal frequency threshold. In short, the left column represents the “overshoot” of the postprocessing step (number of false cloudy pixels), while the right column represents the “stringency” (total number of cloudy pixels within the total scene). The contours are given as percentage of the range between the min. and max. number of cloudy pixels within the region of interest (certain cloudfree, left; or total scene, right). The minimum value most often is very close to the number of cloudy pixels from MAIA.

The geographical differences mainly reflect the general level of frontal gradient values; thus, in the Mediterranean, the contents of the frontal climatology is relatively less significant and above a certain value of *GRAD\_MAX*, arguably a typical Mediterranean Gradient Magnitude, the number of false cloudy pixels becomes virtually independent of both parameters. In regions of larger frontal gradients, the climatological gradient field is crucially important. Overall, it appears from the figures that the present combination (*GRAD\_MAX*=0.20 K/km, frequency threshold=15%) gives rise to a relatively large proportion of false clouds. However, the frontal frequency threshold in most cases must be decreased to between 5 and 10 % to realize a significant benefit in terms of false cloud detections, while the stringency typically decreases accordingly. The exceptions to this are the US East Coast and West Africa, where stringency can be retained or increased while decreasing the number of false cloudy pixels. Overall from these data, it is deemed that decreasing the frontal frequency threshold to 10 % and *GRAD\_MAX* to approximately 0.15 would result in small decreases in stringency while reducing the number of false cloudy pixels in many regions.





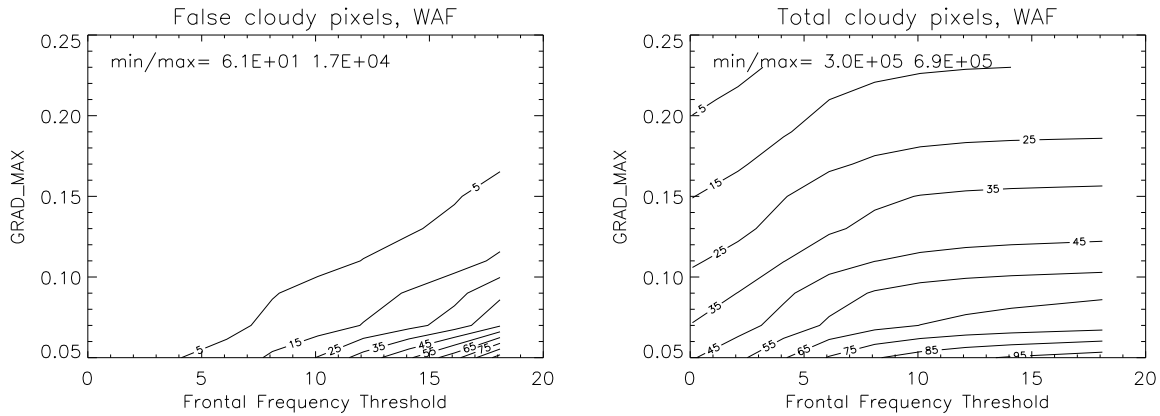


Figure 6

Number of false cloudy pixels within the regions of interest shown in appendix 6 and the total number of cloudy pixels for varying Frontal Frequency Threshold and *GRAD\_MAX*. The contour values are given as percentage of span between min. and max. values. The results are given for the overall regions indicated at the beginning of this section and these regions are referred to with the same abbreviations.

## 5. Summary and conclusions

Preparations for using information on SST front climatology in the cloud masking scheme for the OSISAF Global SST production chain were summarized. A global monthly SST front climatology based on the URI frontal database derived from the Pathfinder SST dataset was presented. The URI climatology showed a good qualitative consistency with overall front patterns. In comparison to the CMS regional data set, used in the present OSISAF North Atlantic Regional SST products. The most notable differences were found near coast or in constricted regions such as in the Alboran Sea close to the Strait of Gibraltar; the CMS data set is higher resolution and more detailed. It was found that the difference in gradient magnitude was consistent with the differences in resolution scale between the two data sets. Hence, the URI gradient magnitudes should be multiplied by a factor 4.5 to be consistent with the CMS gradients. For the purpose of adjusting cloud mask thresholds it is necessary to remove the least frequent fronts. Tentatively a frontal frequency threshold of 15% was derived from visual comparison of the CMS and URI data over the Mediterranean. However, cloud mask experiments performed on a set of AVHRR validation scenes indicated that this filtering was too strict and a 10% threshold together with a stricter setting of the *GRAD\_MAX* parameter (0.15 rather than 0.20) may provide better results. The Mediterranean showed a particularly limited dependence on the frequency threshold, which may be interpreted as an effect of the relatively lower frontal gradients there and/or lack of detail in the URI data. Consequently, the CMS data set was resampled and appended to the URI dataset so that information from both sources can be taken into account over the European regional seas.

The climatologies described here are all stored in one netcdf file per month and at the time of writing they are used in the experimental SST processing chain running at Meteo-France CMS.



Filename	Region	Location	Date	Time	Center (lon,lat)
NSS.LHRR.NL.D05001.S1404.E1408.B2205555.GC.L0397171_Wmed.roi0	Mediterranean: West	East of Gibraltar	2005-01-01	14:04	(2 , 37)
NSS.LHRR.NL.D05001.S1404.E1408.B2205555.GC.L0397171_Wmed.roi1	Mediterranean: West	French Coast	2005-01-01	14:04	(2 , 37)
NSS.LHRR.NL.D05001.S1404.E1408.B2205555.GC.L0397171_Wmed.roi2	Mediterranean: West	French Coast	2005-01-01	14:04	(2 , 37)
NSS.LHRR.NL.D05004.S1329.E1333.B2209797.GC.L0397191_Wmed.roi0	Mediterranean: East	Adriatic Sea	2005-01-04	13:29	(2 , 37)
NSS.LHRR.NL.D05004.S1329.E1333.B2209797.GC.L0397191_Wmed.roi1	Mediterranean: East	Tyrrhenian Sea	2005-01-04	13:29	(2 , 37)
NSS.LHRR.NM.D05003.S1200.E1212.B1314141.WI.L0397181_Nwaf.roi0	West Africa: North	Coast of Western Sahara	2005-01-03	12:00	(-18 , 25)
NSS.LHRR.NM.D05004.S1137.E1149.B1315555.WI.L0397201_Nwaf.roi0	West Africa: North	Coast of Southern part of Western Sahara	2005-01-04	11:37	(-18 , 25)
NSS.LHRR.NM.D05013.S1132.E1143.B1328383.WI.L0397221_Nwaf.roi0	West Africa: North	Coast of Southern part of Western Sahara	2005-01-13	11:32	(-18 , 25)
NSS.LHRR.NL.D05010.S1342.E1353.B2218182.GC.L0464311_Wsaf.roi0	South Africa: West Coast	NorthWest South Africa	2005-01-10	13:42	(20 , -30)
NSS.LHRR.NL.D05016.S1232.E1243.B2226566.GC.L0464321_Esaf.roi0	South Africa: East Coast	Madagascar	2005-01-16	12:32	(45 , -20)
NSS.LHRR.NL.D05027.S1348.E1359.B2242122.GC.L0464331_Wsaf.roi0	South Africa: West Coast	Namibia	2005-01-27	13:48	(15 , -20)
NSS.LHRR.NL.D05027.S1348.E1359.B2242122.GC.L0464331_Wsaf.roi1	South Africa: West Coast	Namibian/South African border	2005-01-27	13:48	(10 , -30)
NSS.LHRR.NL.D05044.S1354.E1405.B2266162.GC.L0464341_Wsaf.roi0	South Africa: West Coast	Namibia	2005-02-13	13:54	(12 , -25)
NSS.LHRR.NL.D05044.S1354.E1405.B2266162.GC.L0464341_Wsaf.roi1	South Africa: West Coast	South Africa	2005-02-13	13:54	(10 , -30)
NSS.LHRR.NL.D05045.S1342.E1354.B2267576.GC.L0464351_Ssaf.roi0	South Africa: South Coast	South Africa	2005-02-14	13:42	(20 , -30)
NSS.LHRR.NL.D05045.S1342.E1354.B2267576.GC.L0464351_Wsaf.roi0	South Africa: West Coast	South Africa	2005-02-14	13:42	(18 , -30)
NSS.HRPT.NM.D03262.S1544.E1558.B0642828.WI.L9827001_ec.roi0	US East Coast	West Florida (Middle)	2003-09-19	15:44	(-80 , 30)
NSS.HRPT.NM.D04024.S1608.E1622.B0823535.WI.L9827011_ec.roi0	US East Coast	West Florida (Middle)	2004-01-24	16:08	(-80 , 30)
NSS.HRPT.NM.D04127.S1531.E1544.B0970000.WI.L9827021_ec.roi0	US East Coast	Virginia + N. Carolina	2004-05-06	15:31	(-80 , 40)
Hrpt_noaa15_20040807_1552_32412.11b_egl.roi0	Greenland East Coast	SouthWest of Svalbard	2004-08-07	15:52	(10 , 75)
Hrpt_noaa17_20040715_1351_10695.11b_egl.roi0	Greenland East Coast	SouthEast Greenland	2004-07-15	13:51	(-40 , 63)
Hrpt_noaa17_20040811_1157_11078.11b_polfmnt.roi0	Polar Front	South Iceland	2004-08-11	11:57	(-15 , 63)

**Table 3:** List of AVHRR validation scenes. All scenes are LAC datasets obtained from the NOAA archives; except the last four, which are locally received hrpt files.



## 6. References

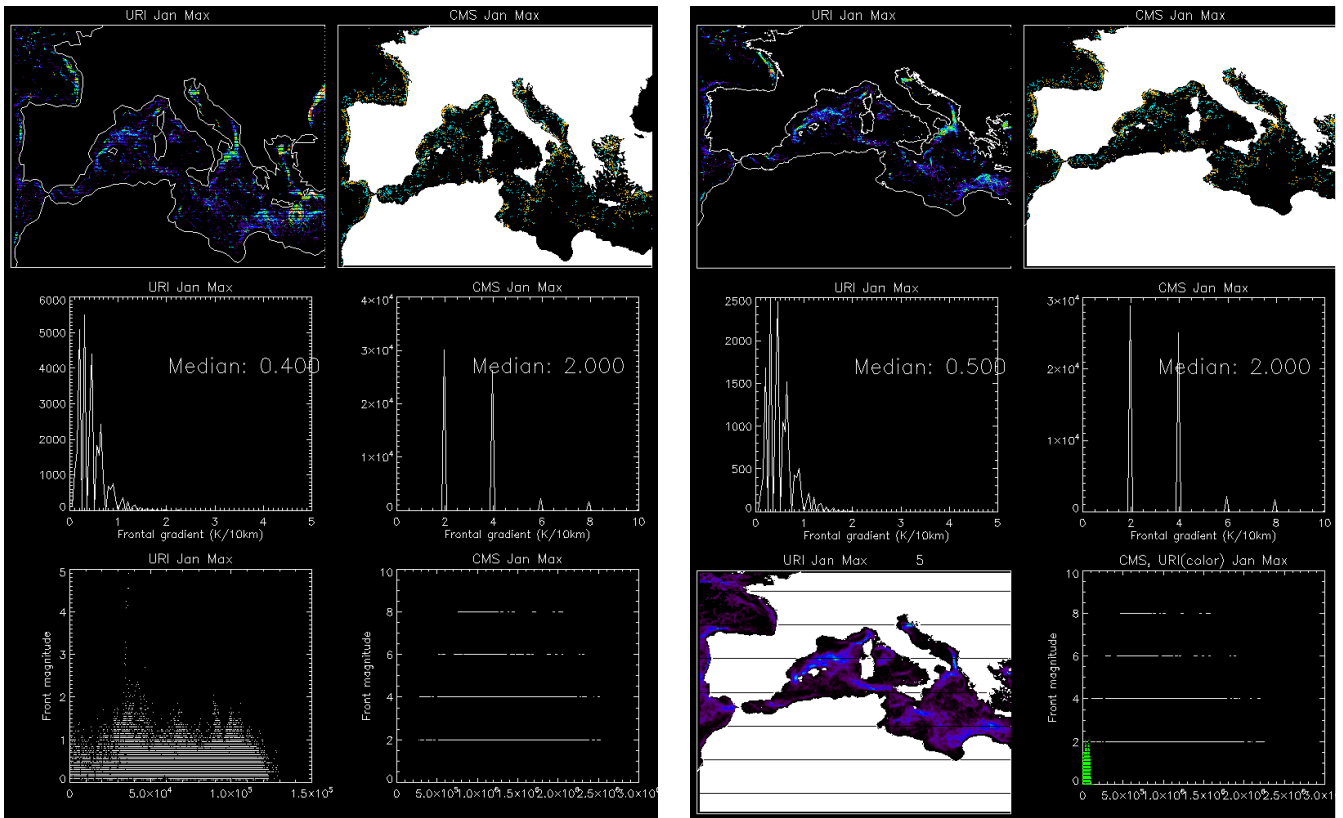
- Belkin, I.M., P. C. Cornillon, D. S. Ullman, and Z. Shan (2006) Global survey of oceanic fronts from satellite SST data, *Progress in Oceanography* (in preparation).
- Cayula, J.-F., and P. Cornillon (1992) Edge detection algorithm for SST images, *J. Atm. Oc. Tech.*, 9(1), 67-80.
- Cayula, J.-F., and P. Cornillon (1995) Multi-image edge detection for SST images. *J. Atm. Oc. Tech.*, 12(4), 821-829.
- Cayula, J.-F., and P. Cornillon (1996) Cloud detection from a sequence of SST images, *Rem. Sens. Envir.*, 55(1), 80-88.
- Cayula, J.-F., P. Cornillon, R. Holyer, and S. Peckinpaugh (1991) Comparative study of two recent edge-detection algorithms designed to process sea-surface temperature fields, *IEEE Trans. Geosci. Rem. Sens.*, 29(1), 175-177.
- LeBorgne (2006a) Making and use of an Atlas of thermal fronts at CMS. Informal memo, Meteo\_France CMS.
- LeBorgne (2006b) Annex on the use of spatial variability.
- Ullman, D. S. and P. C. Cornillon (1999) Surface temperature fronts off the East Coast of North America from AVHRR imagery, *J. Geophys. Res.*, 104(C10), 23,459-23,478.
- Ullman, D. S. and P. C. Cornillon (2000) Evaluation of front detection methods for satellite-derived SST data using in situ observations, *J. Atm. Oceanic Tech.*, 17(12), 1667-1675.
- Ullman, D. S. and P. C. Cornillon (2001) Continental shelf surface thermal fronts in winter off the north-east US coast, *Cont. Shelf Res.*, 21(11-12), 1139-1156.

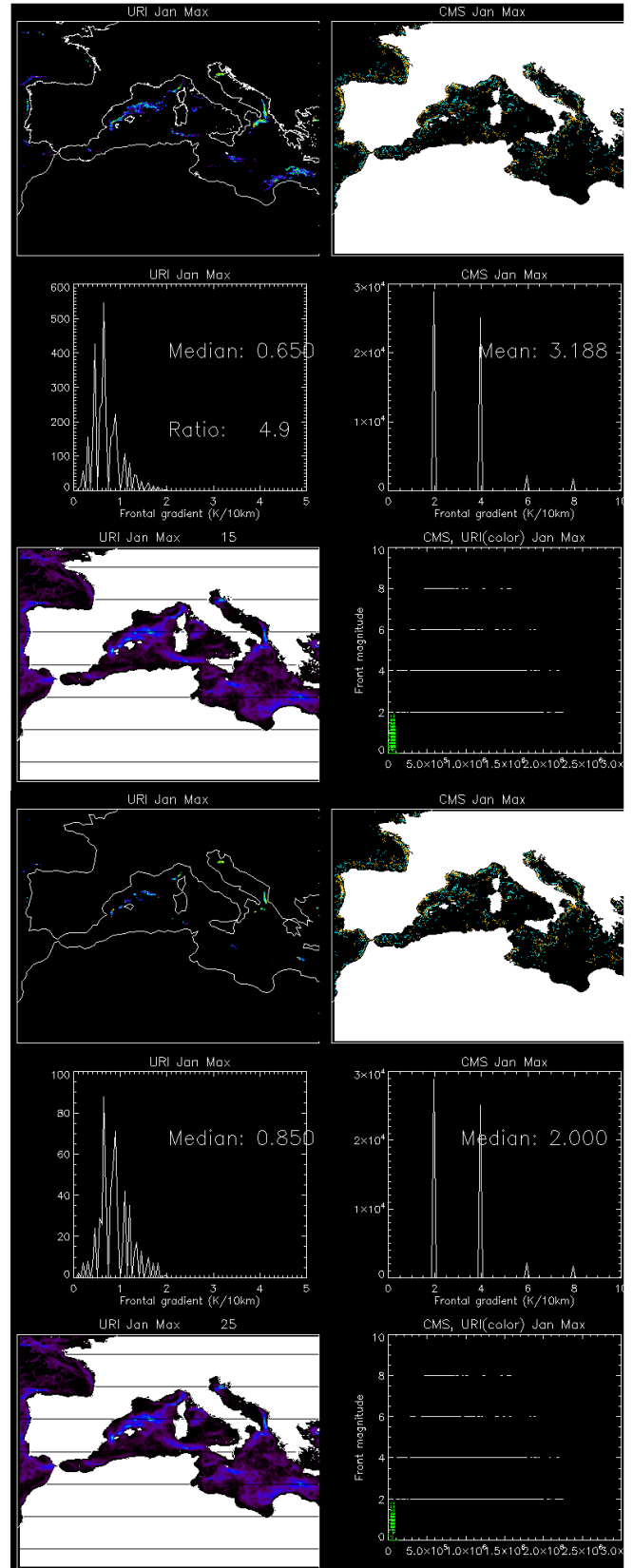
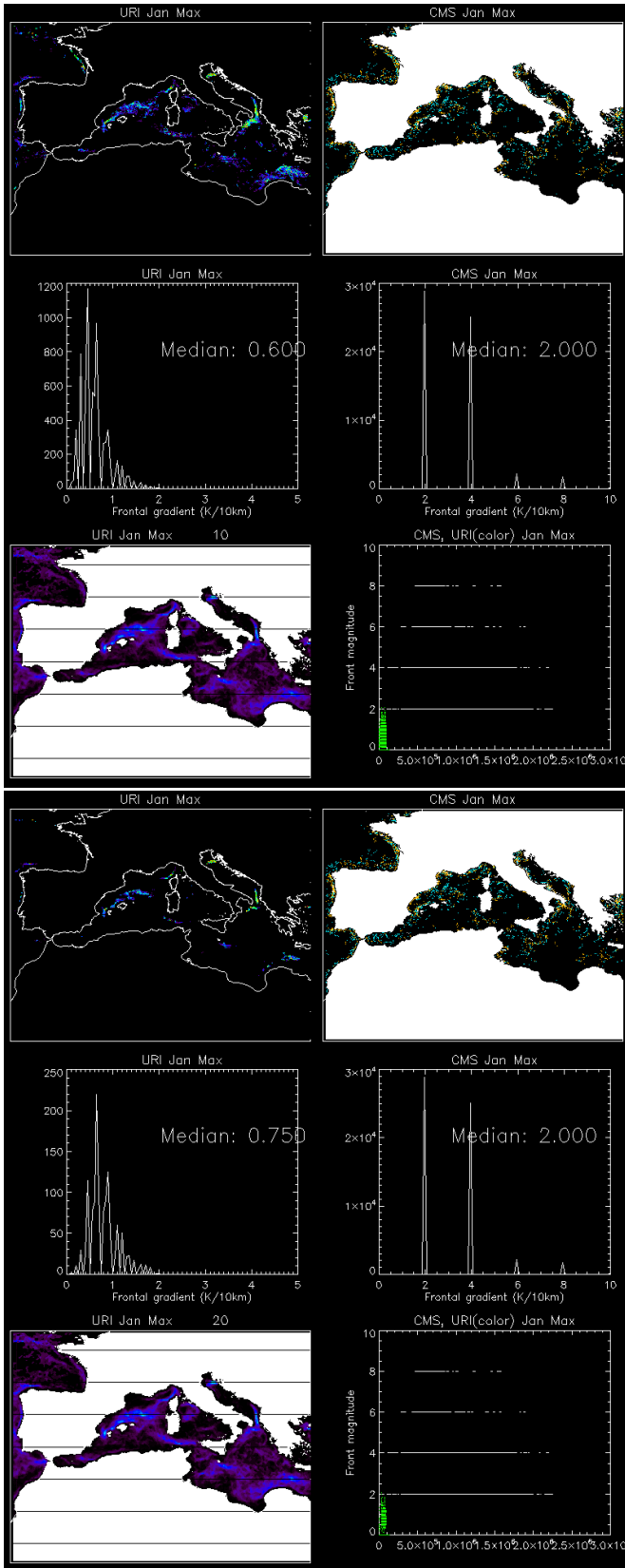


## Appendix 1: Comparisons between CMS and URI fields

In the following, comparisons between CMS and URI maximum gradient fields are presented for different months and URI frequency thresholds from 0 to 25 % (left-right, top-bottom: First row is 0 and 5 %, second row 10 and 15%, third row 20 and 25%). Each plot shows (from left to right, top to bottom) the thresholded URI field, the CMS field, the histogram of the URI field, the histogram of the CMS field. The bottom row shows either the unthresholded URI field or a scatter plot of the URI values (left) and a scatter plot of the CMS values and in some cases the thresholded URI values in green dots (right).

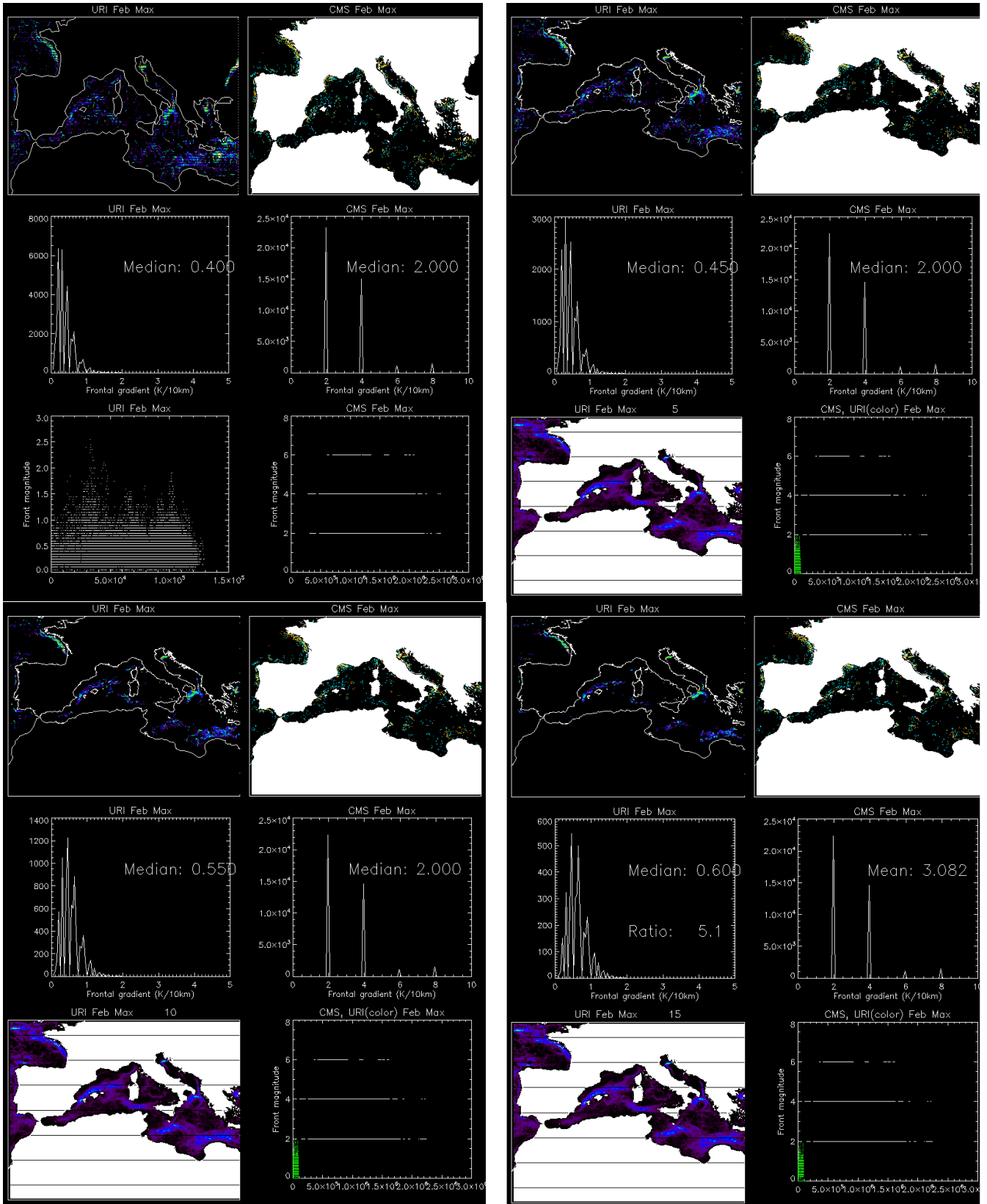
### January

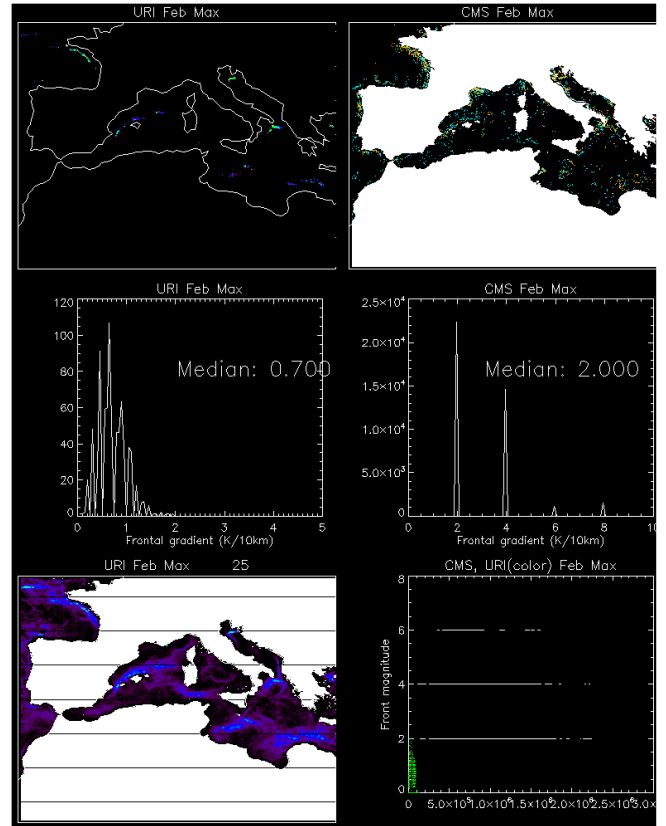
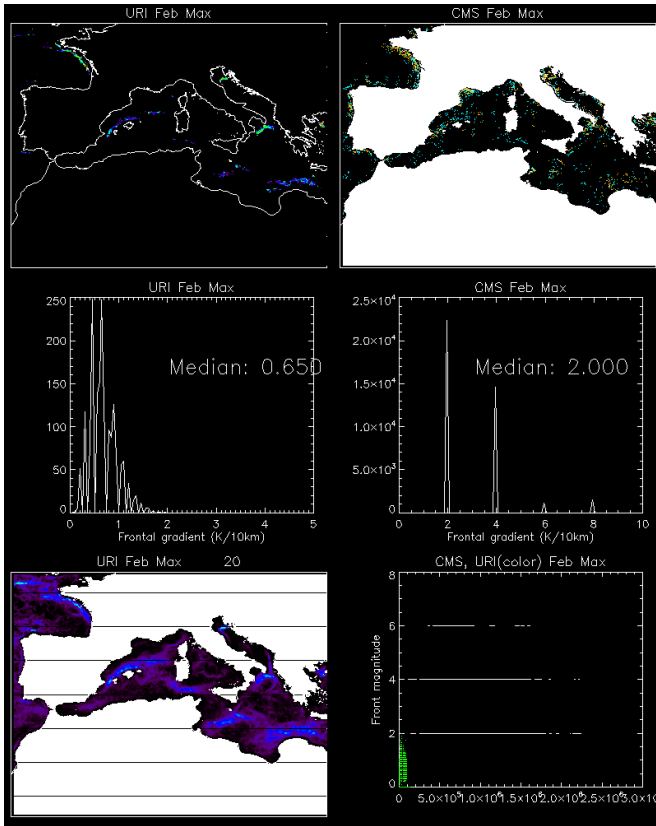




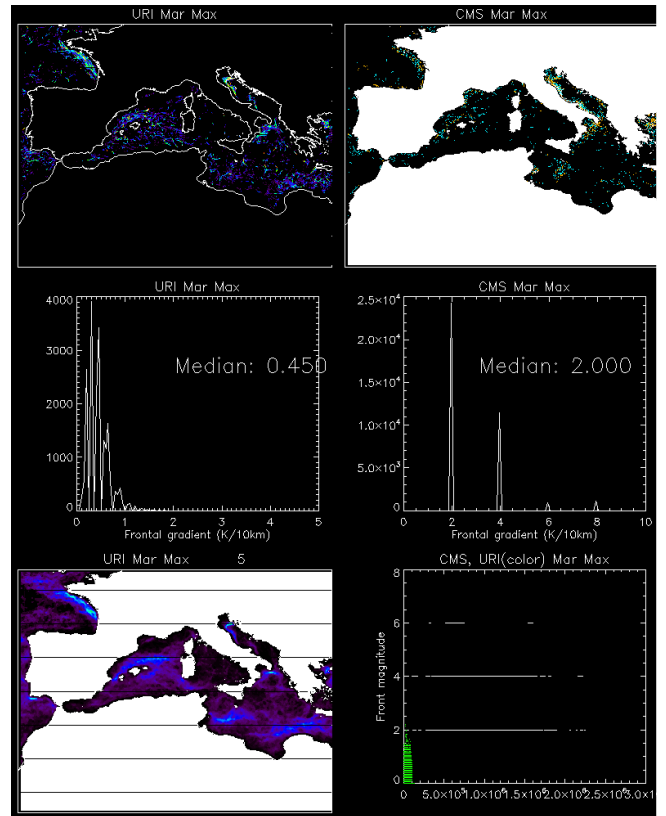
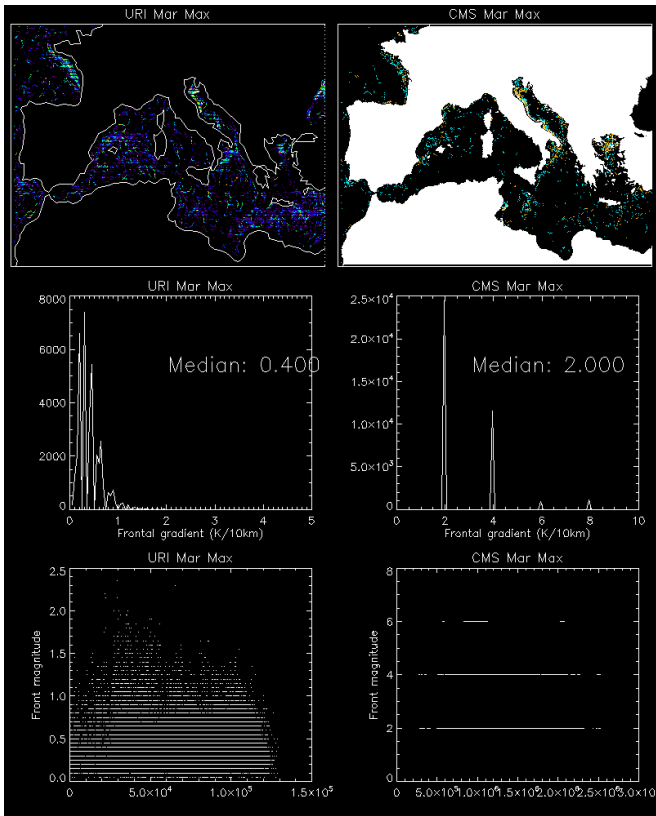


# February





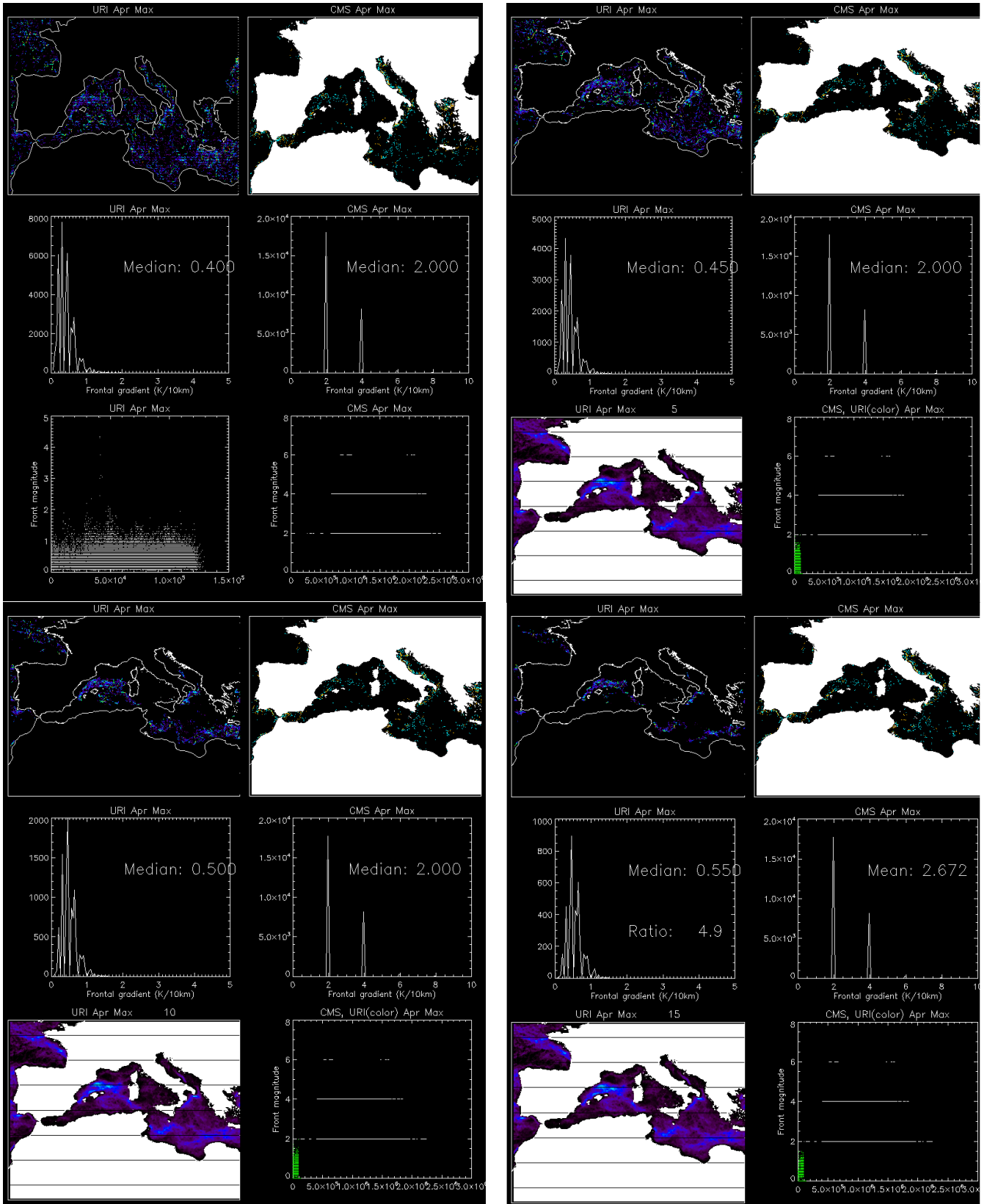
### March

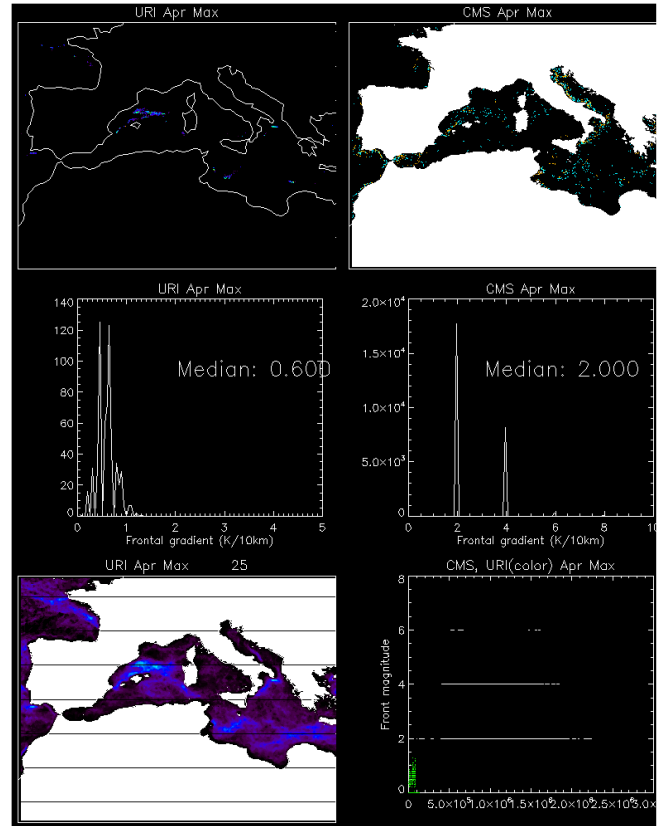
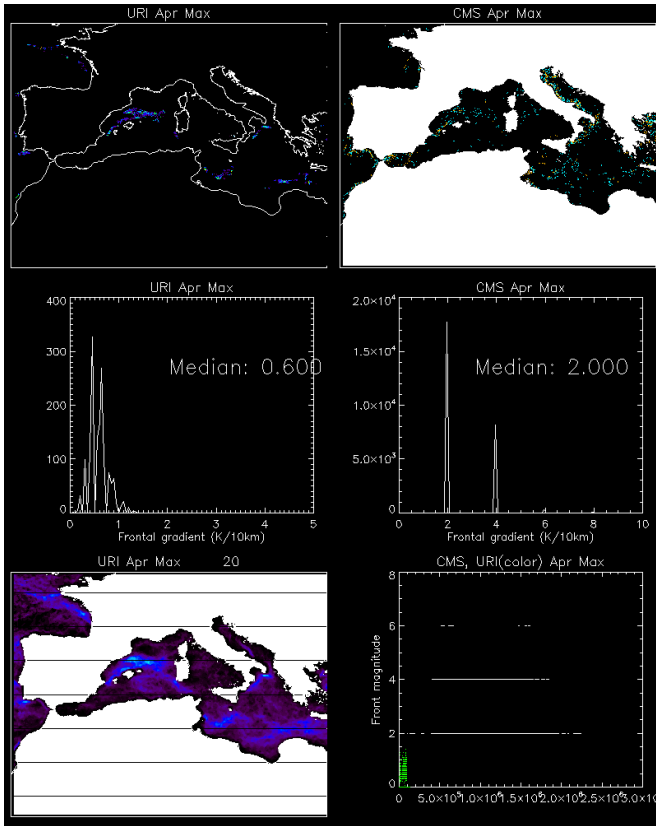




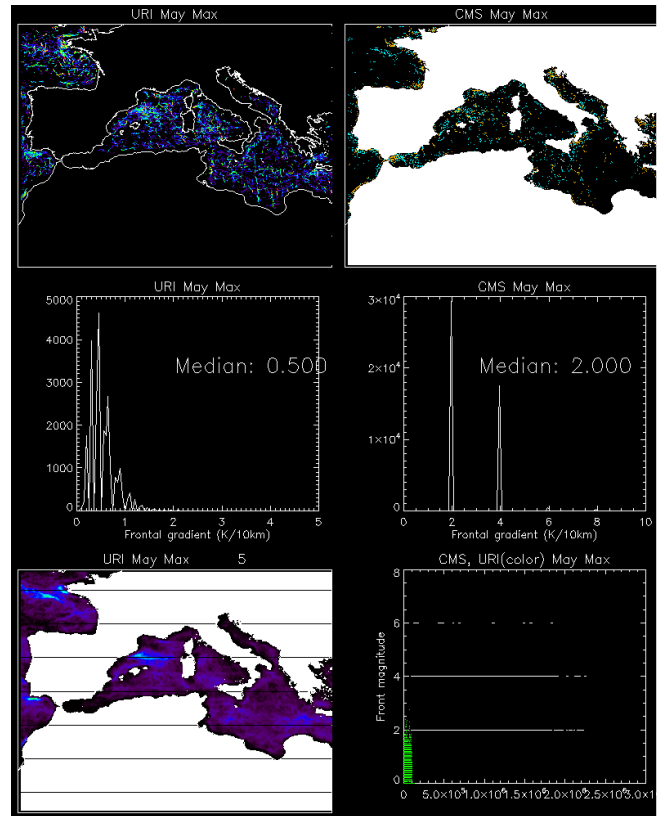
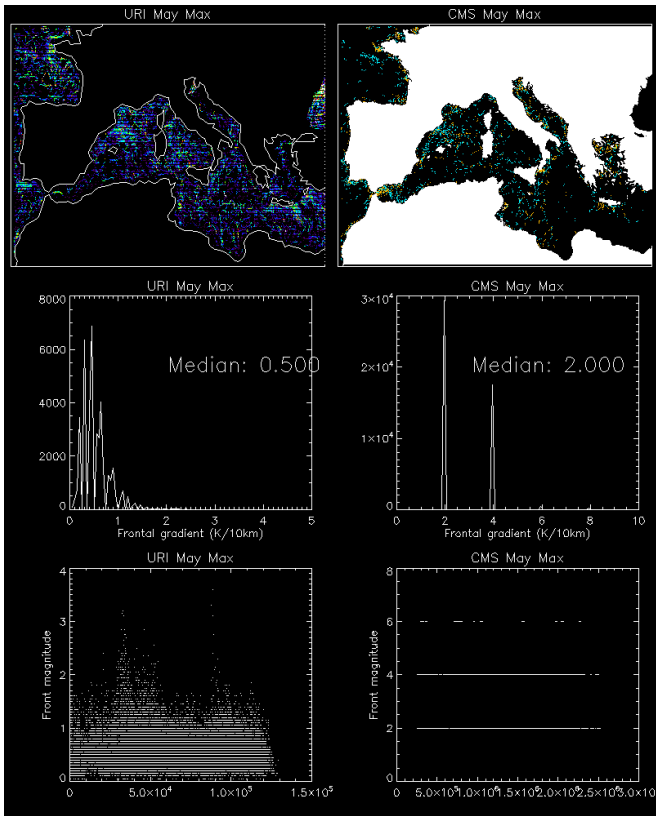


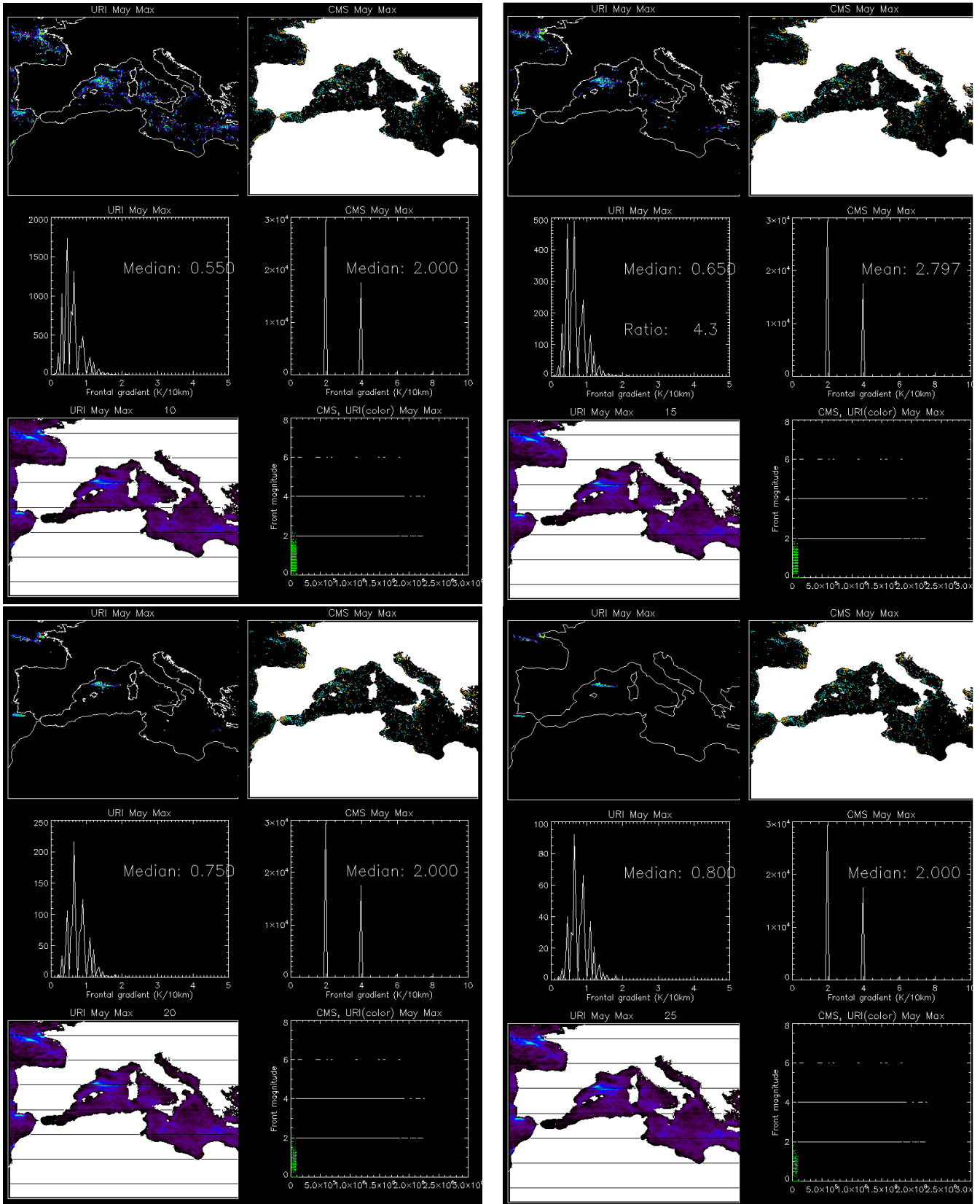
# April





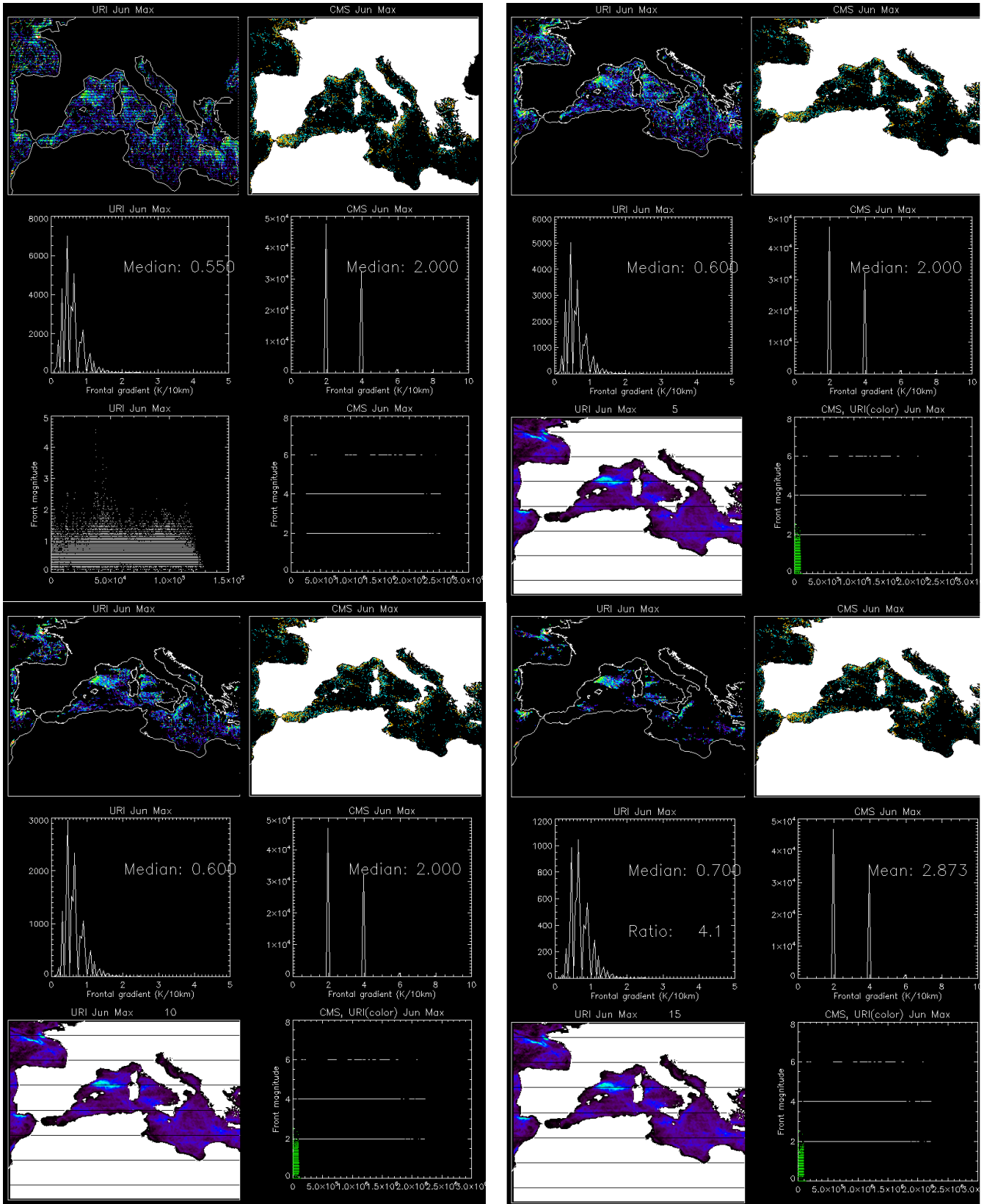
## May

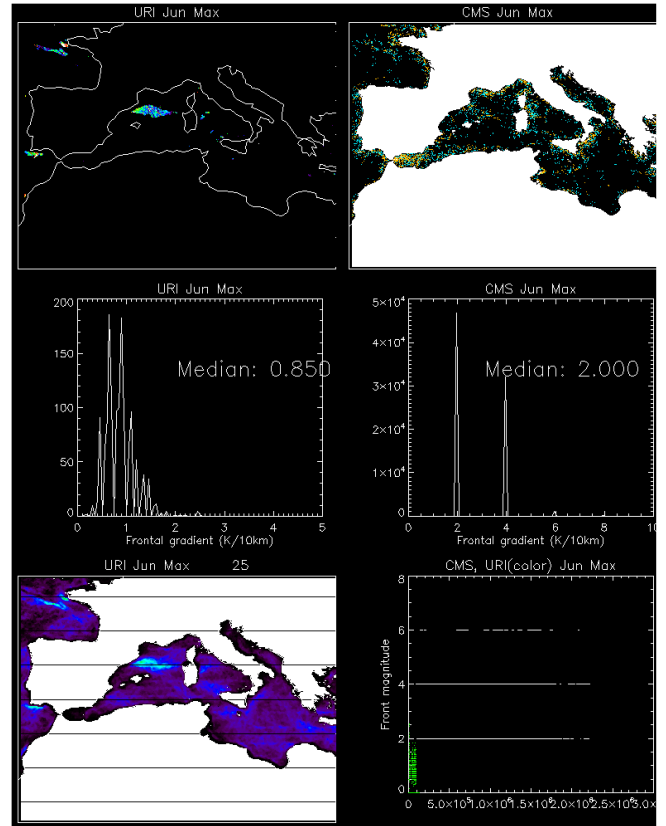
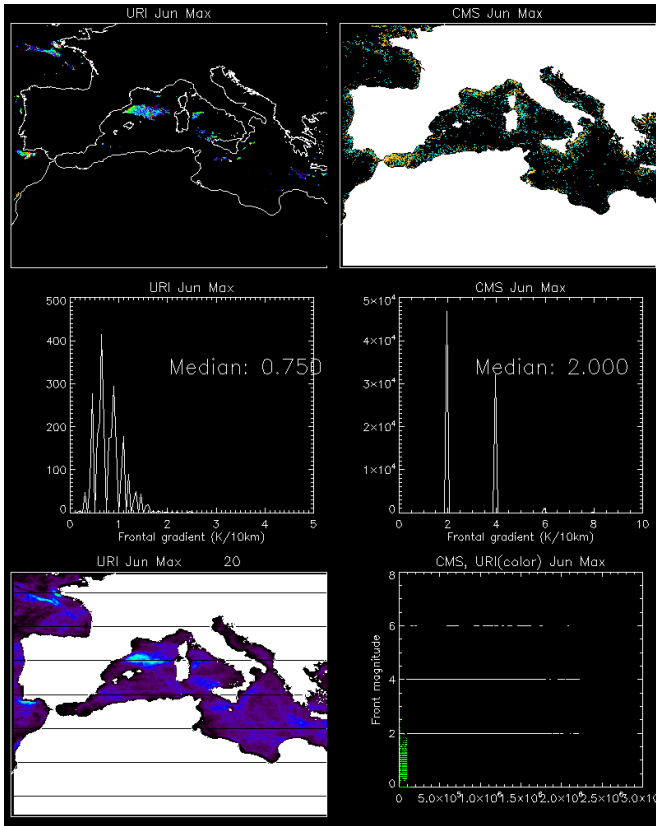




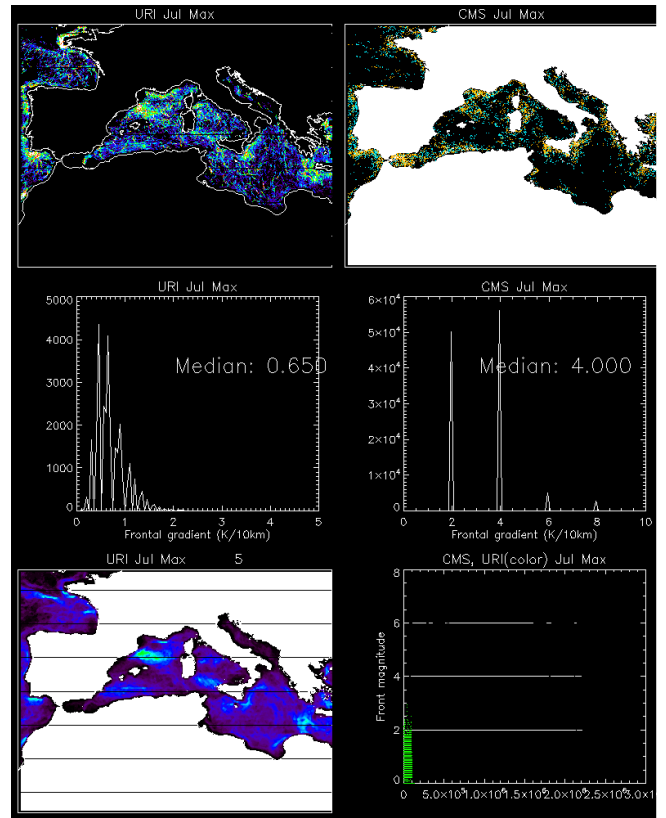
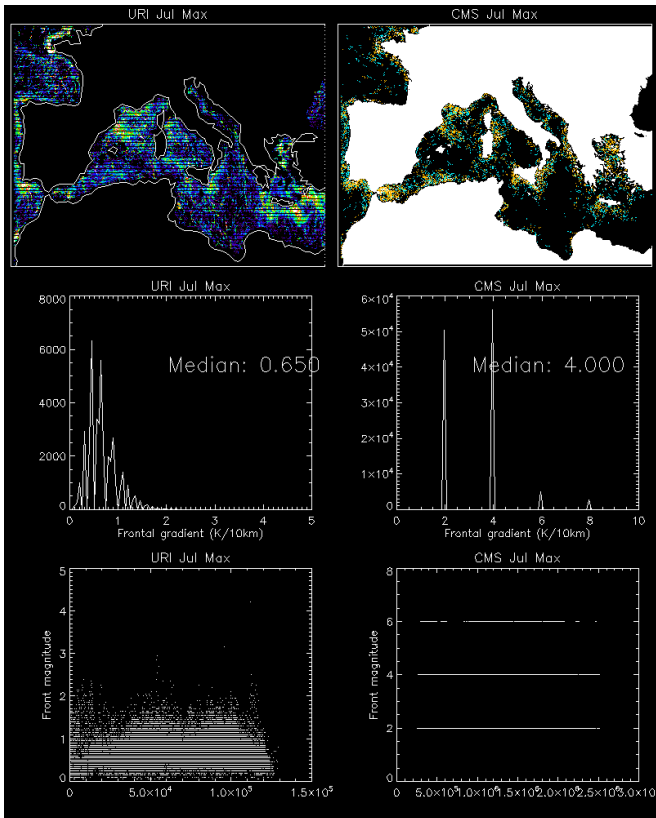


# June





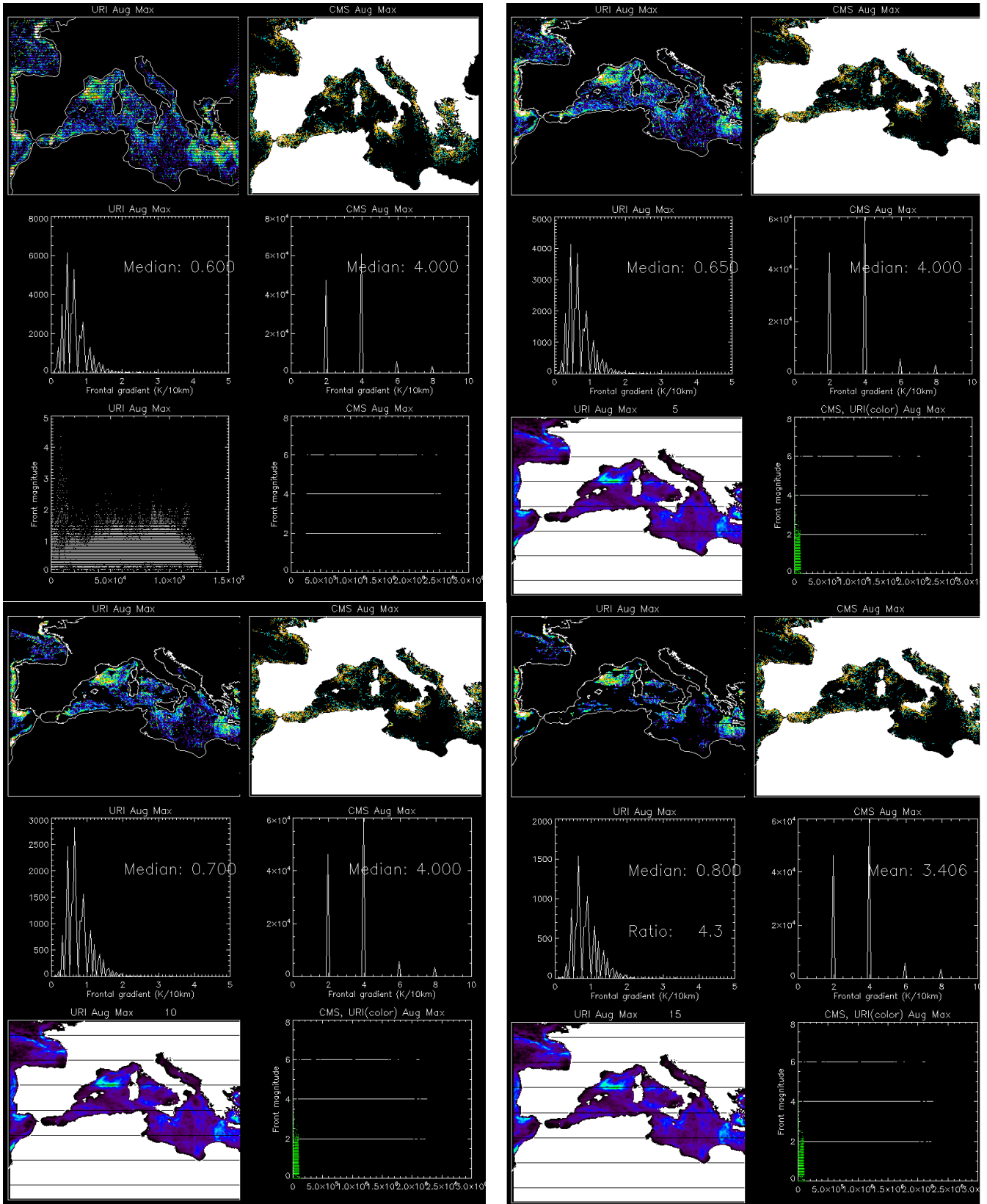
## July



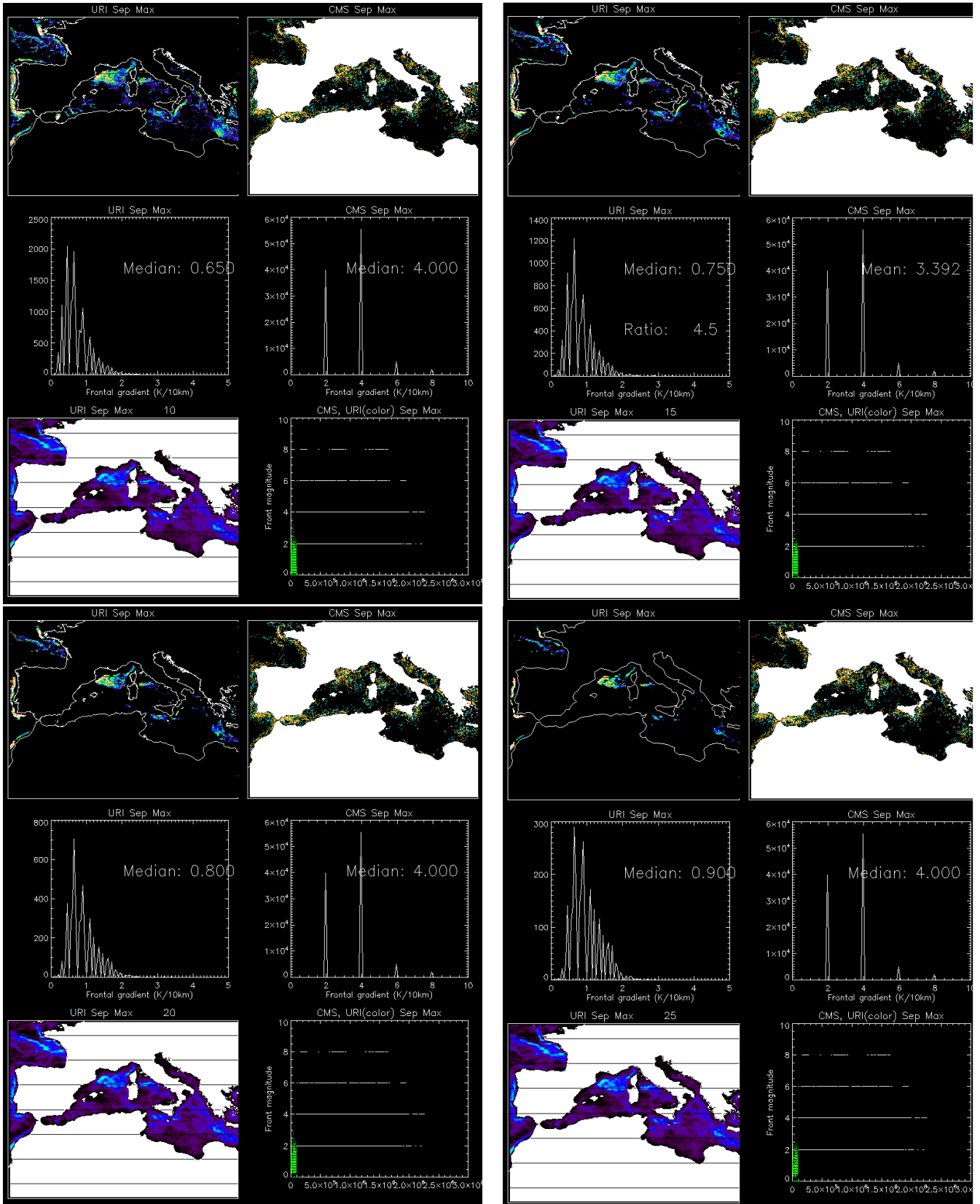




# August

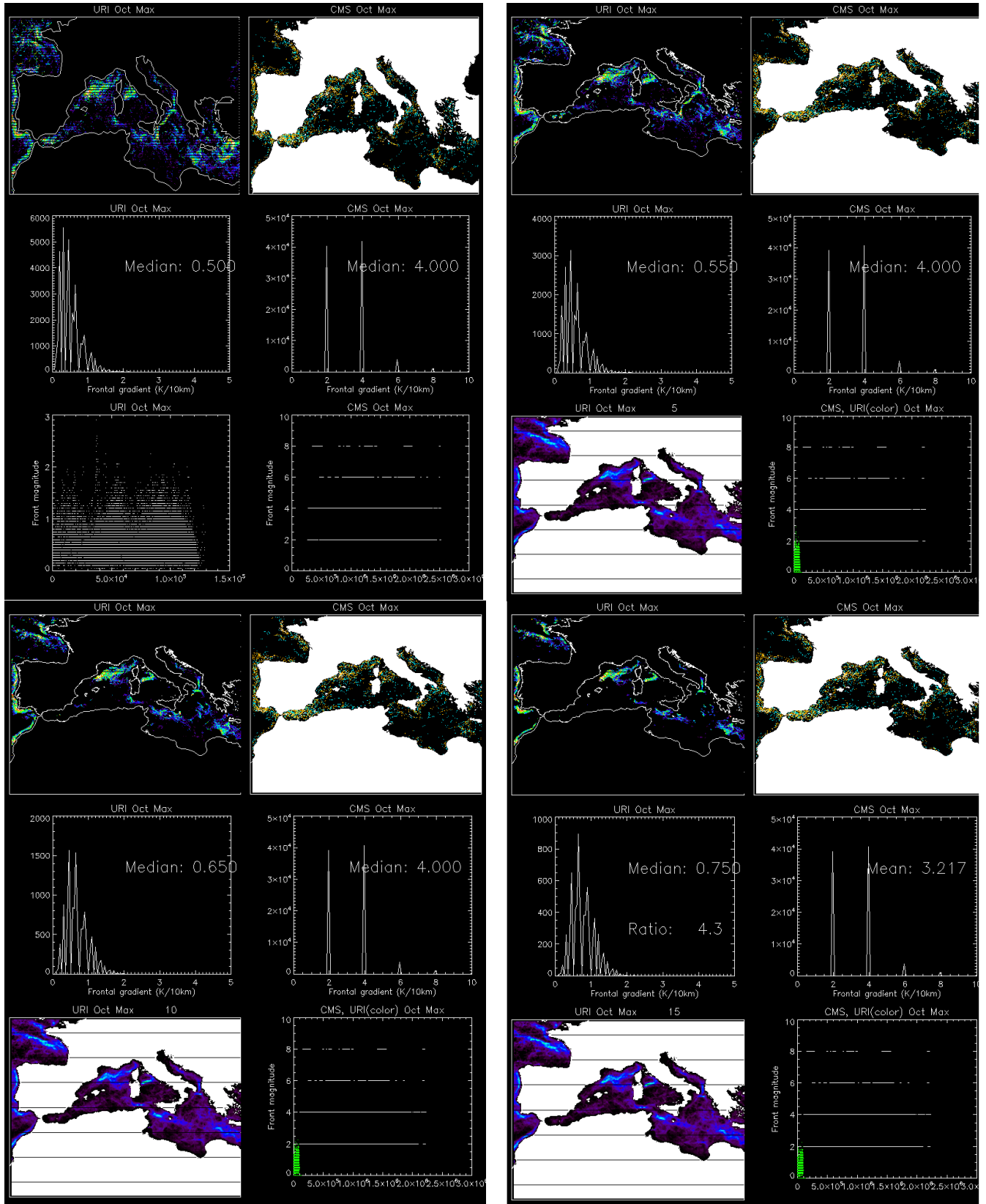


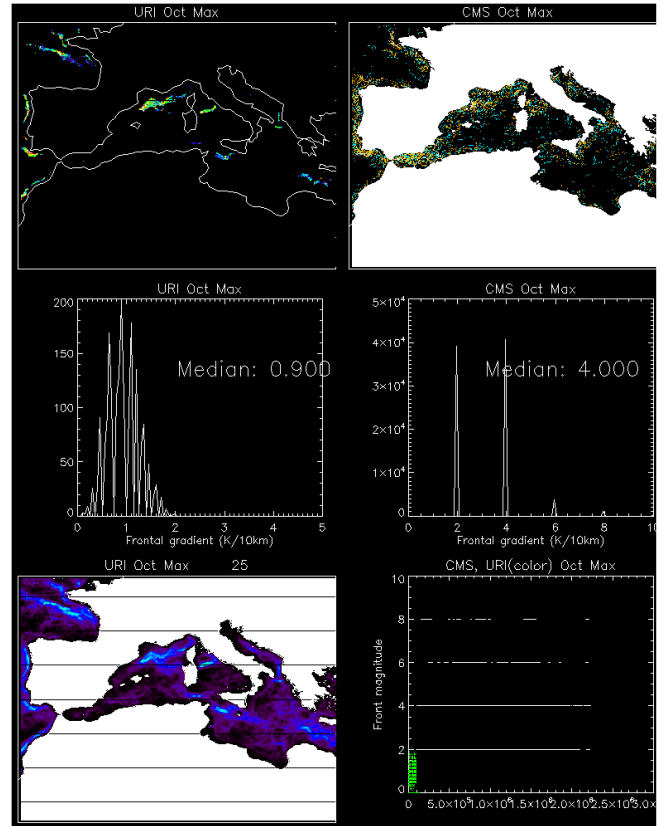
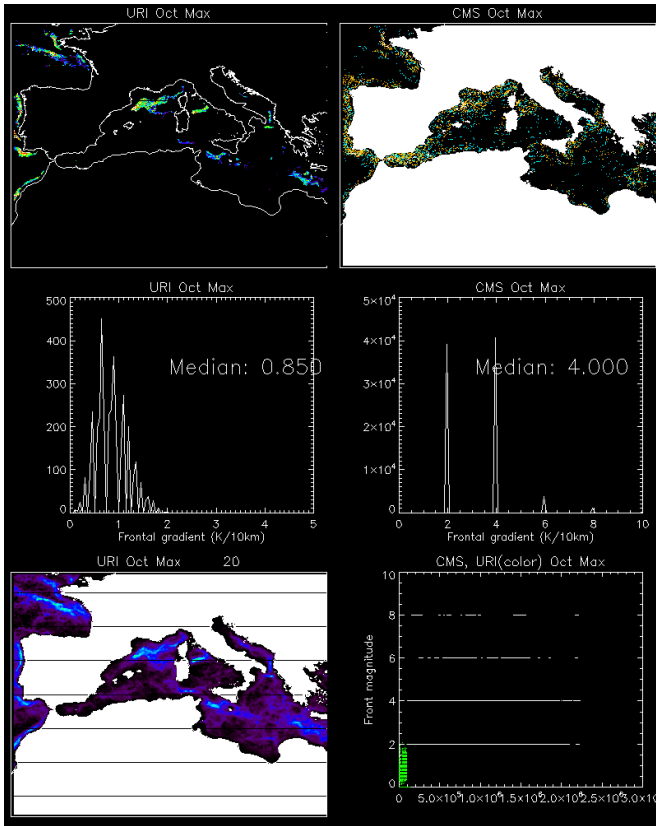




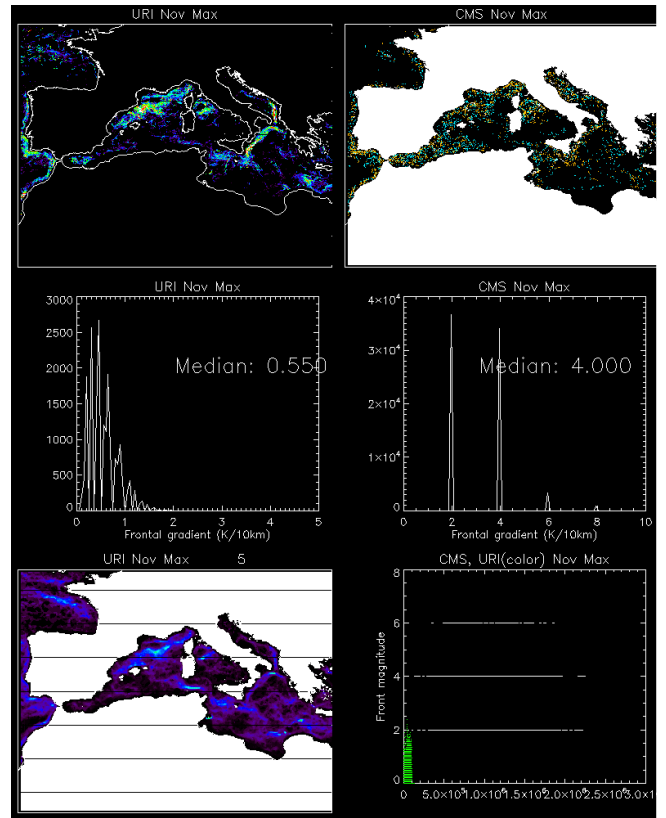
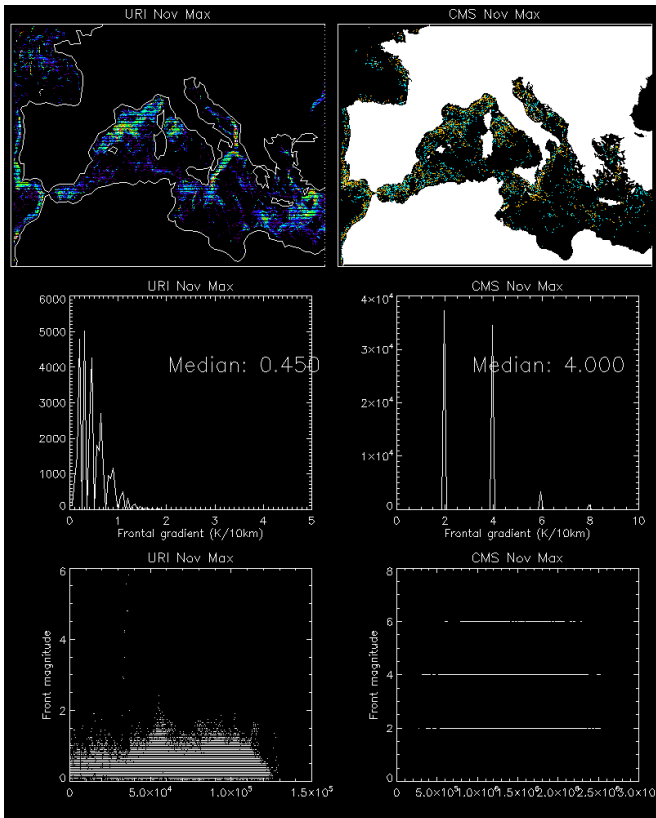


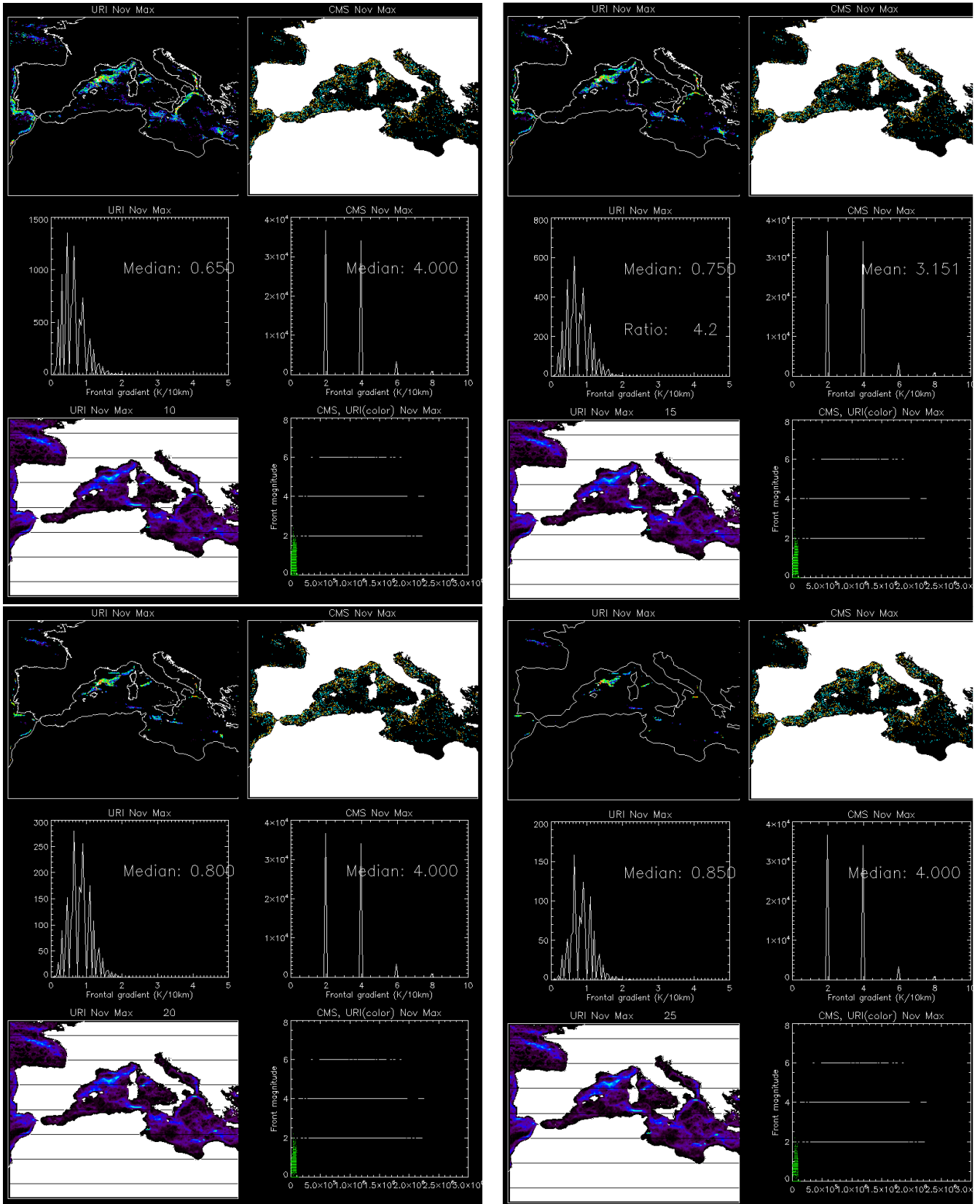
# October





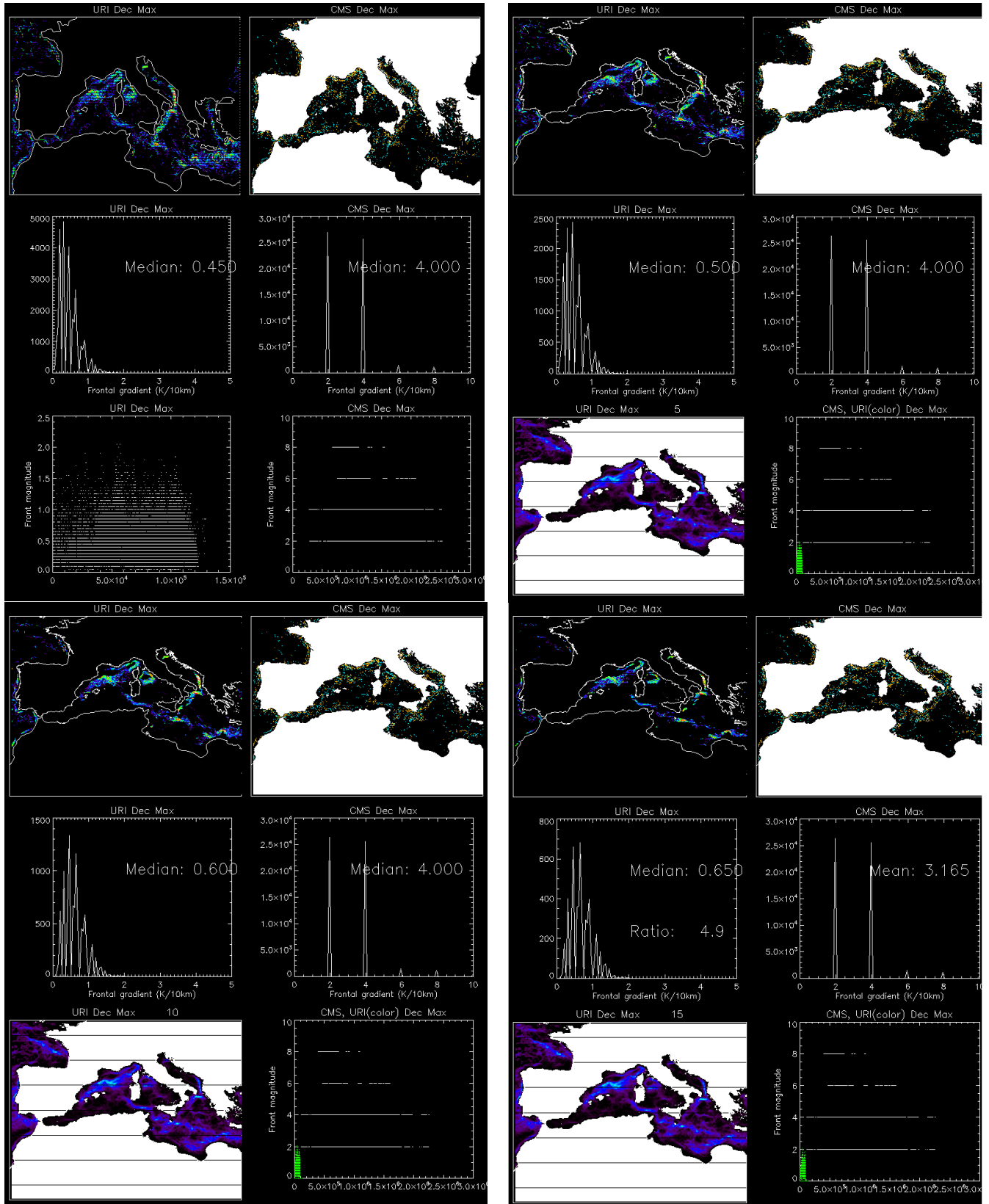
### November

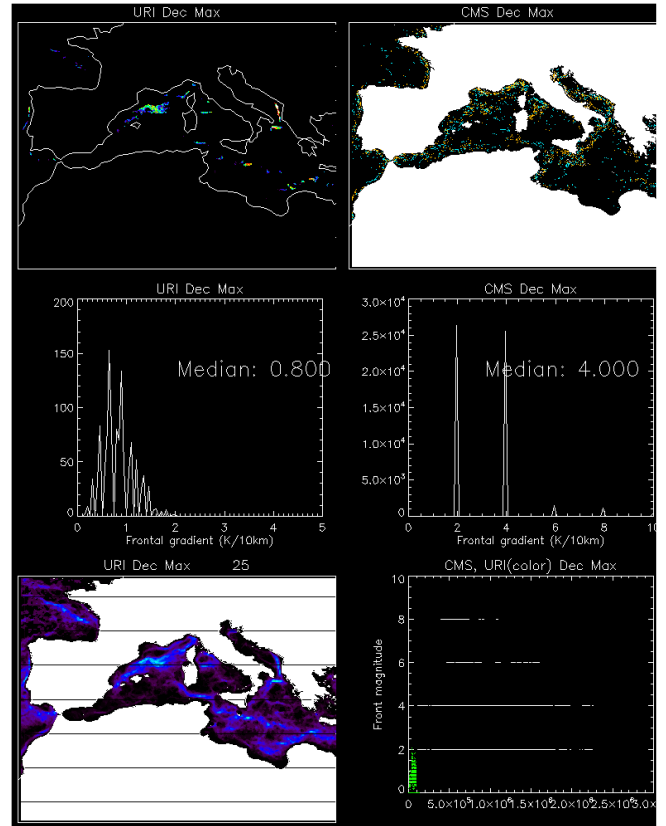
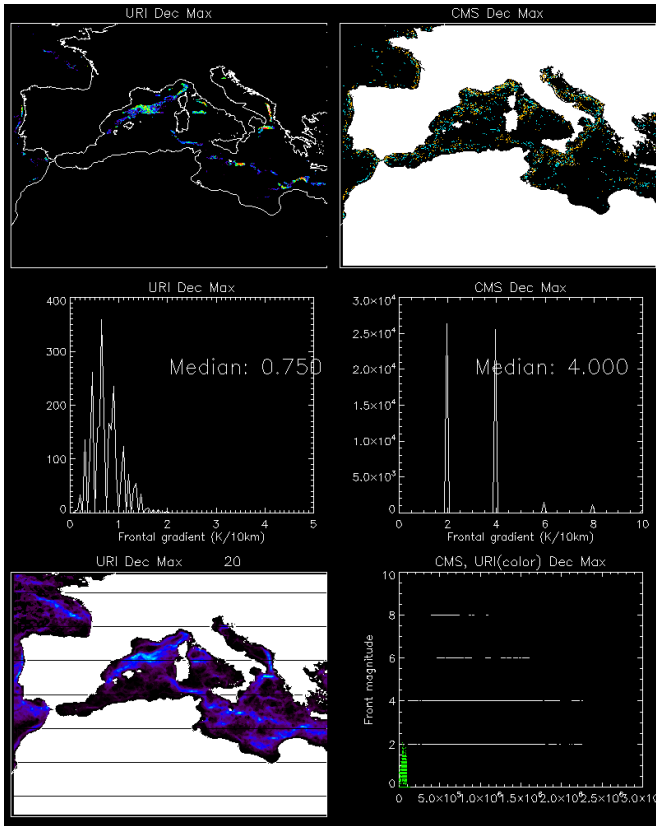






# December



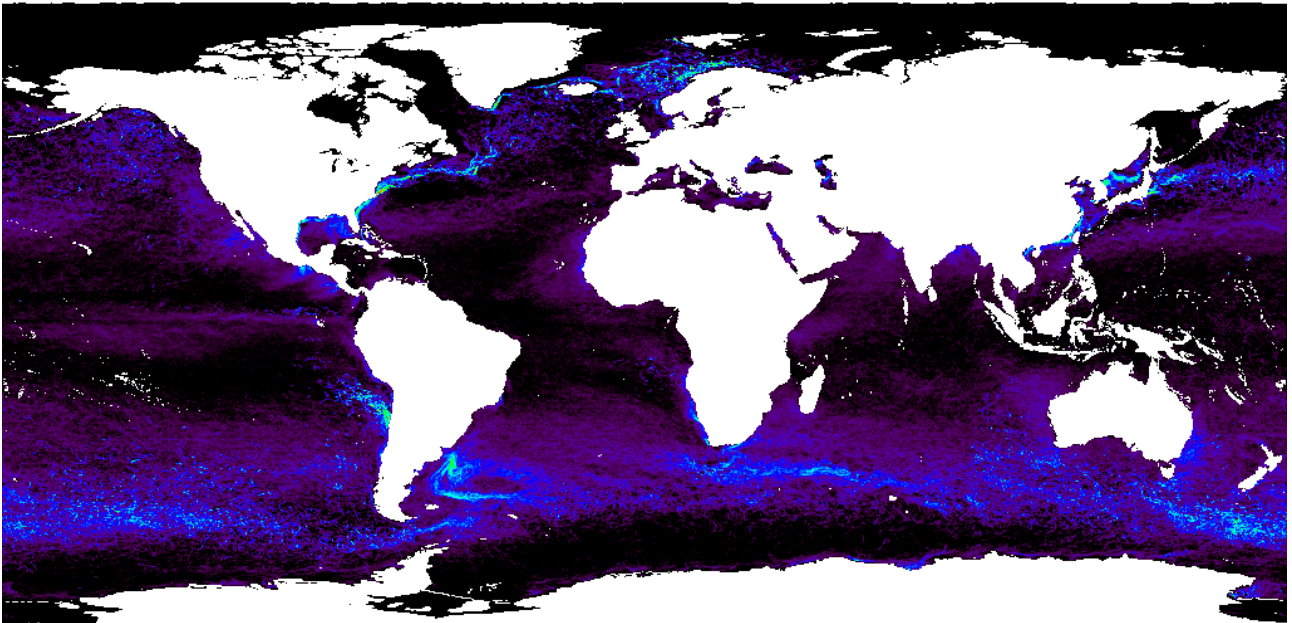




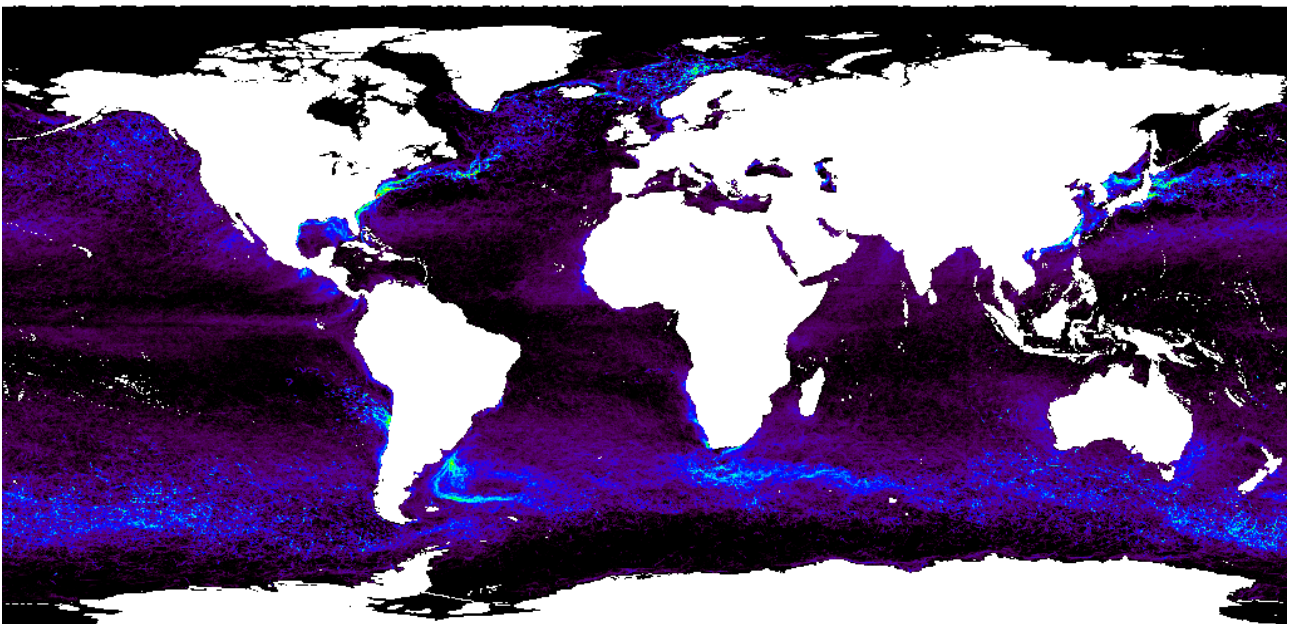
K/10km

## Appendix 2: Original URI max gradient fields

Pathfinder resolution maximum gradient expressed in K/10km



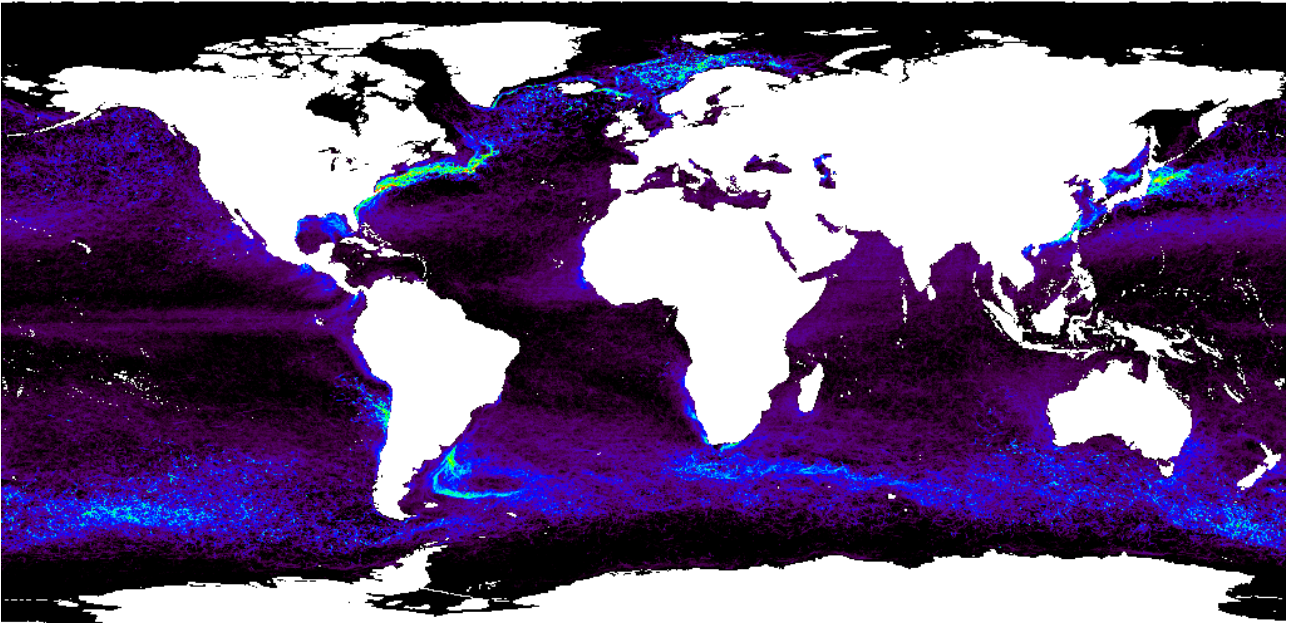
Jan



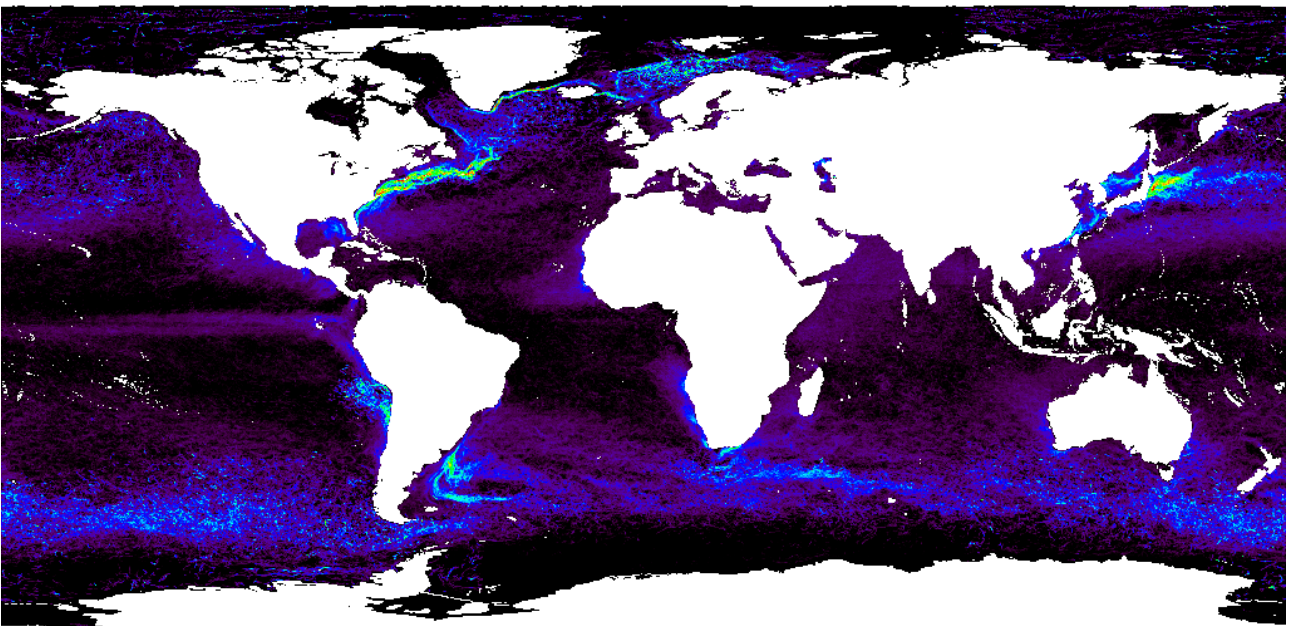
Feb



K/10km



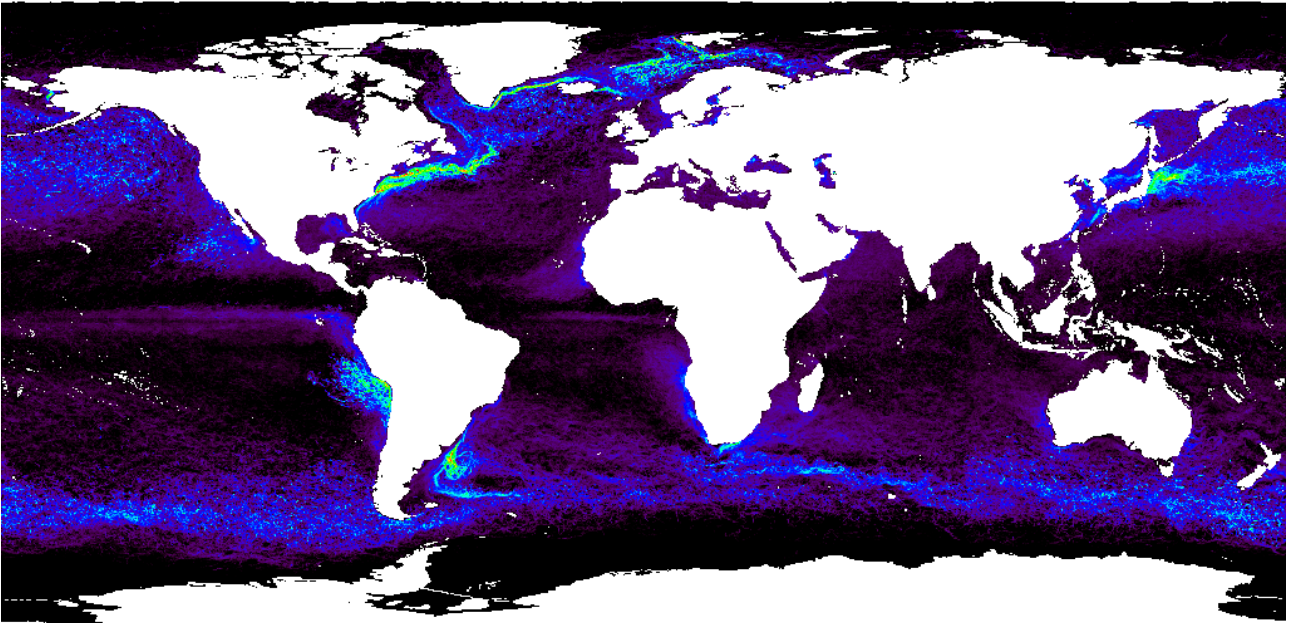
Mar



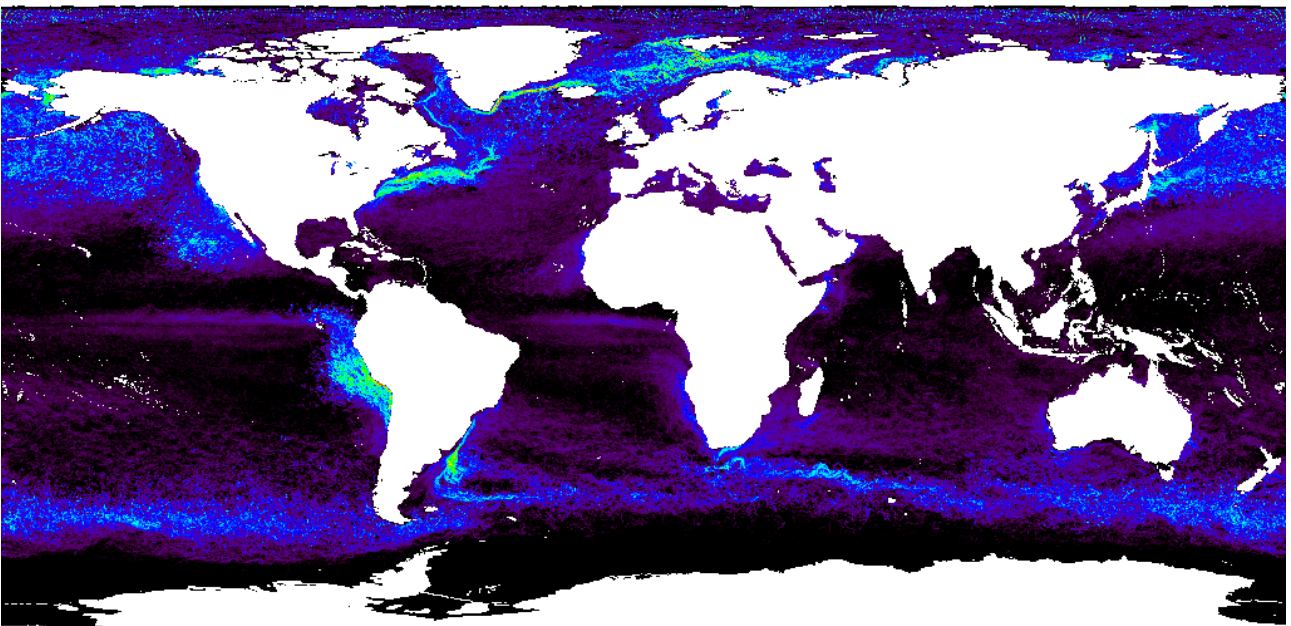
Apr



K/10km



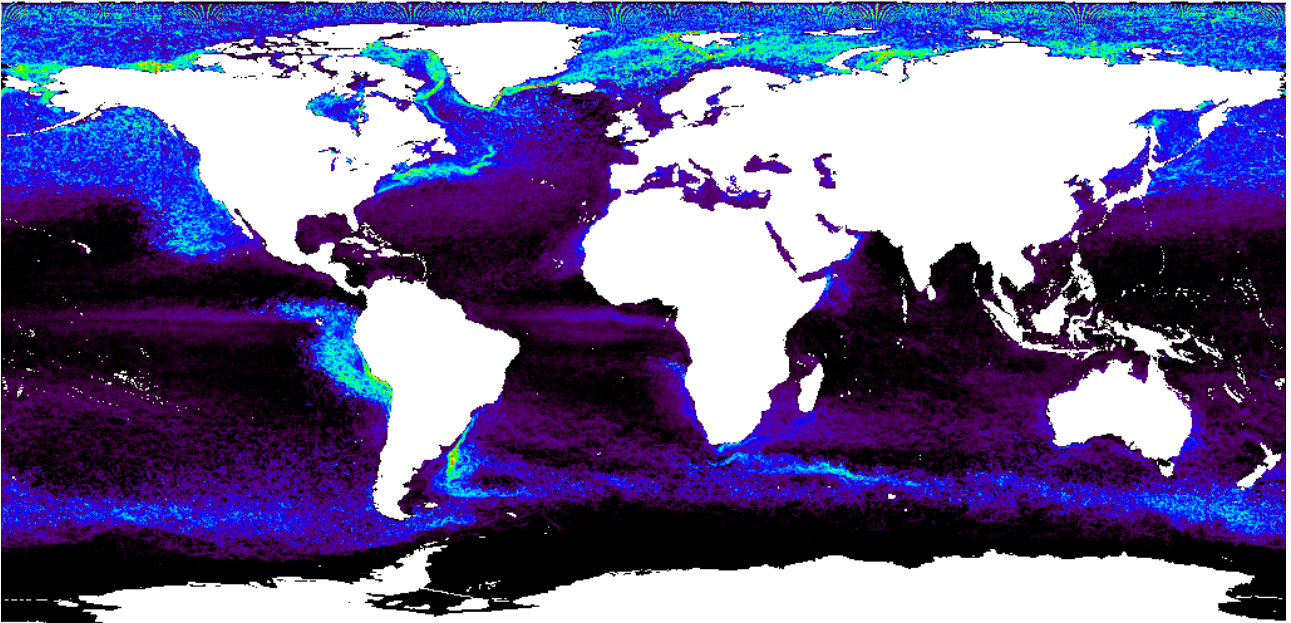
May



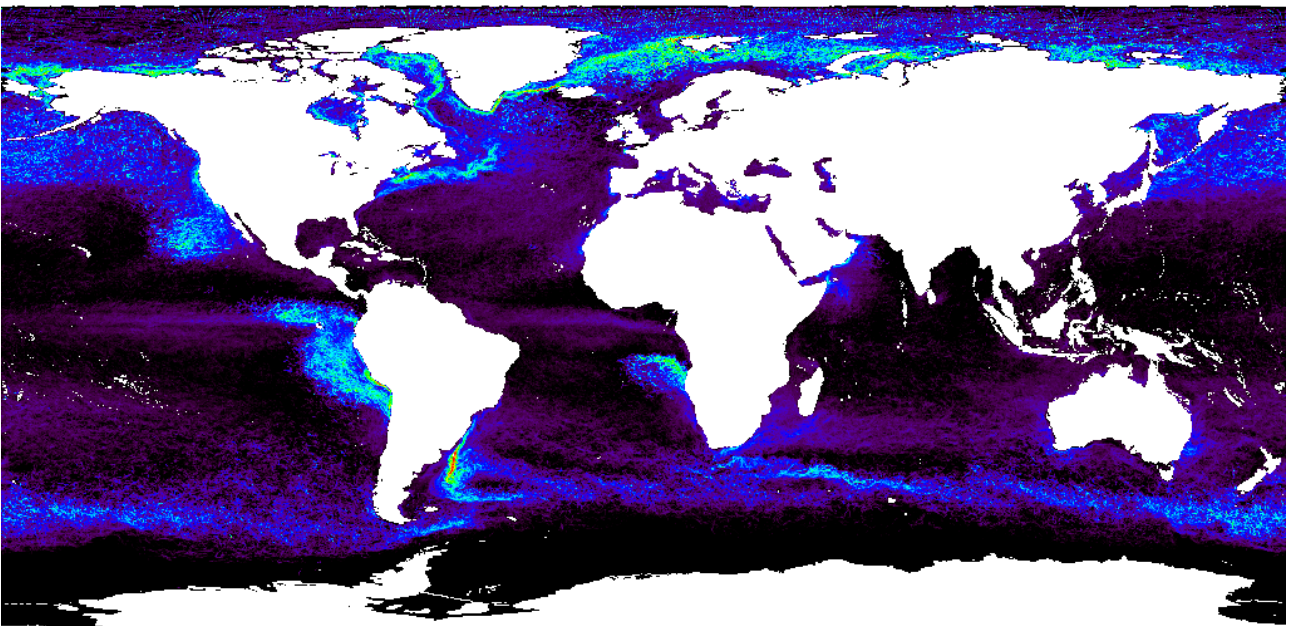
Jun



K/10km



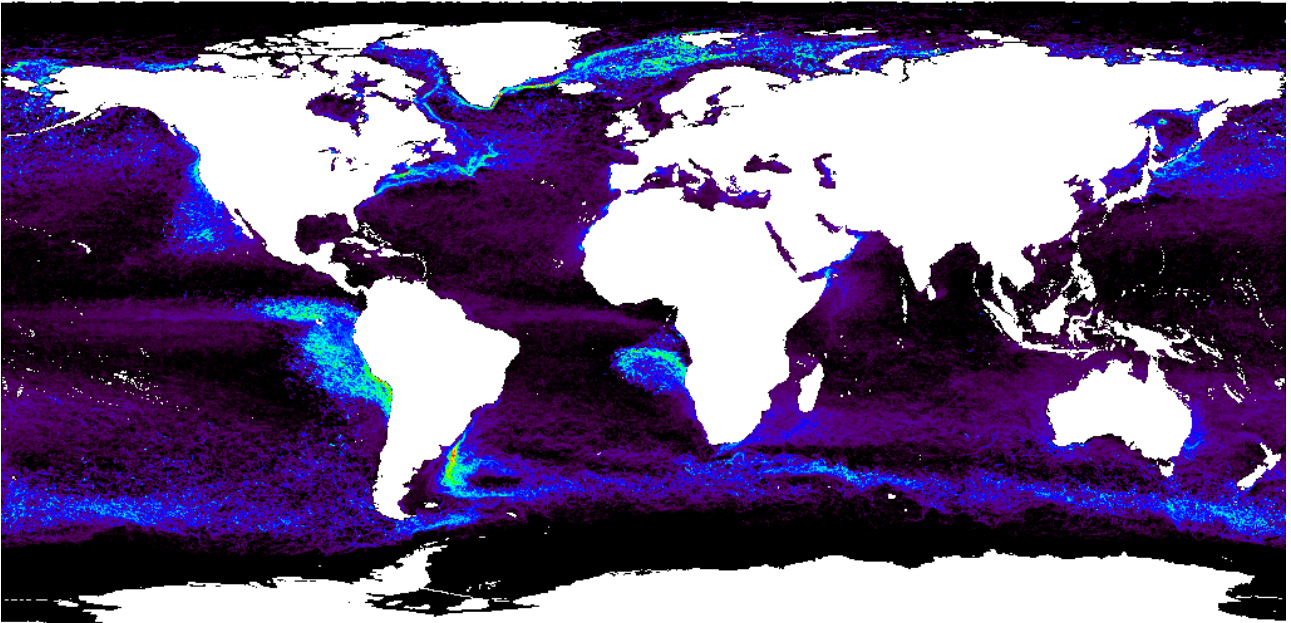
Jul



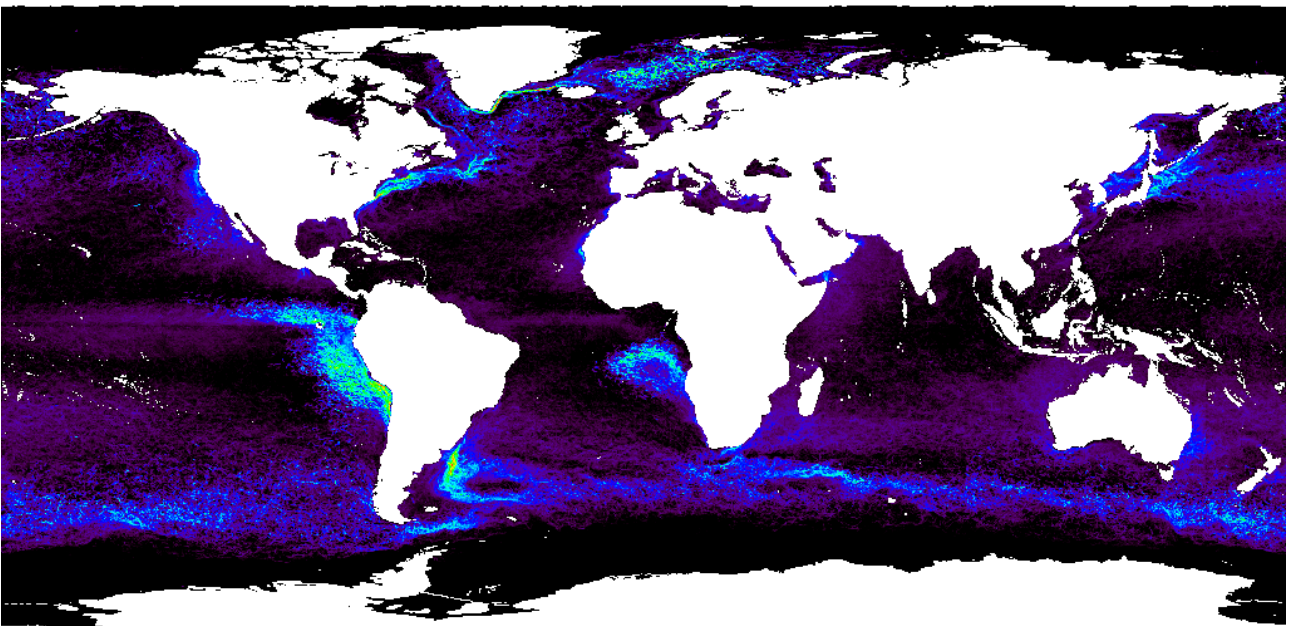
Aug



K/10km



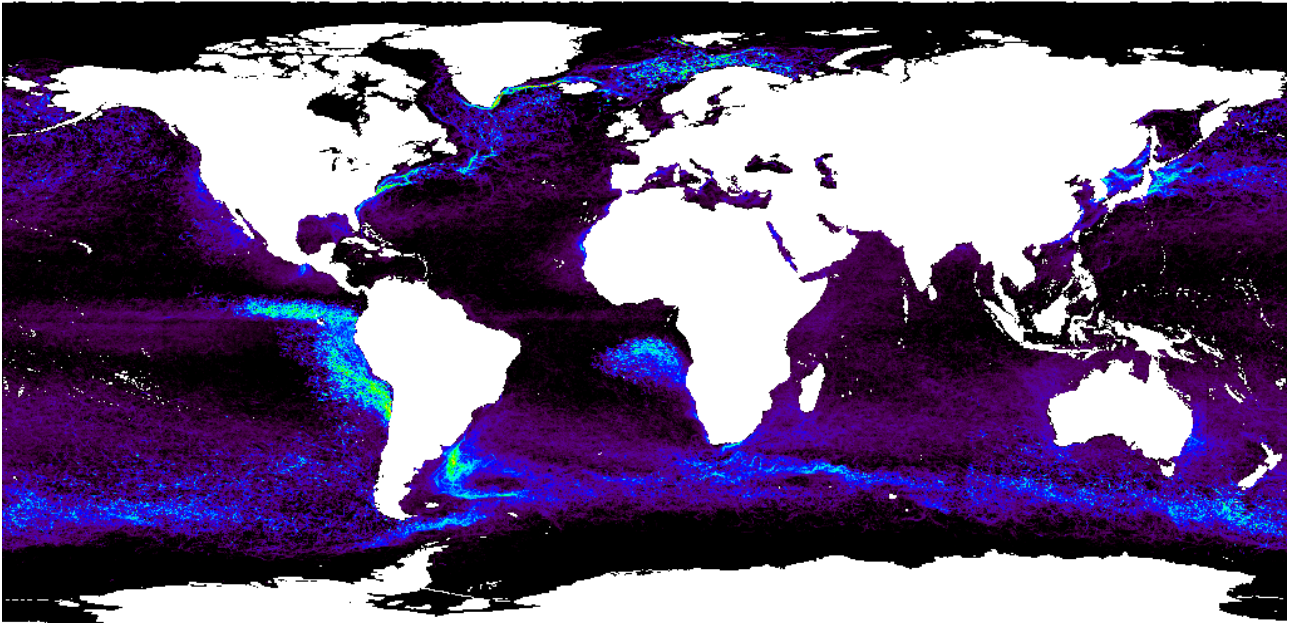
Sep



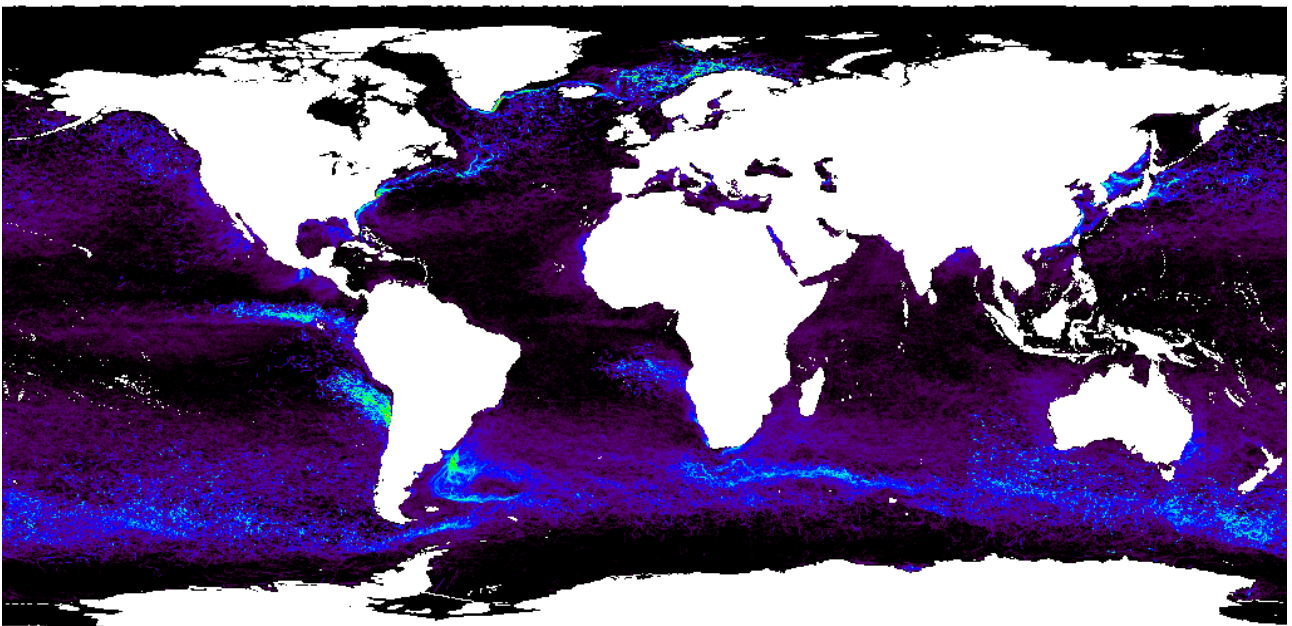
Oct



K/10km



Nov

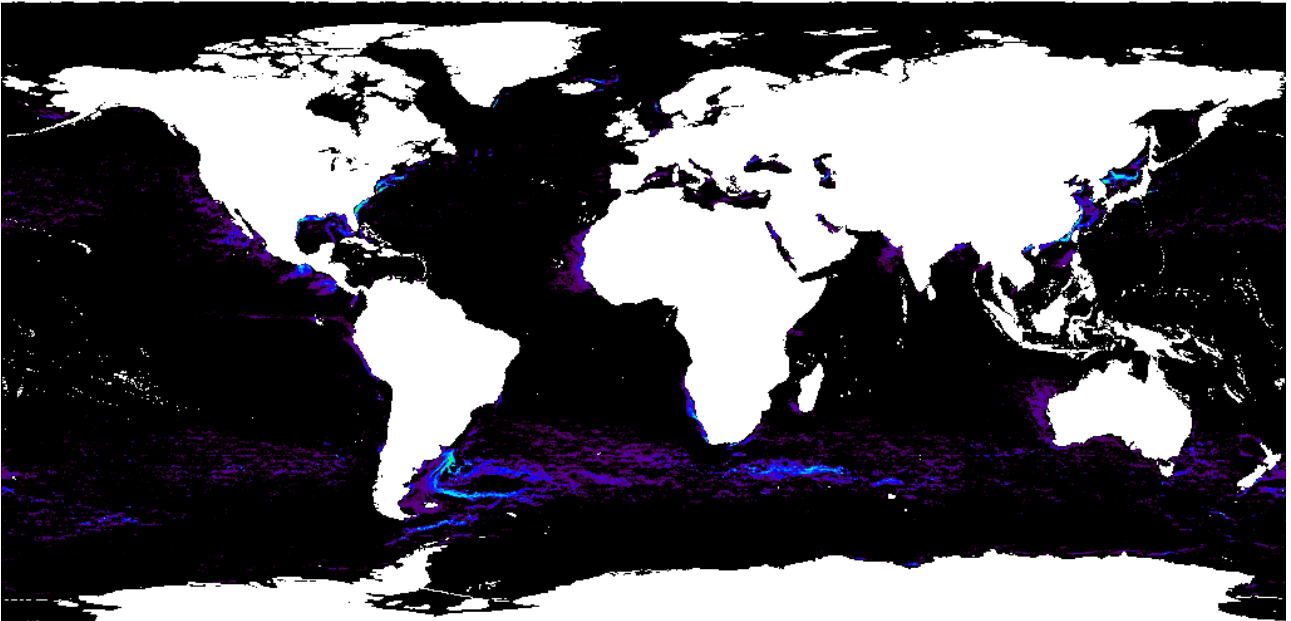


Dec

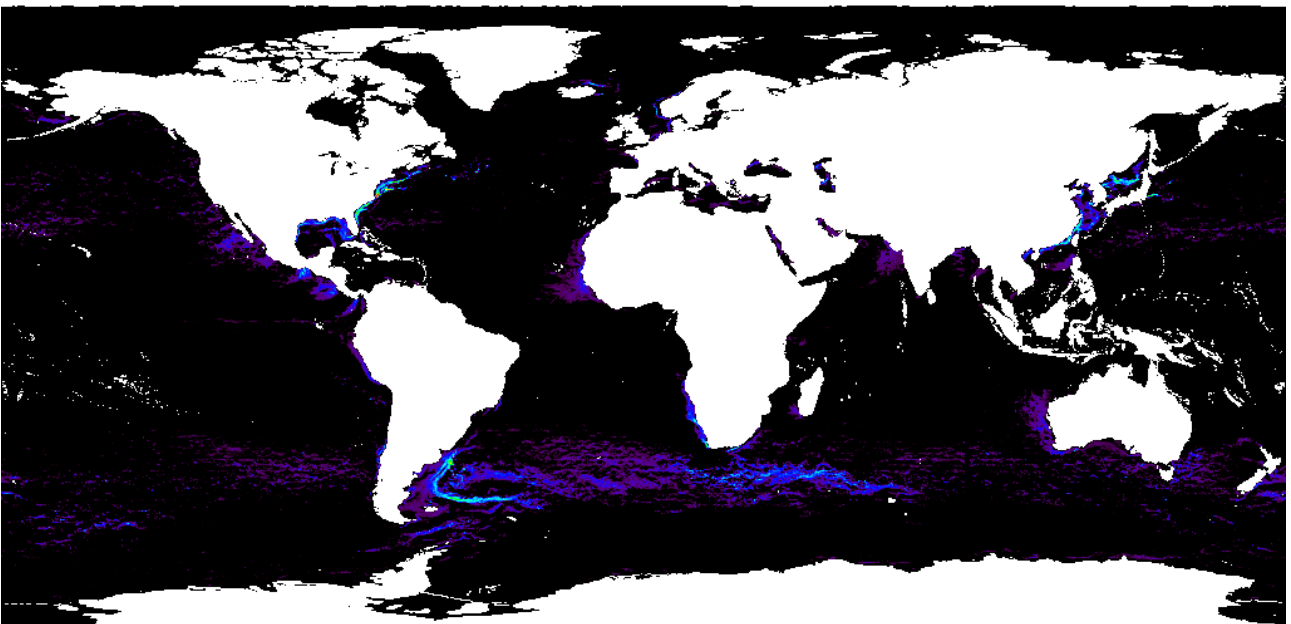


K/10km

## Appendix 3: URI max gradient fields thresholded at 15 % frequency



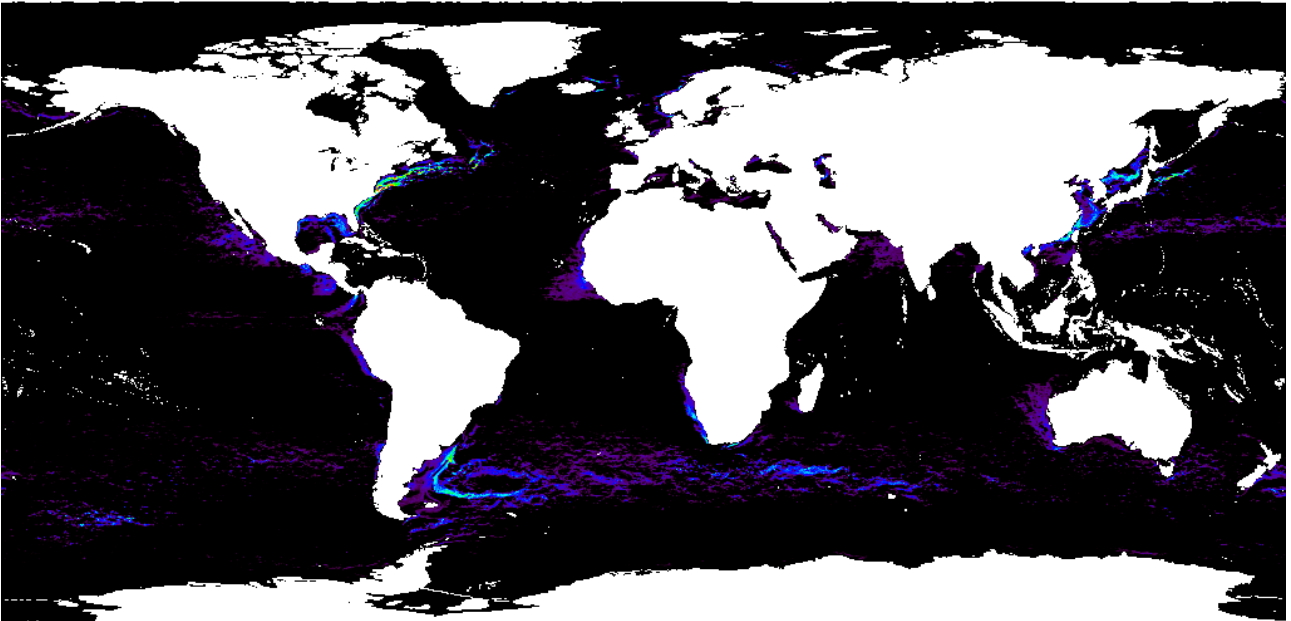
Jan



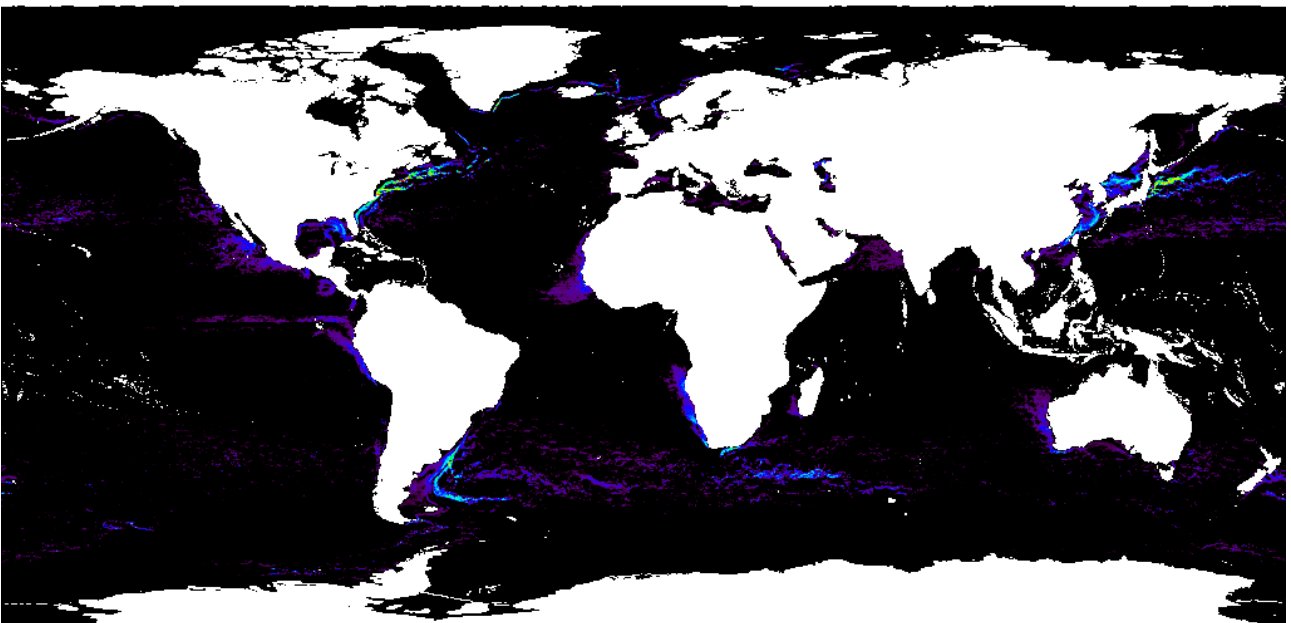
Feb



K/10km



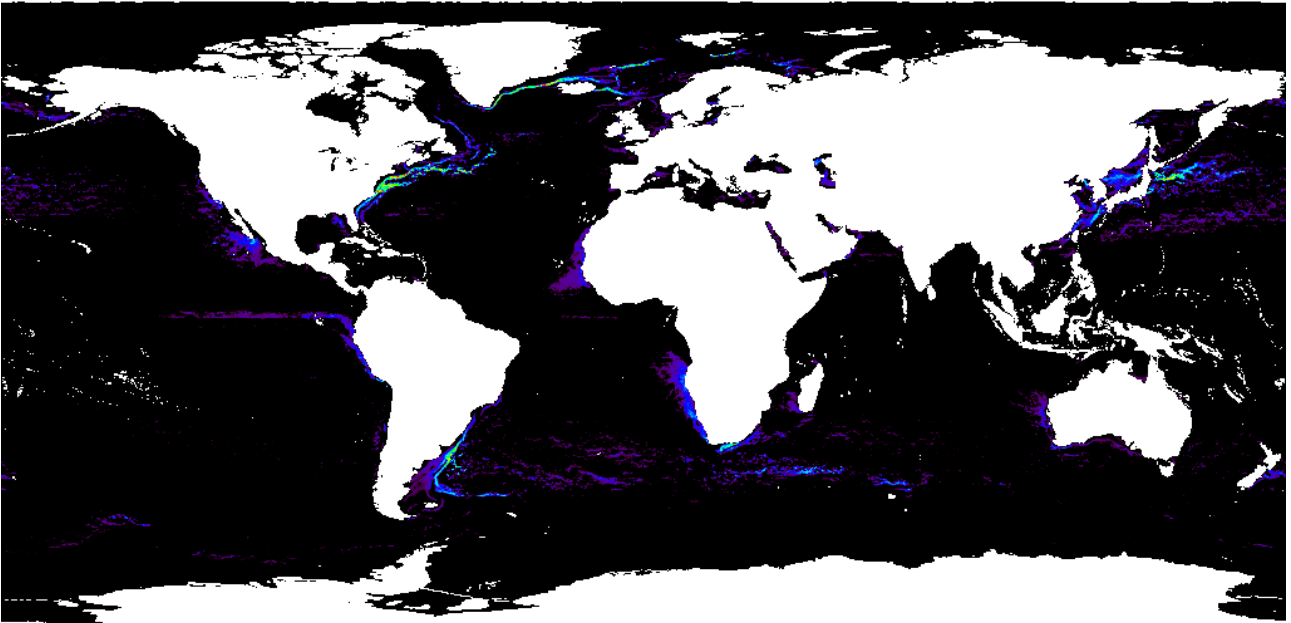
Mar



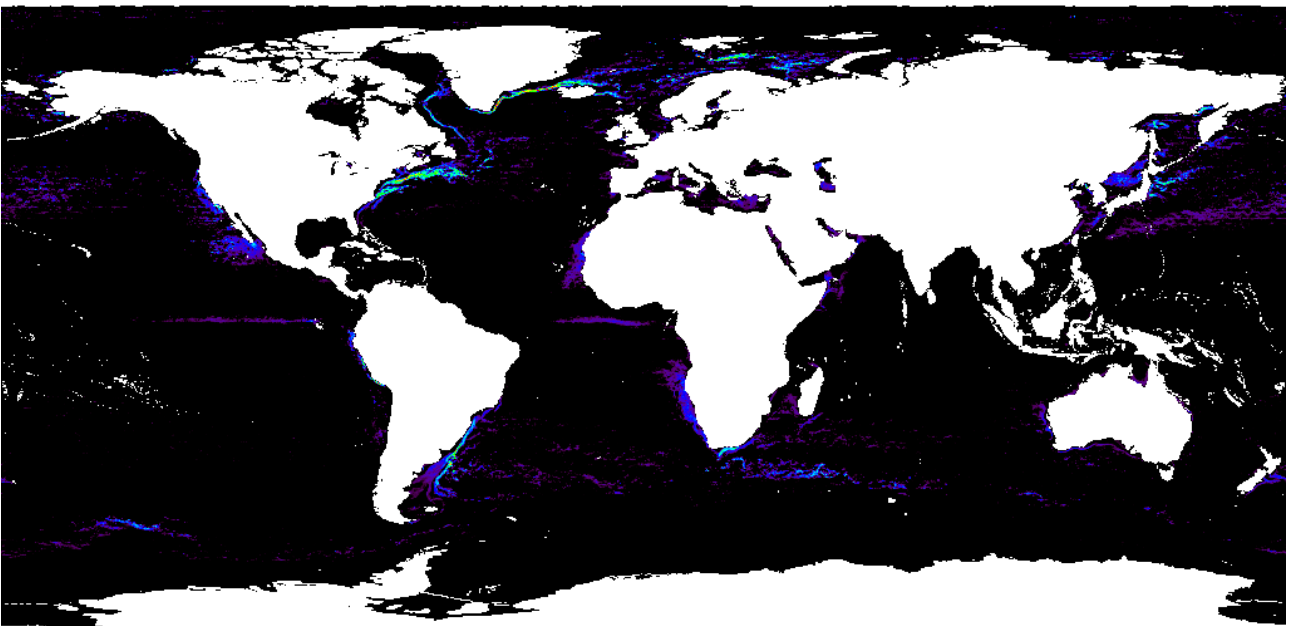
Apr



K/10km



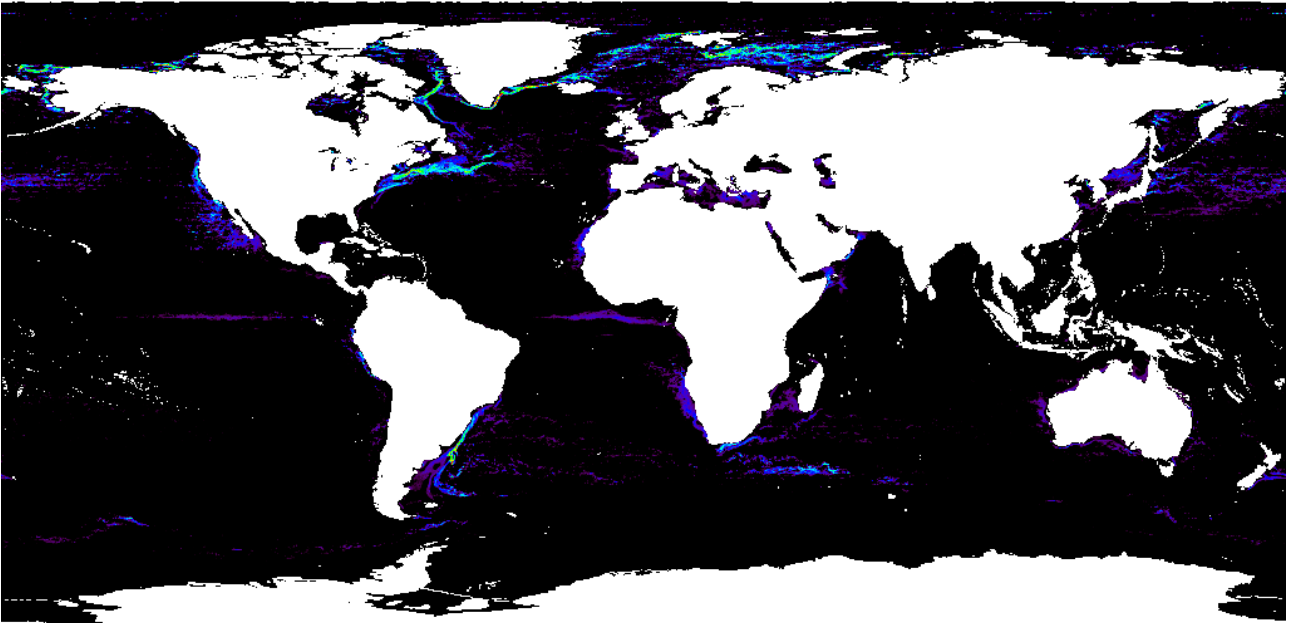
May



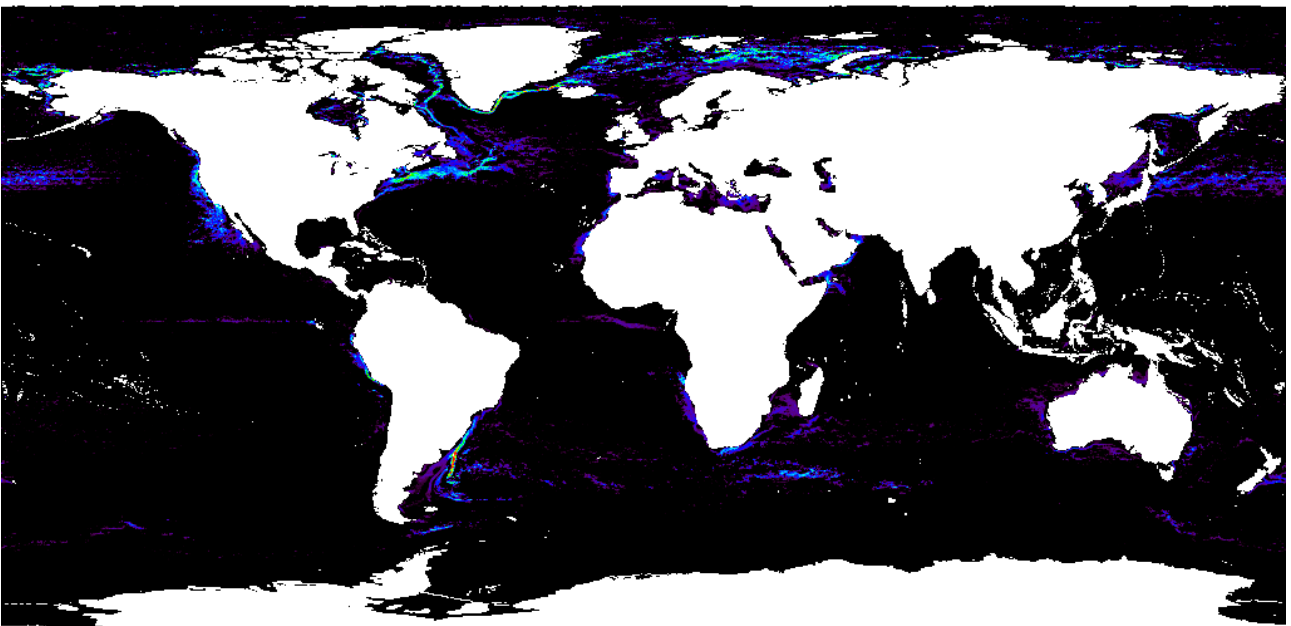
Jun



K/10km



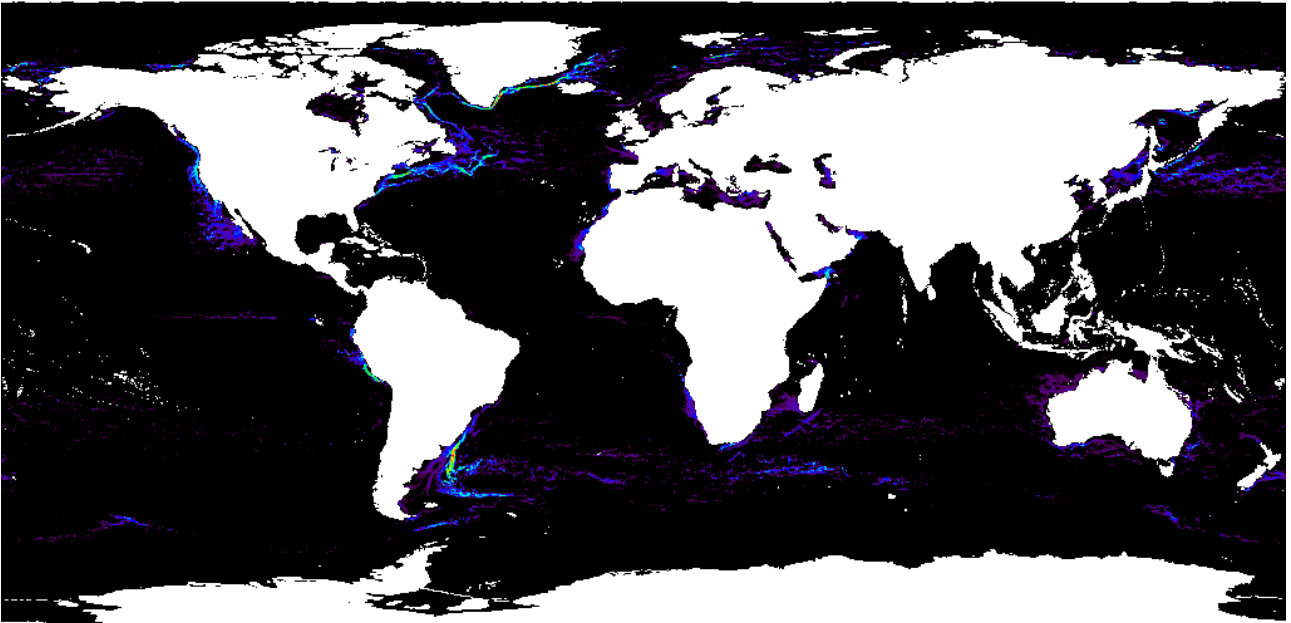
Jul



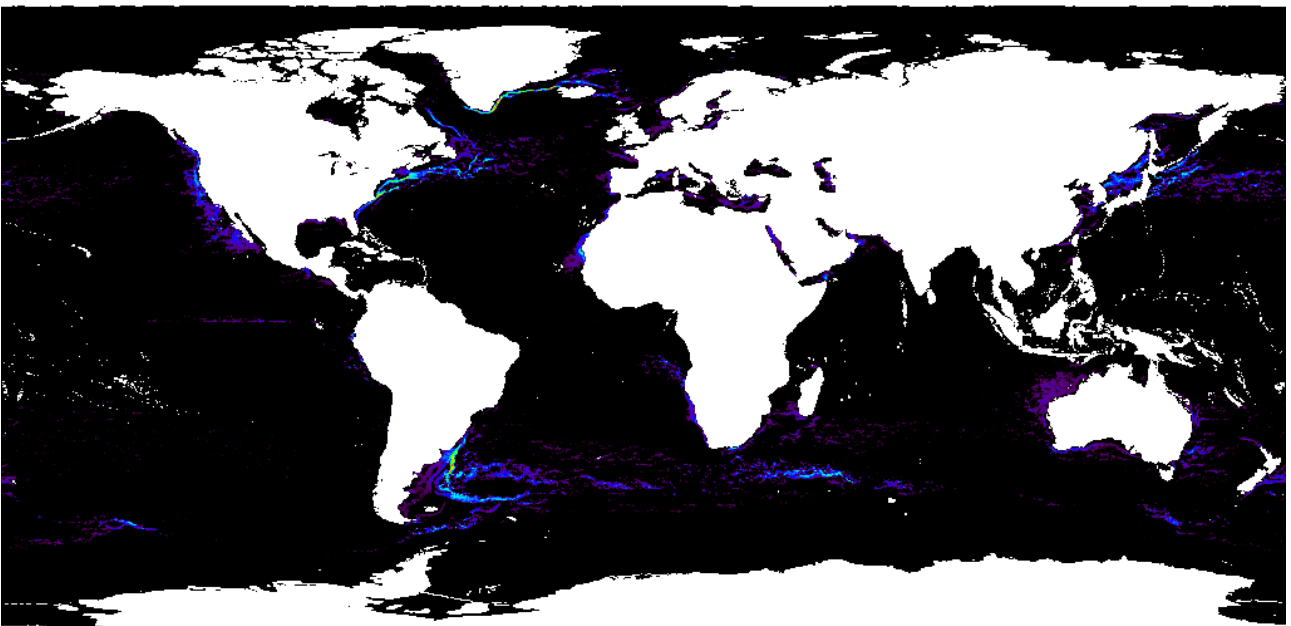
Aug



K/10km



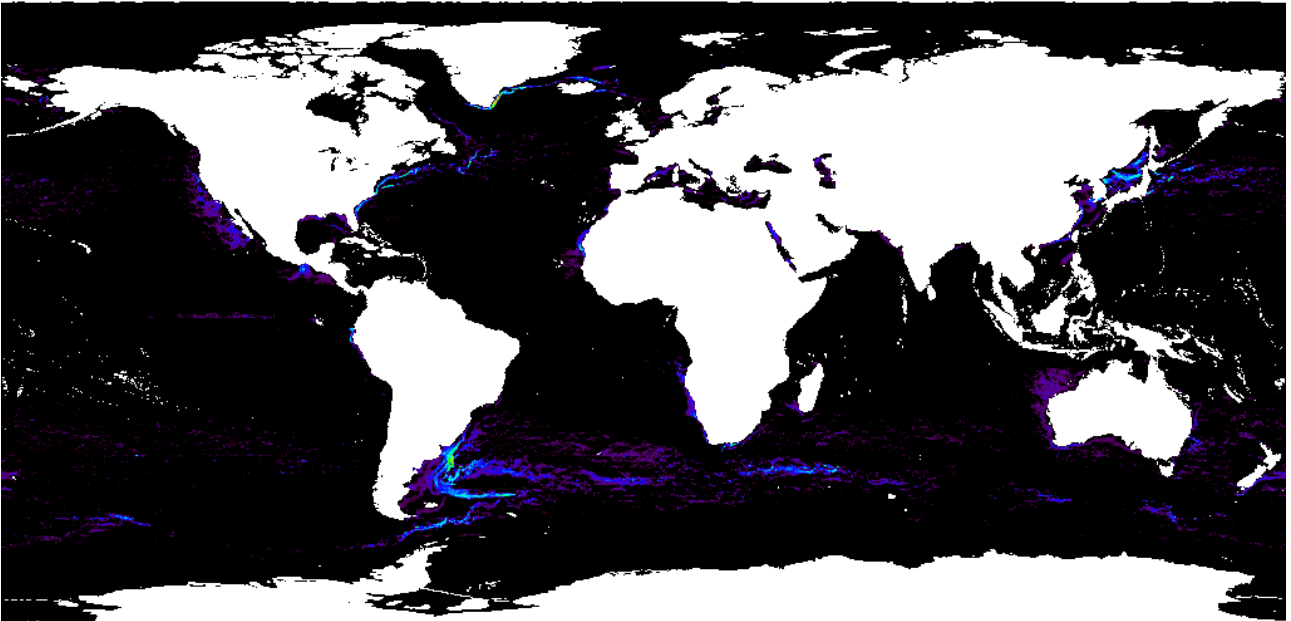
Sep



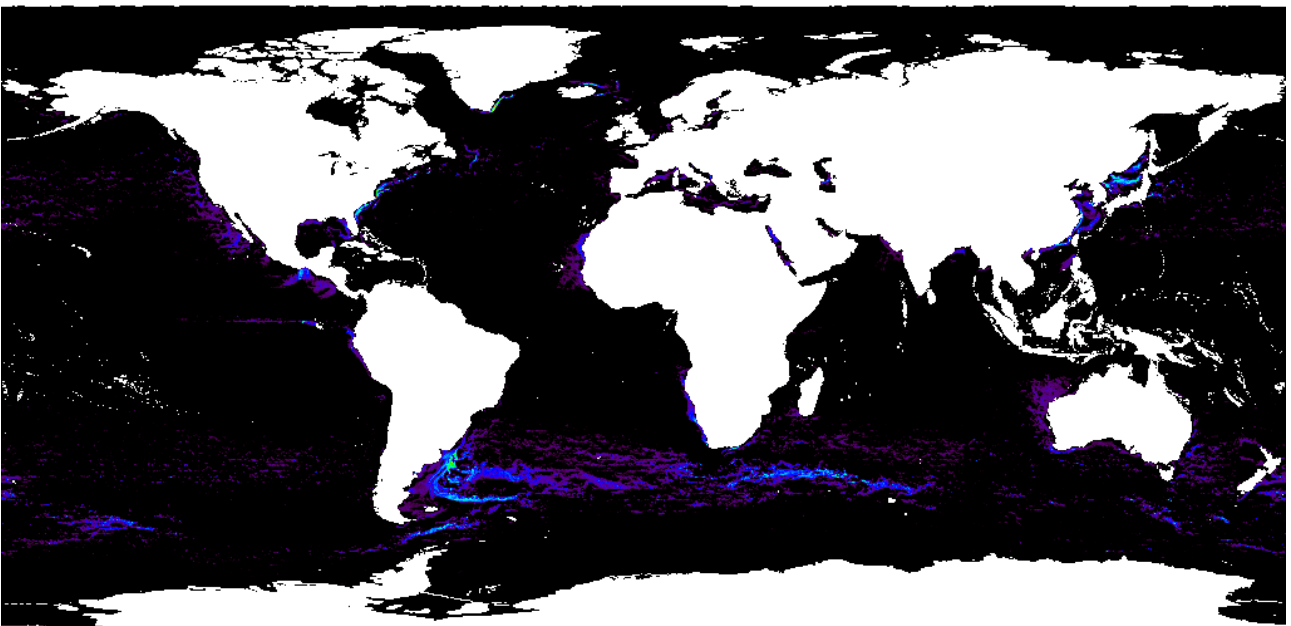
Oct



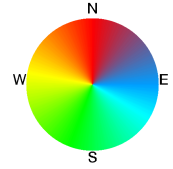
K/10km



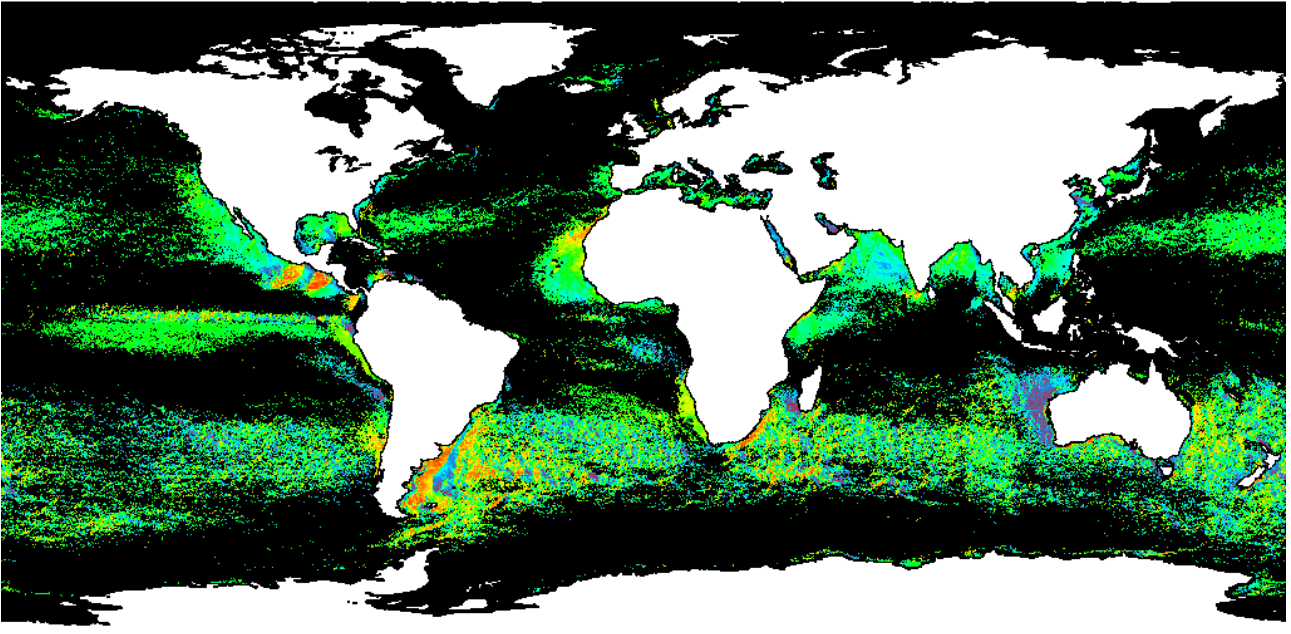
Nov



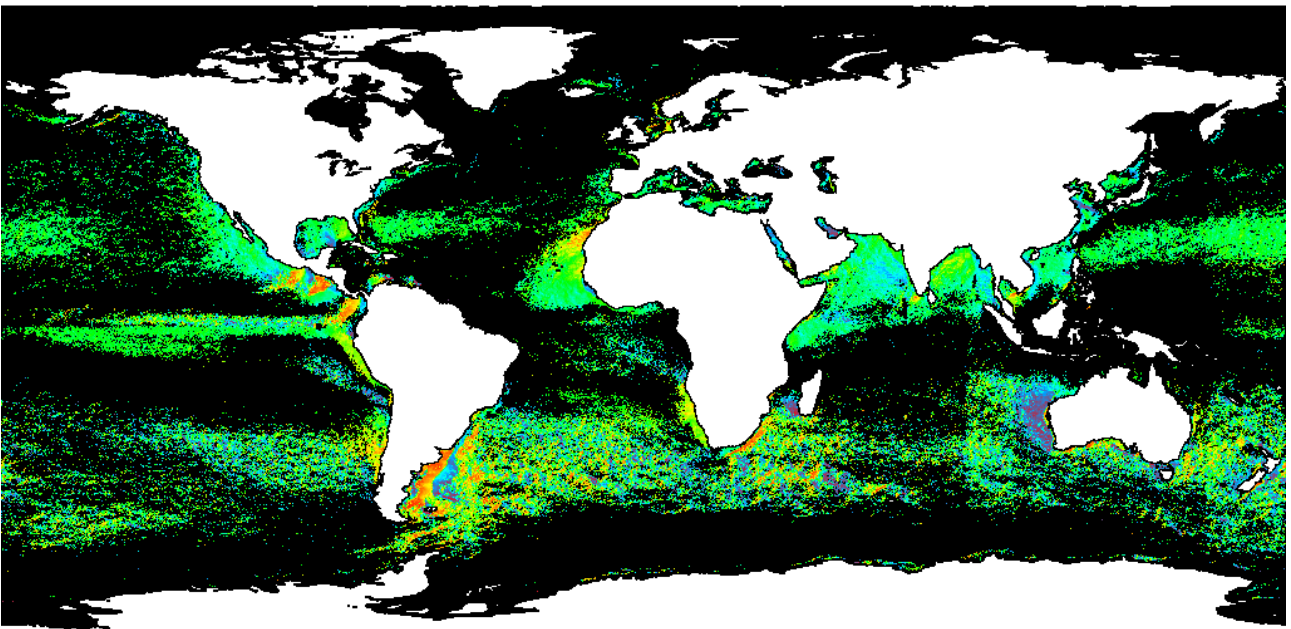
Dec



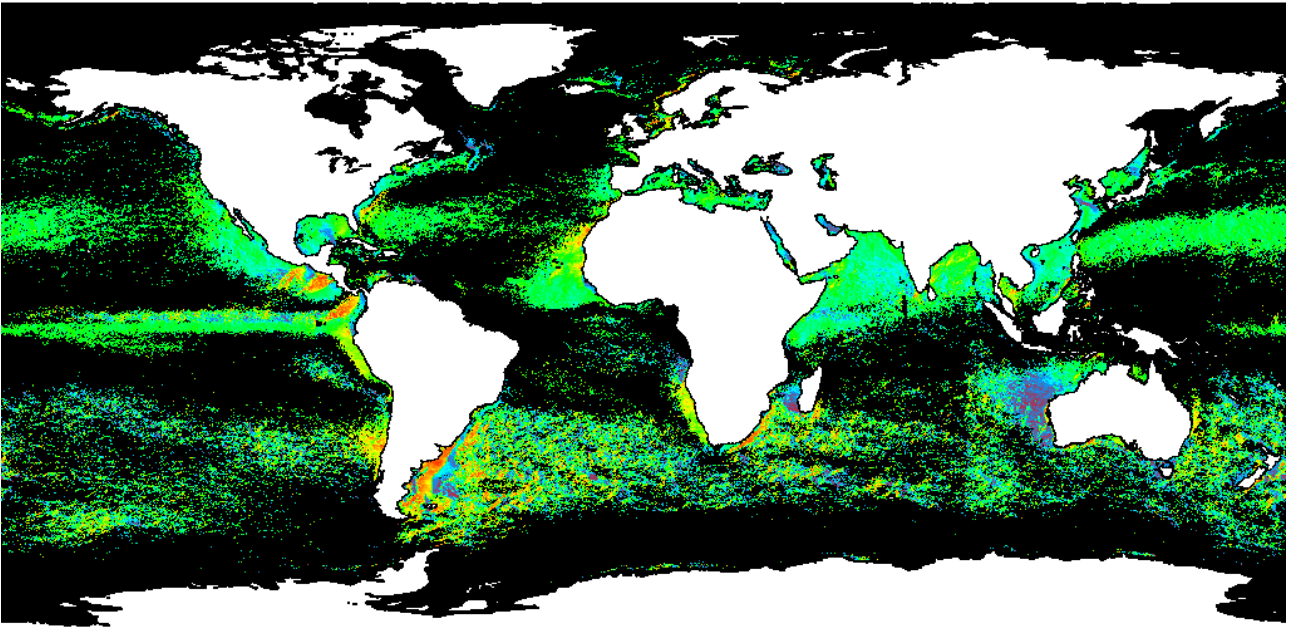
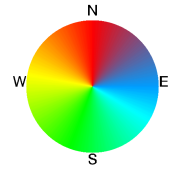
## Appendix 4 Original monthly gradient direction fields



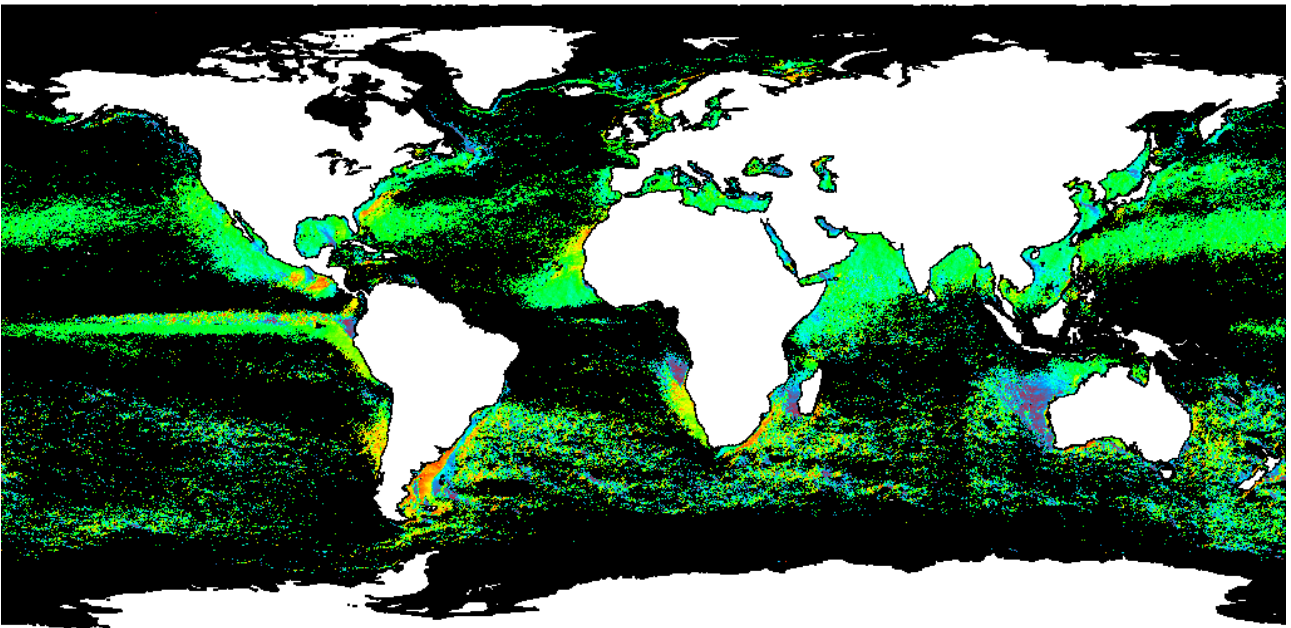
Jan



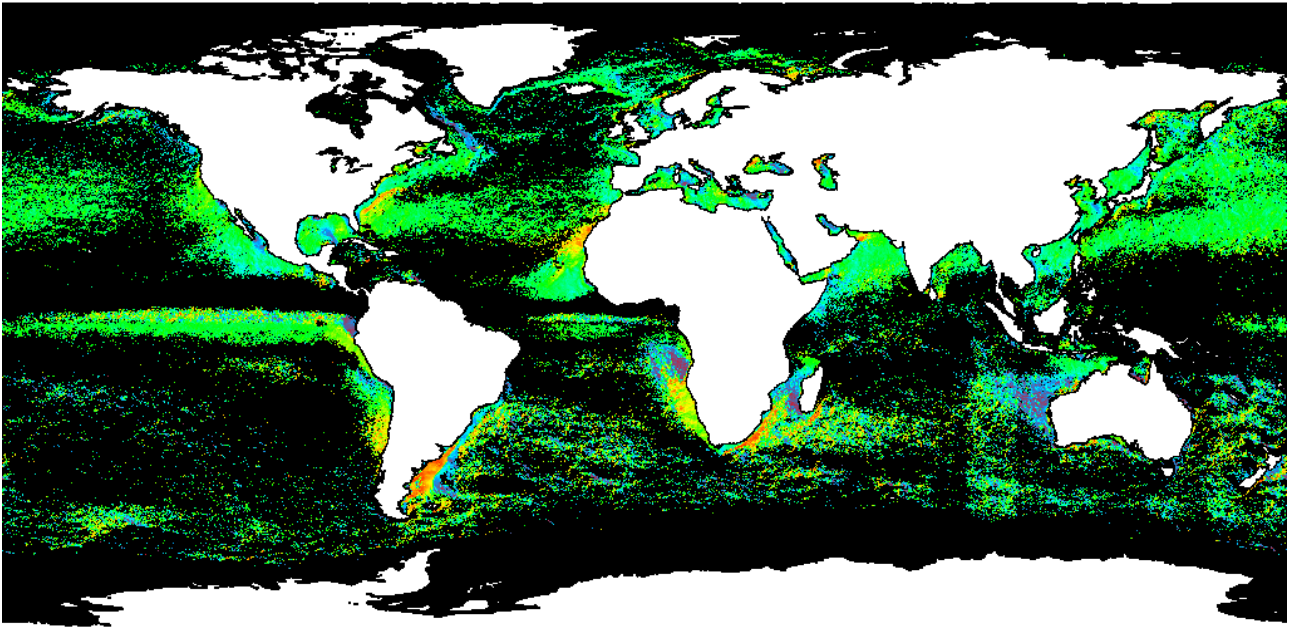
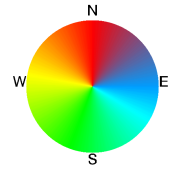
Feb



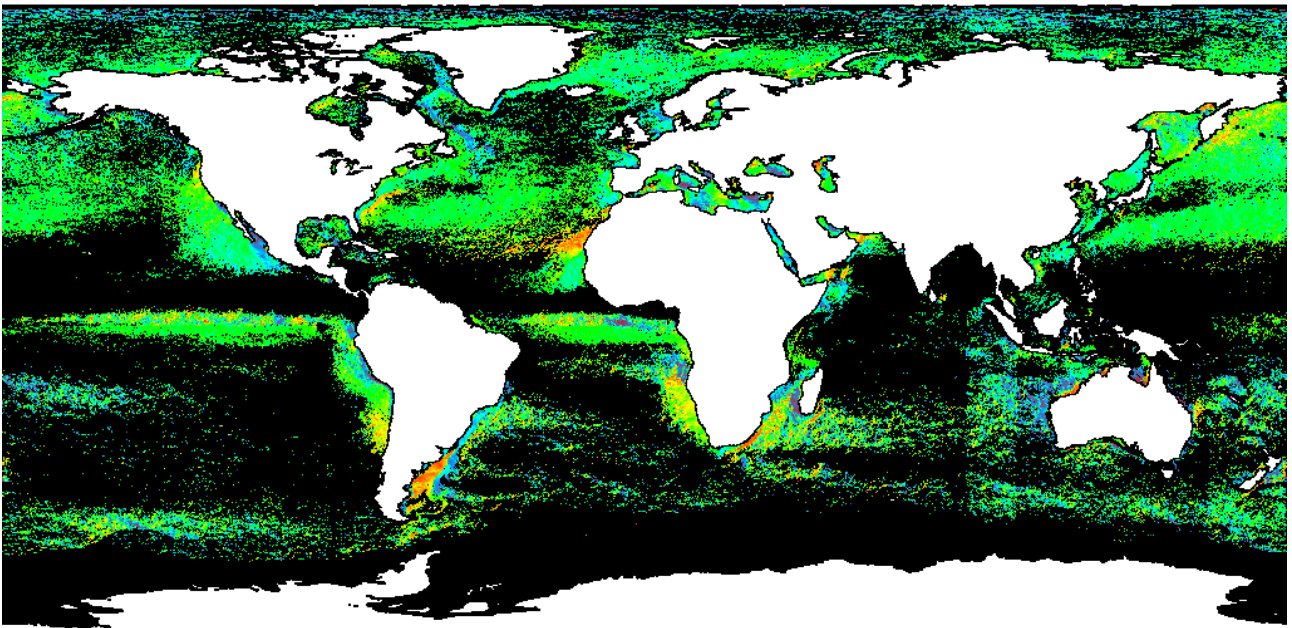
Mar



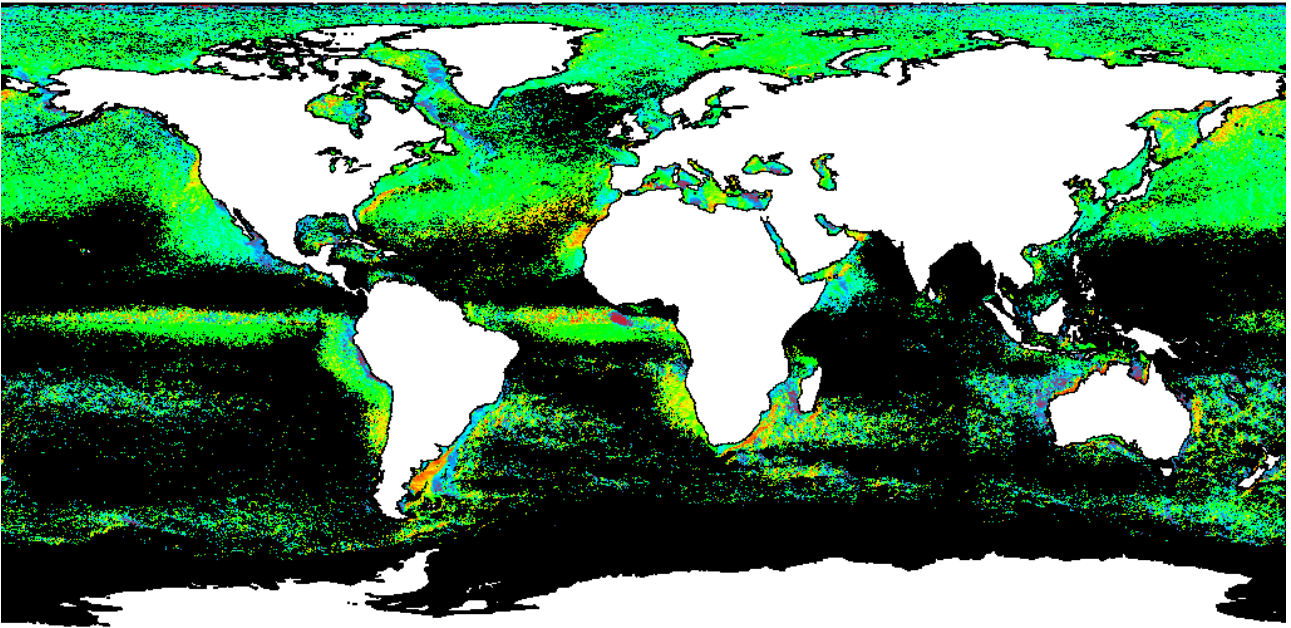
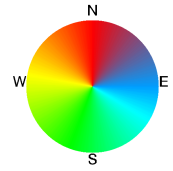
Apr



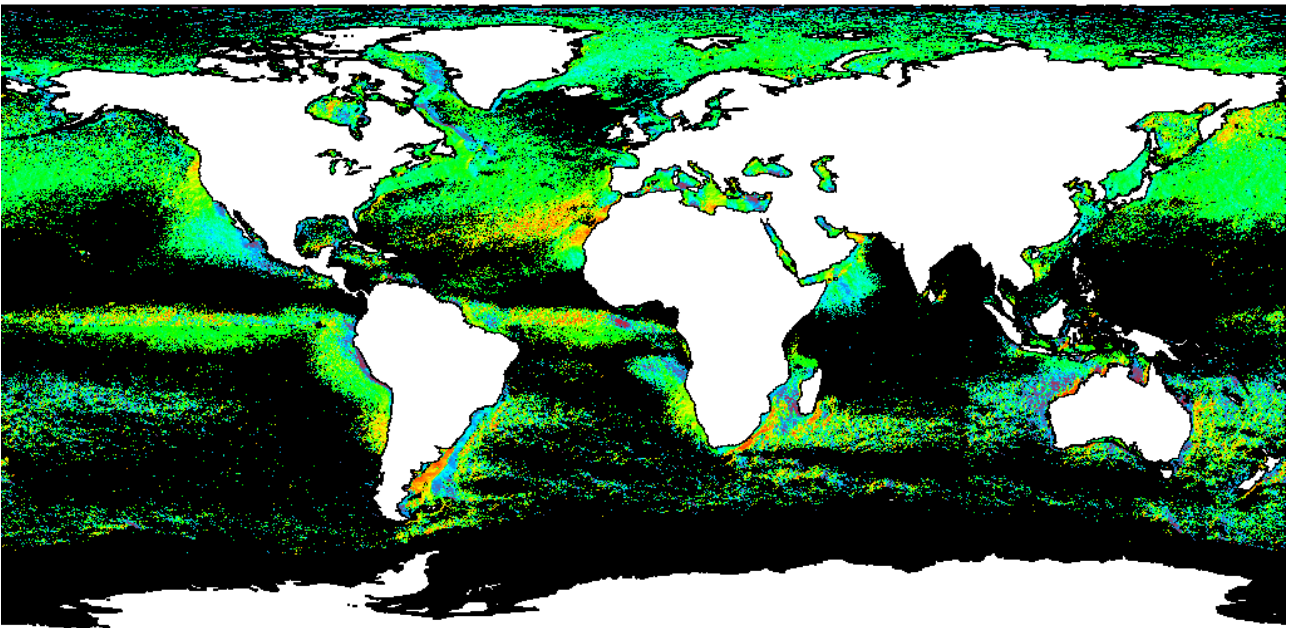
May



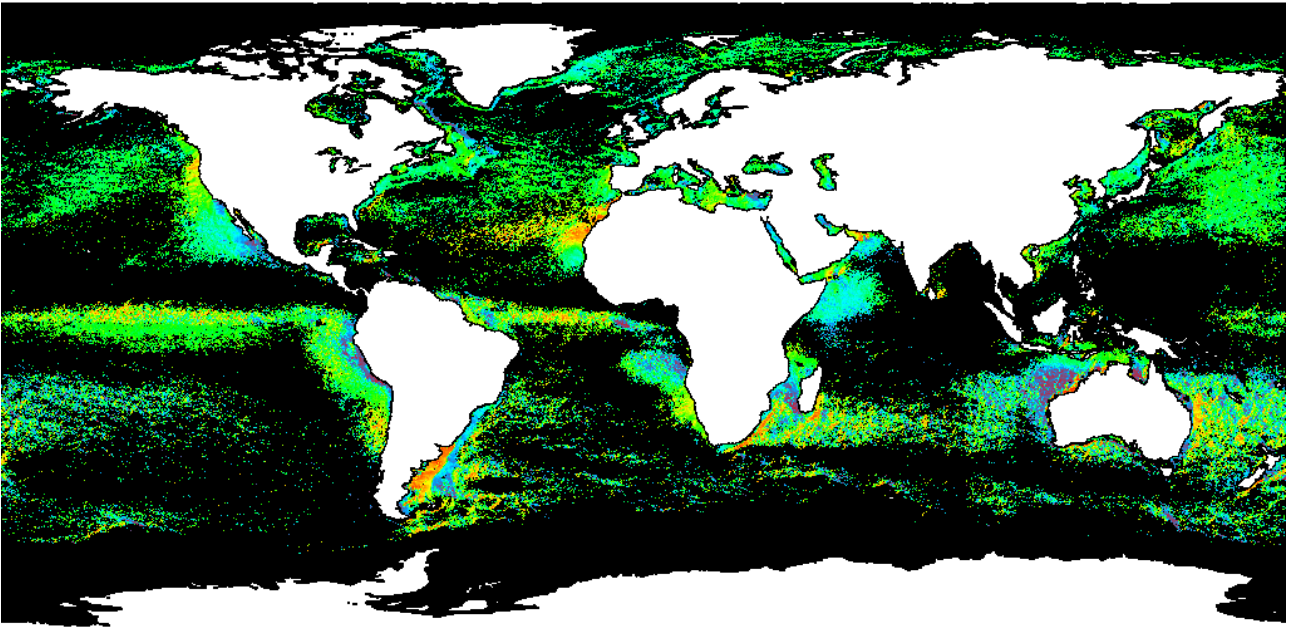
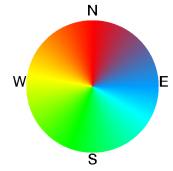
Jun



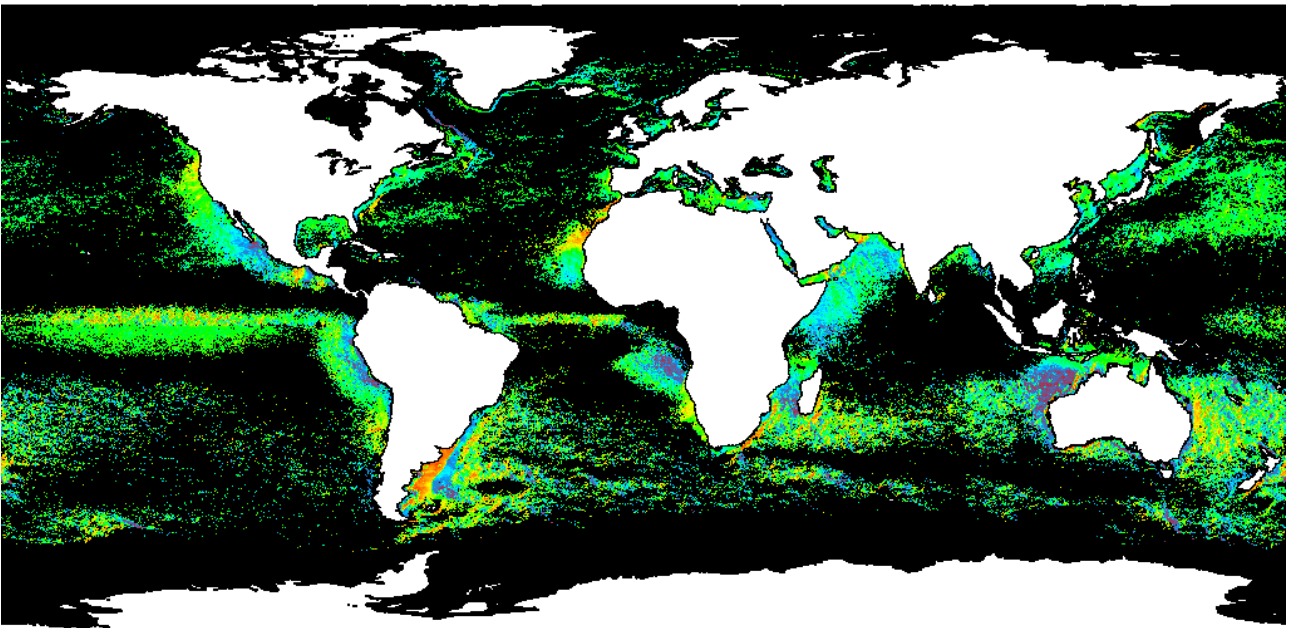
Jul



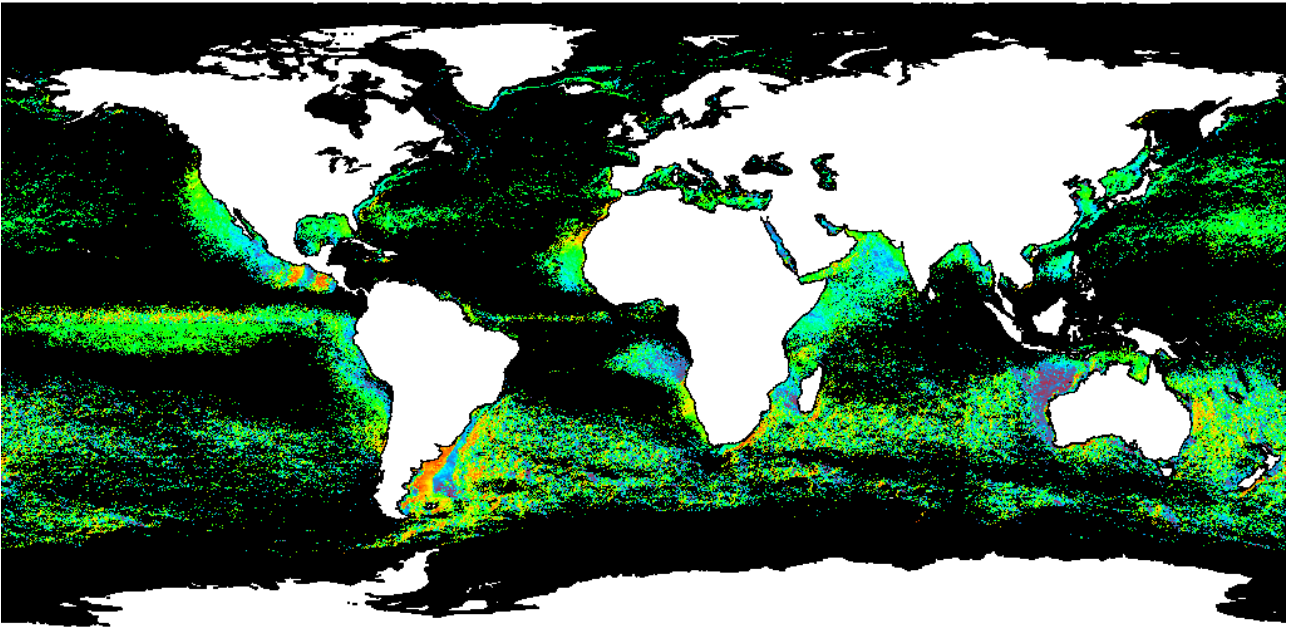
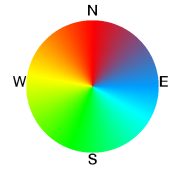
Aug



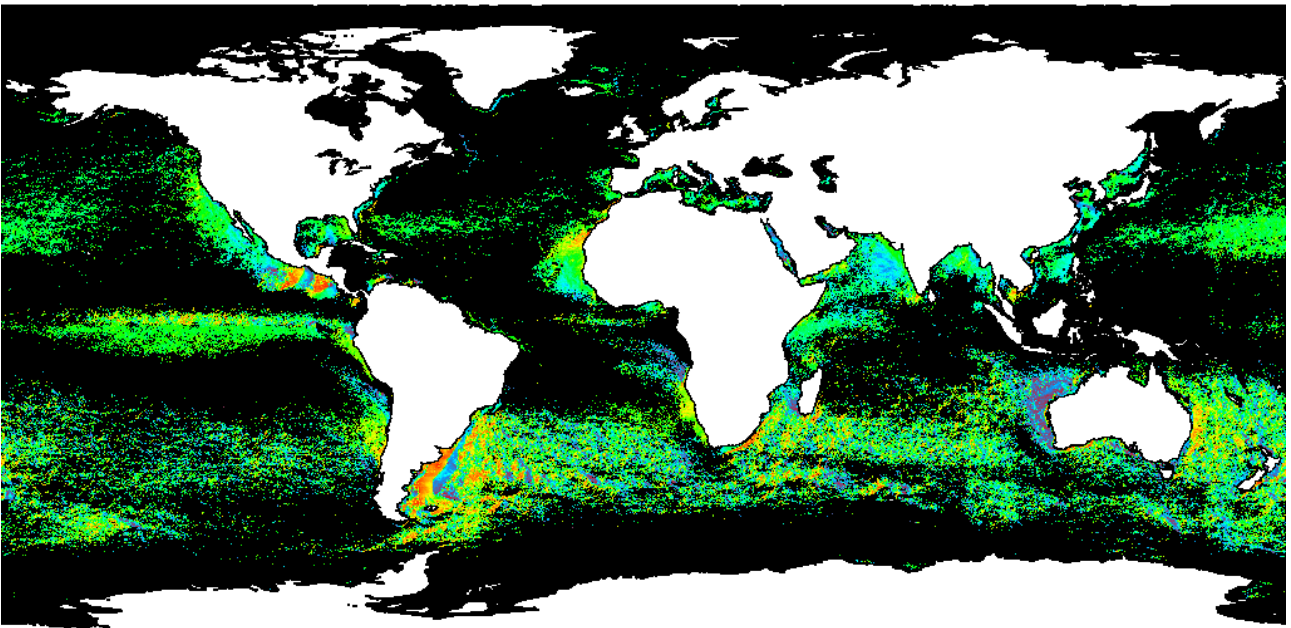
Sep



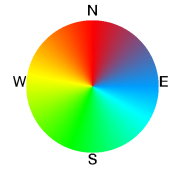
Oct



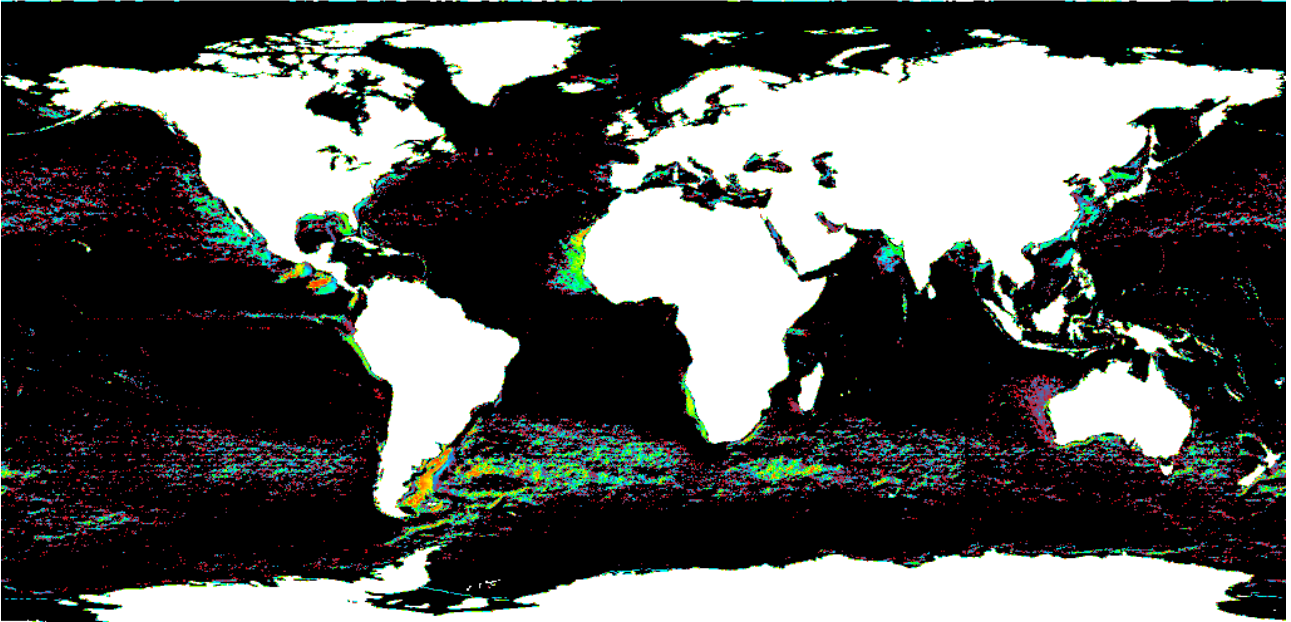
Nov



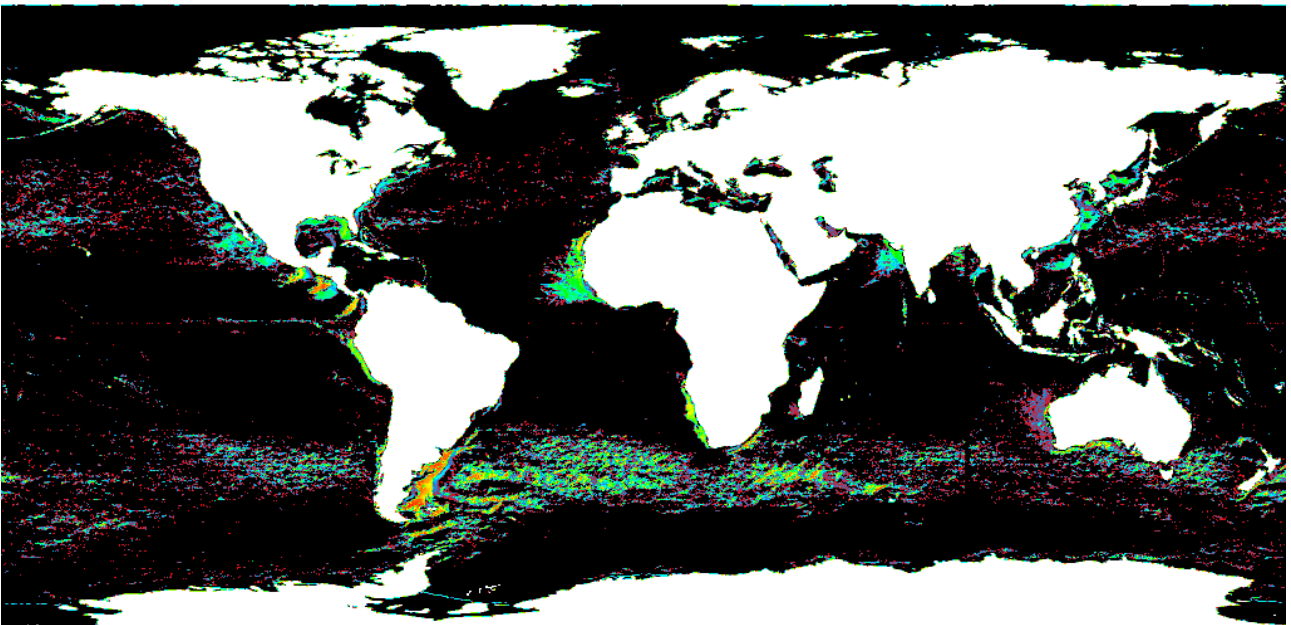
Dec



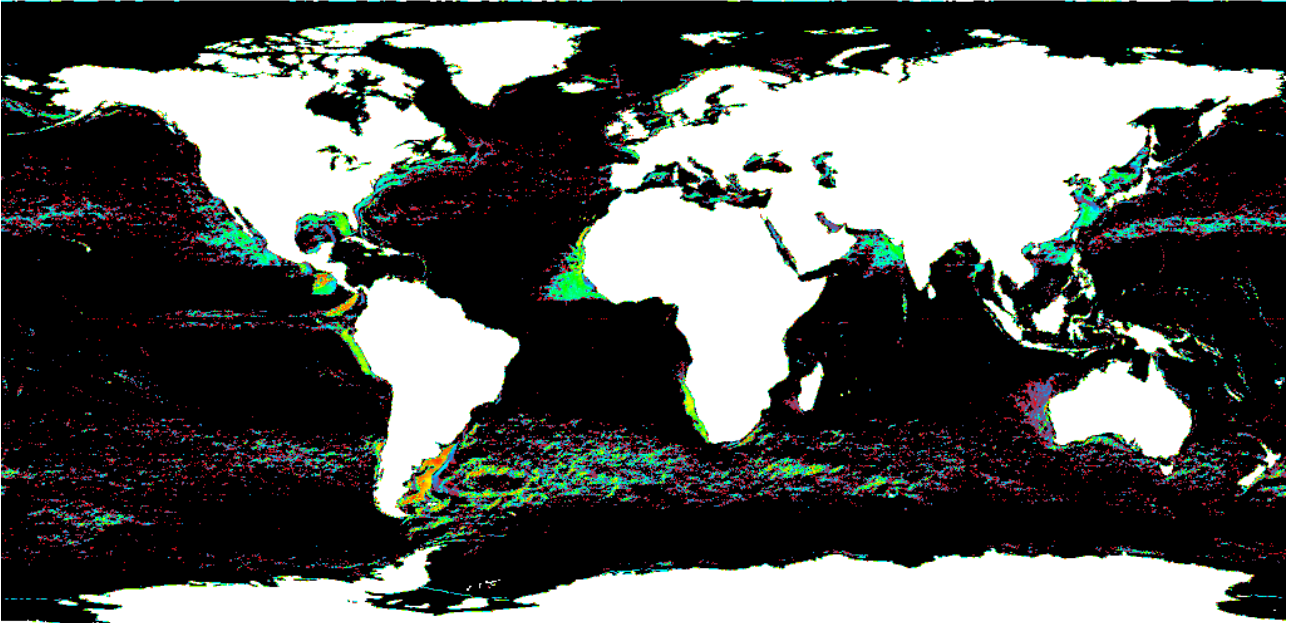
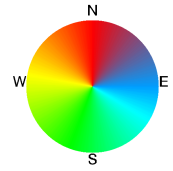
## Appendix 5 Gradient direction fields thresholded at 15% frequency



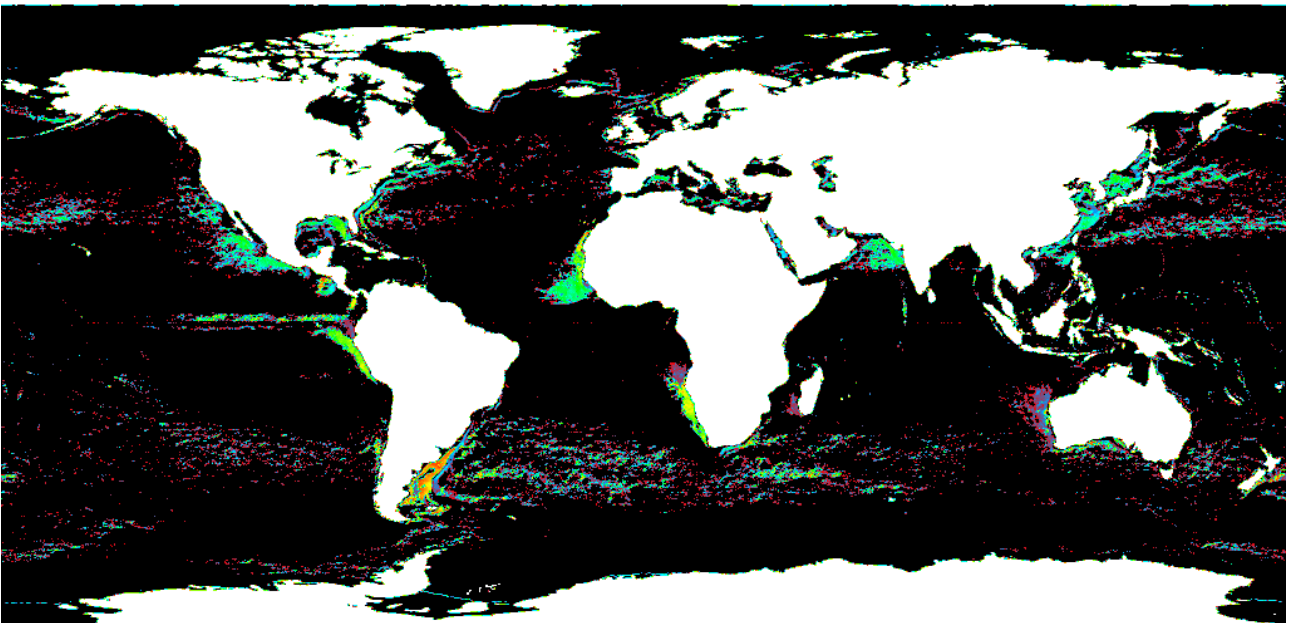
Jan



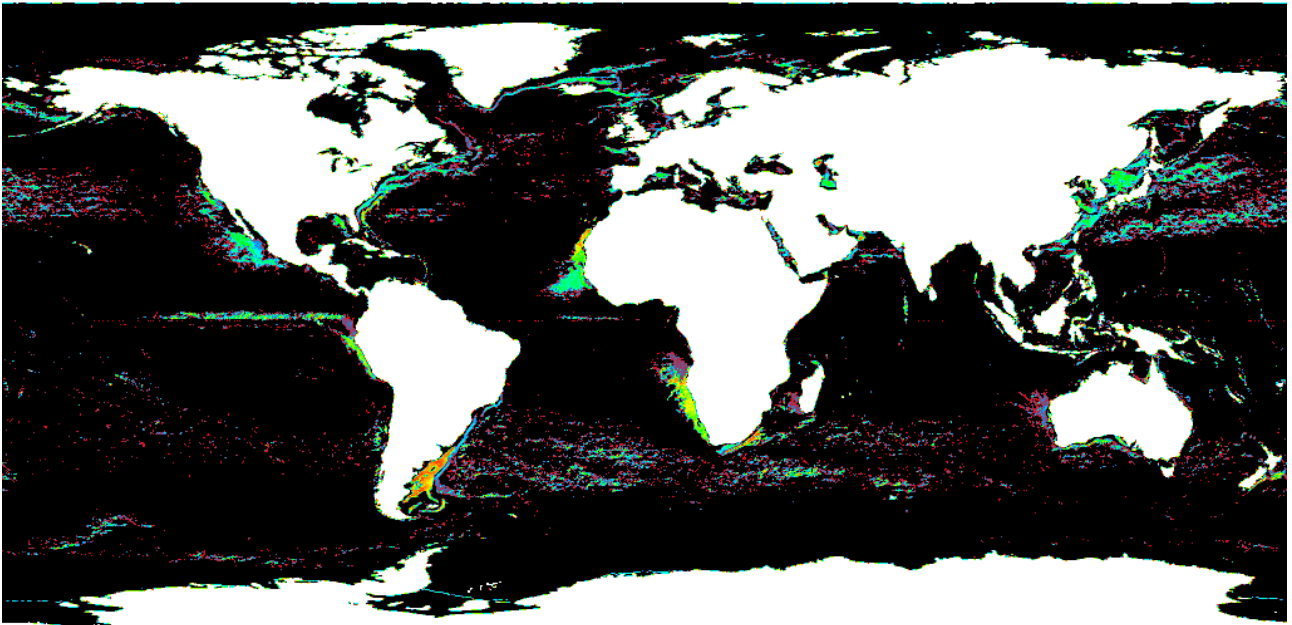
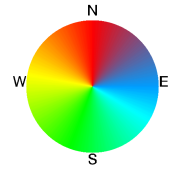
Feb



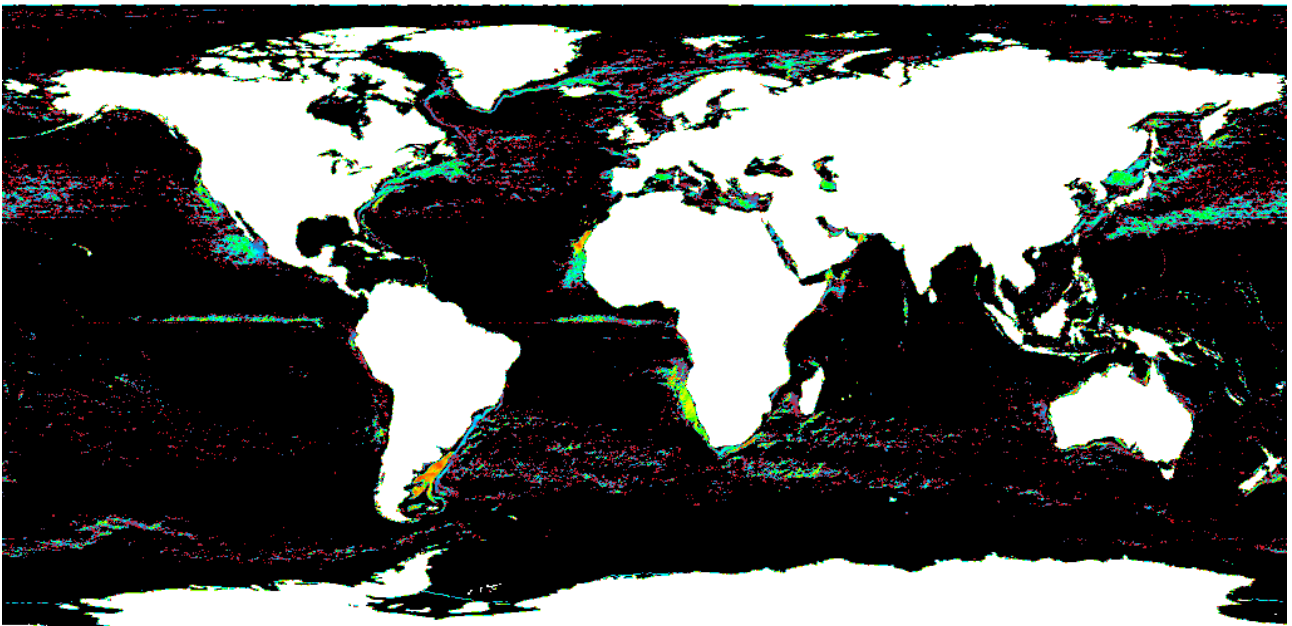
Mar



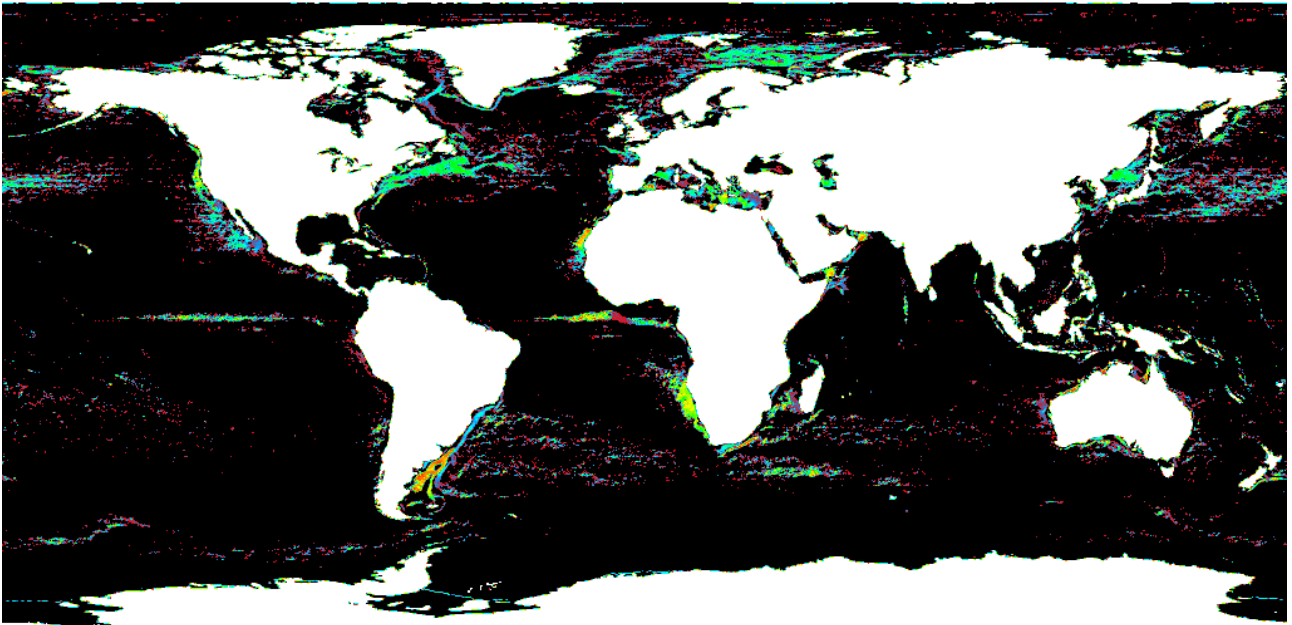
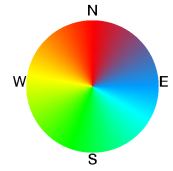
Apr



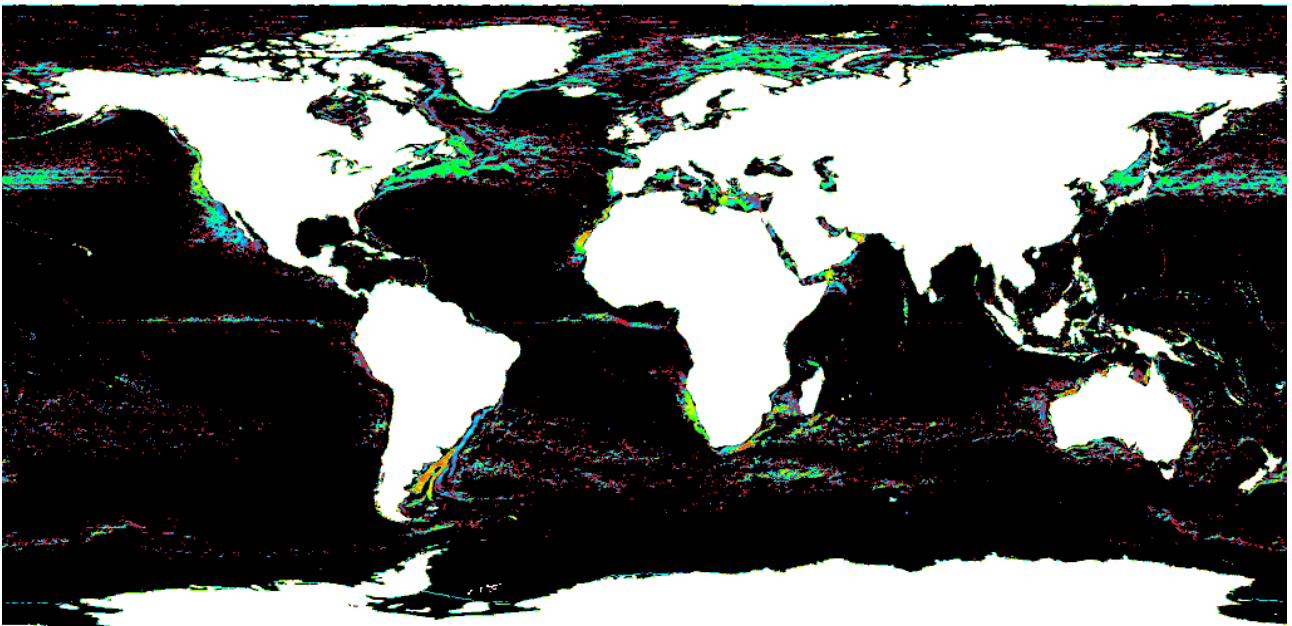
May



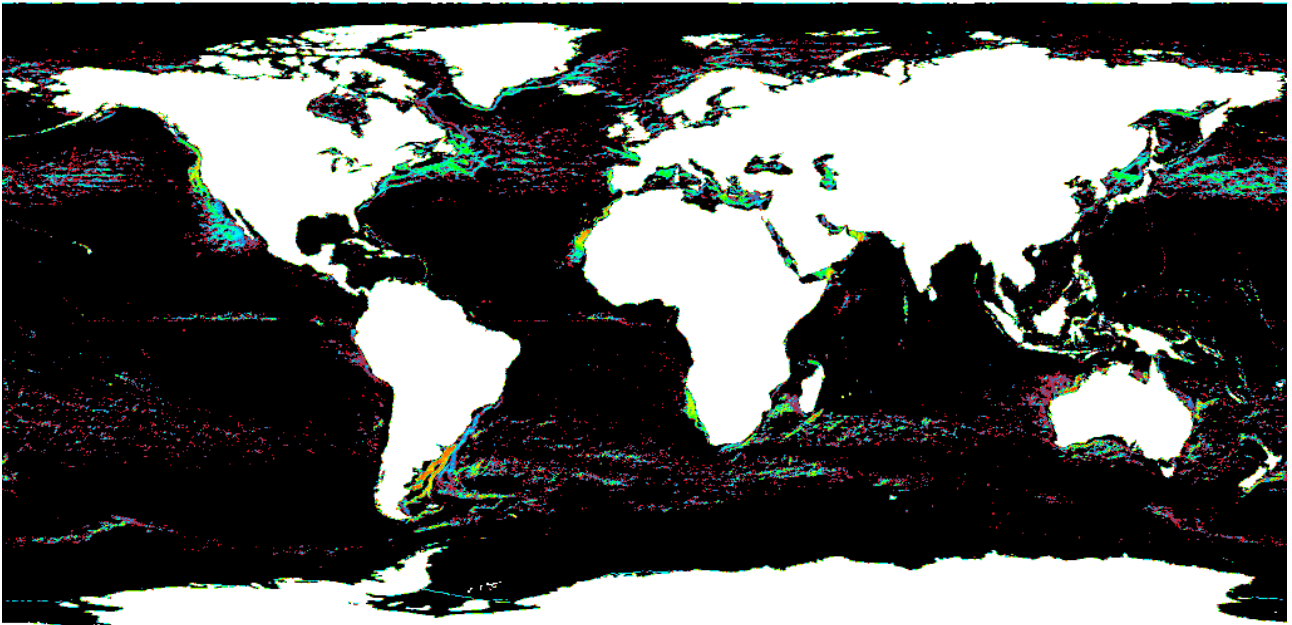
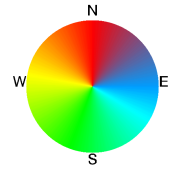
Jun



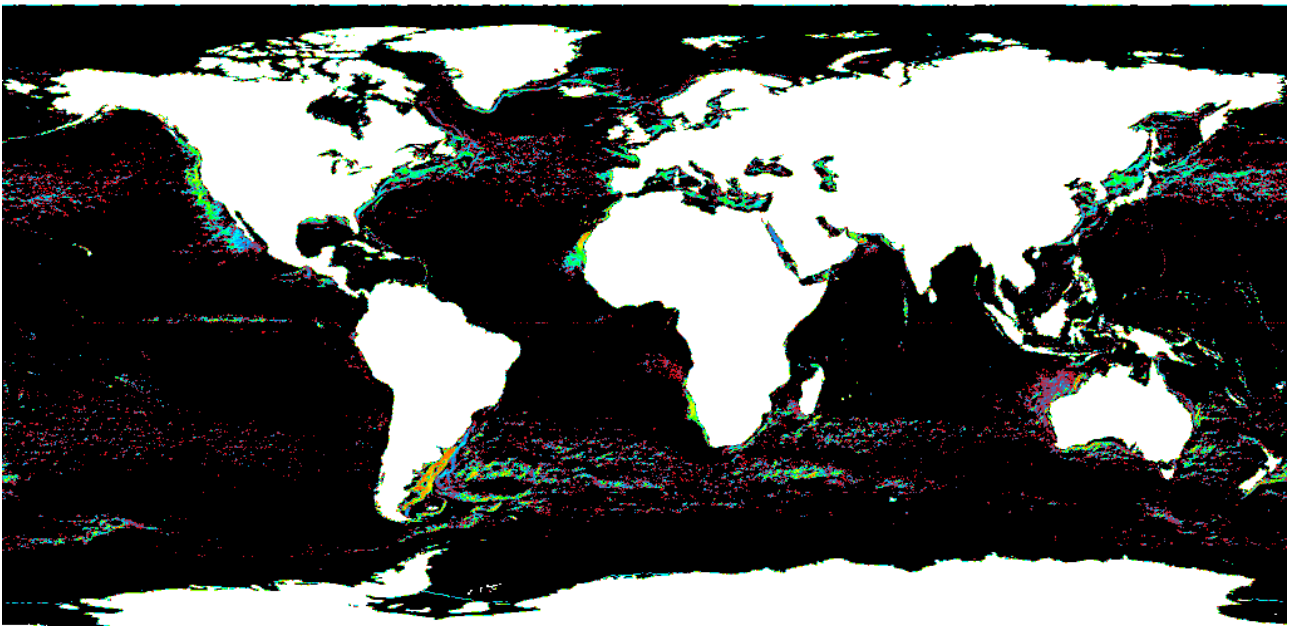
Jul



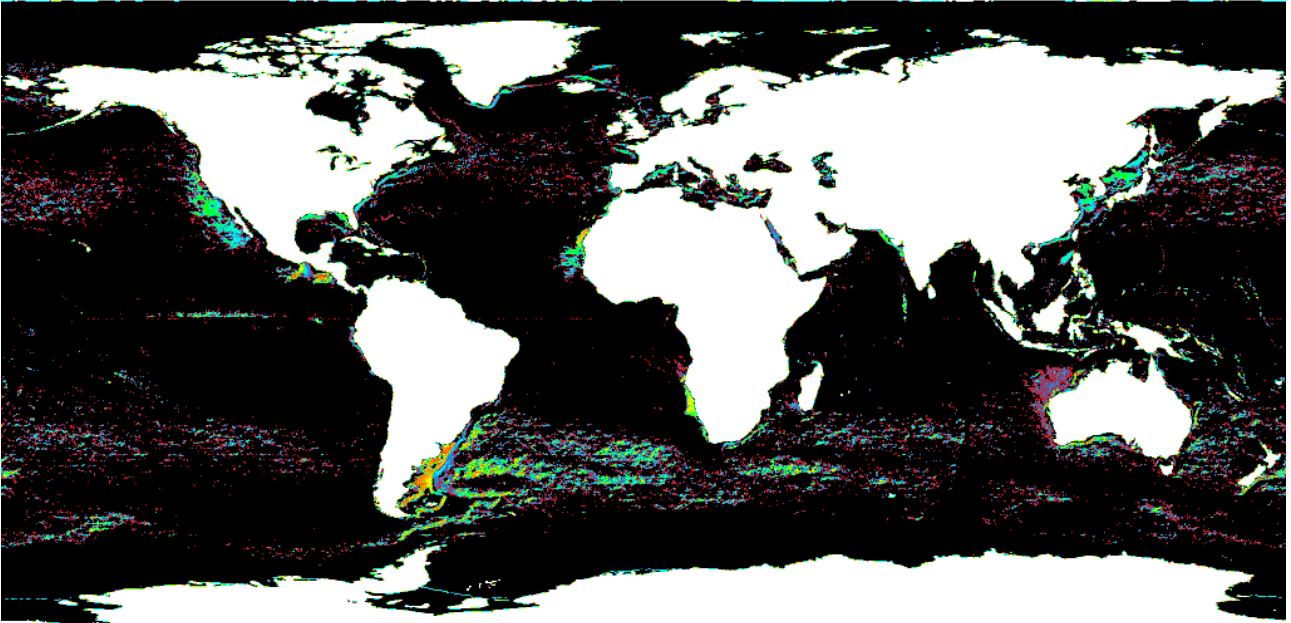
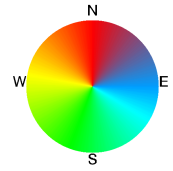
Aug



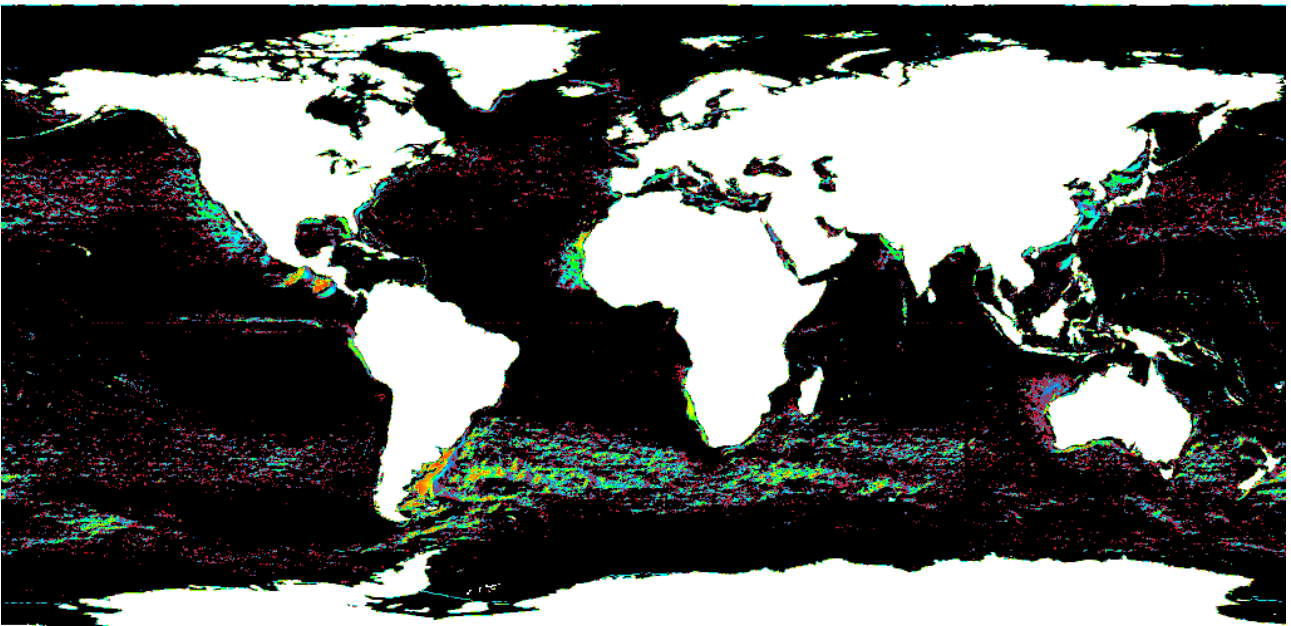
Sep



Oct



Nov



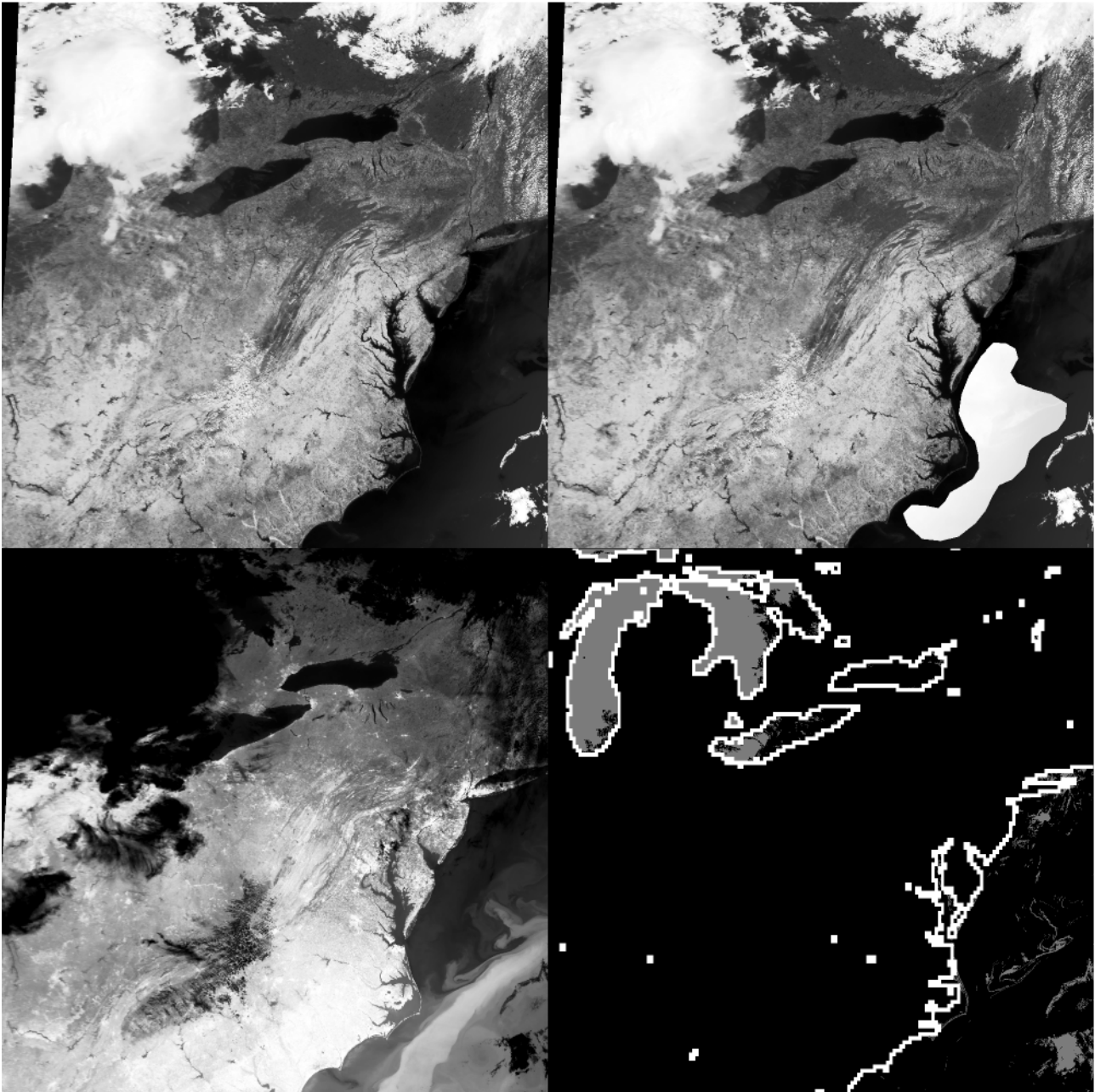
Dec



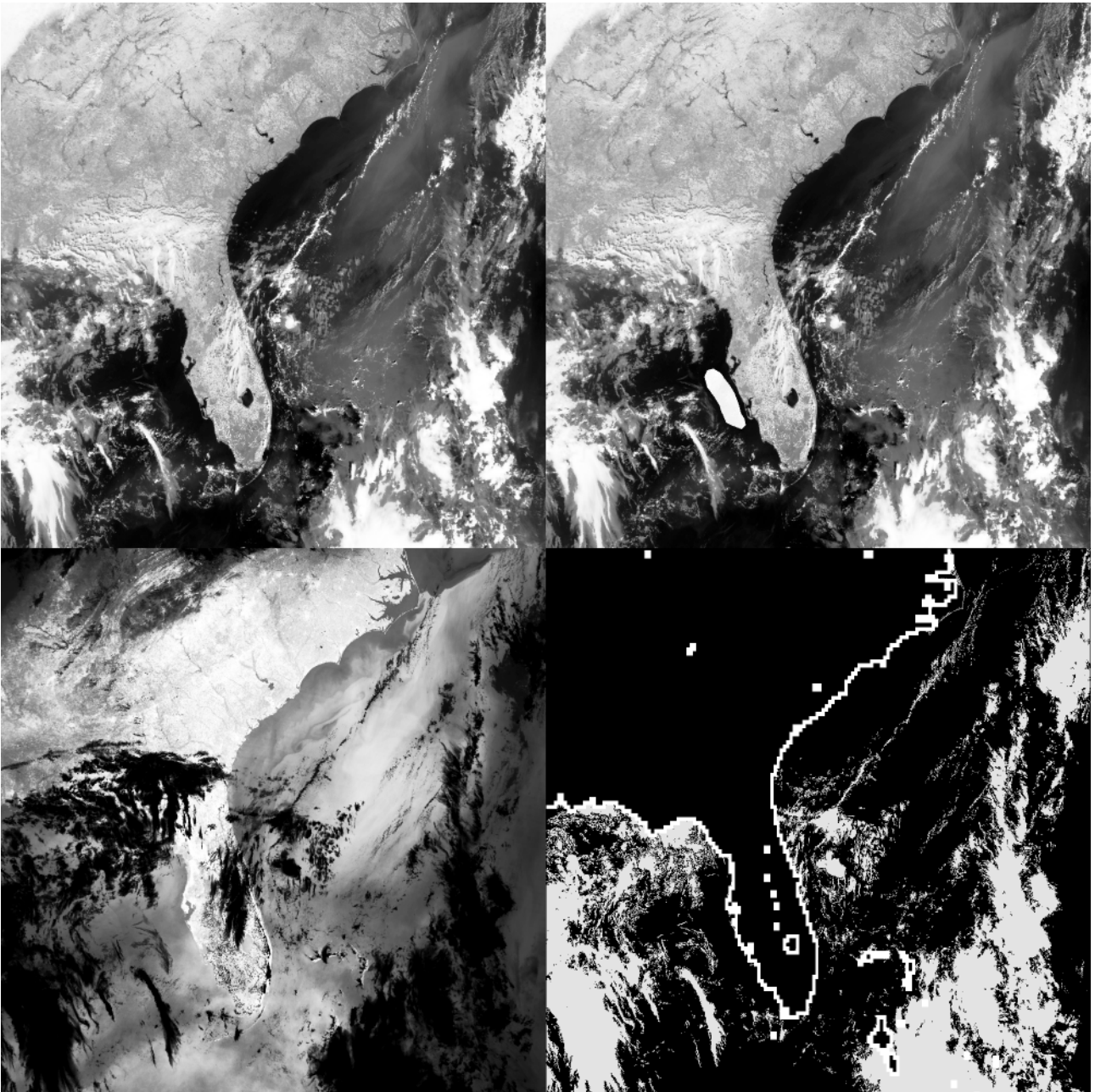
## Appendix 6: Validation data

In the following, the AVHRR scenes used for validating the procedure are presented. Images are top-left: channel 2; top-right: channel 2 with cloud free region of interest; bottom-left: channel 4; bottom-right: MAIA Marine Clear classification. Scene names refer to Table 3.

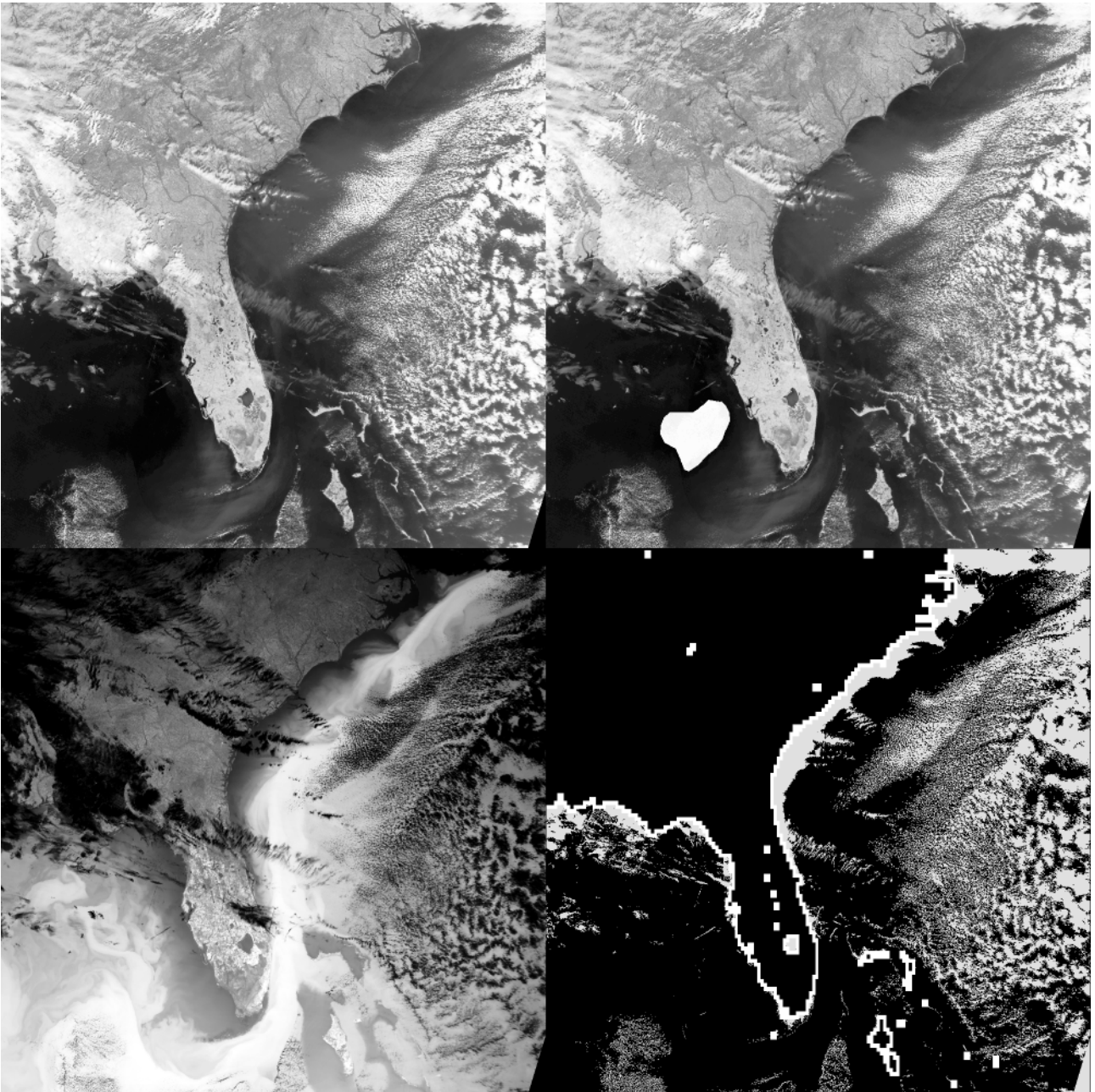
### US East Coast



NSS.HRPT.NM.D04127.S1531.E1544.B0970000.W1L9827021\_ec



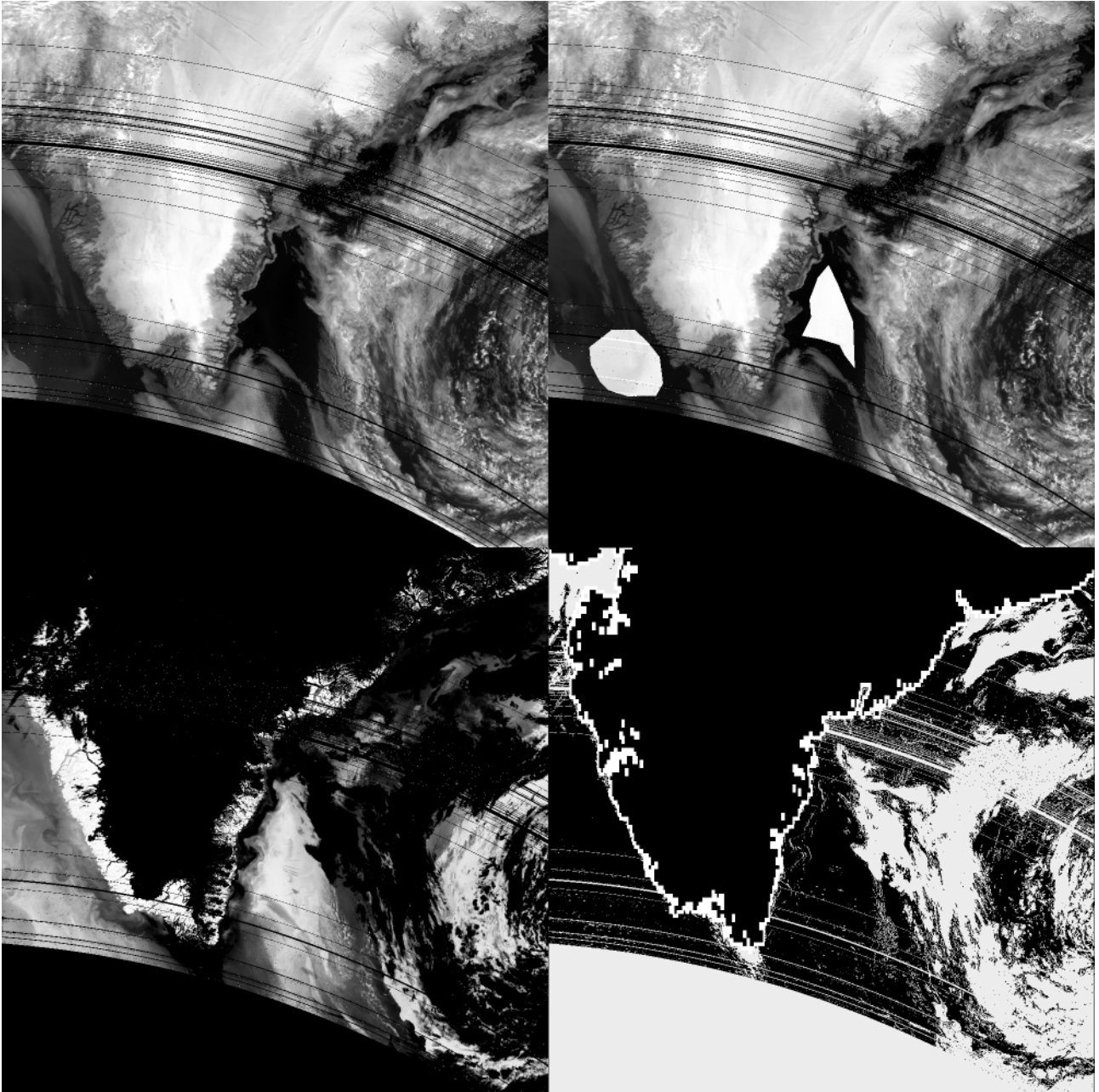
NSS.HRPT.NM.D03262.S1544.E1558.B0642828.WI.L9827001\_ec

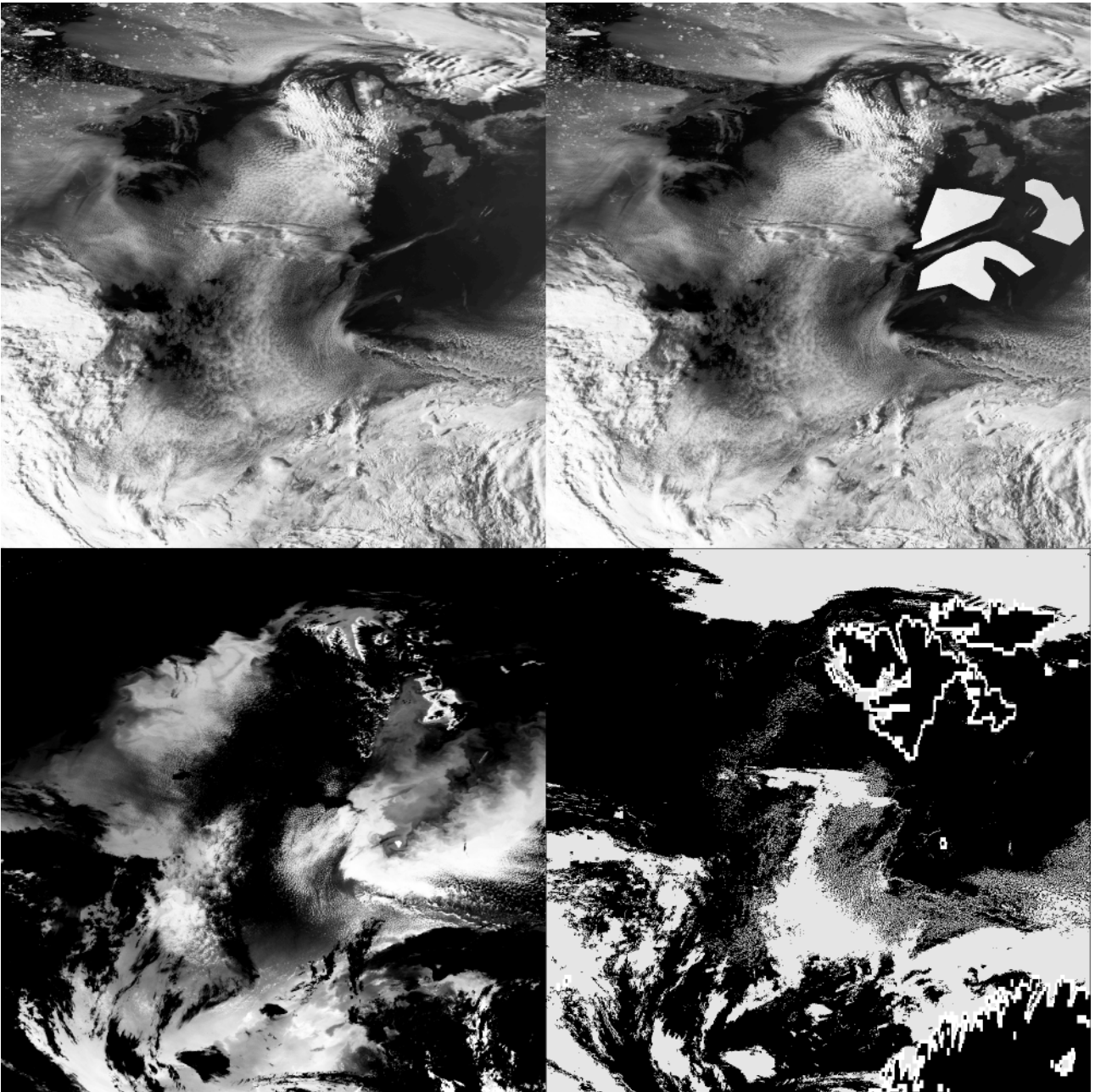


NSS.HRPT.NM.D04024.S1608.E1622.B0823535.WIL9827011\_ec



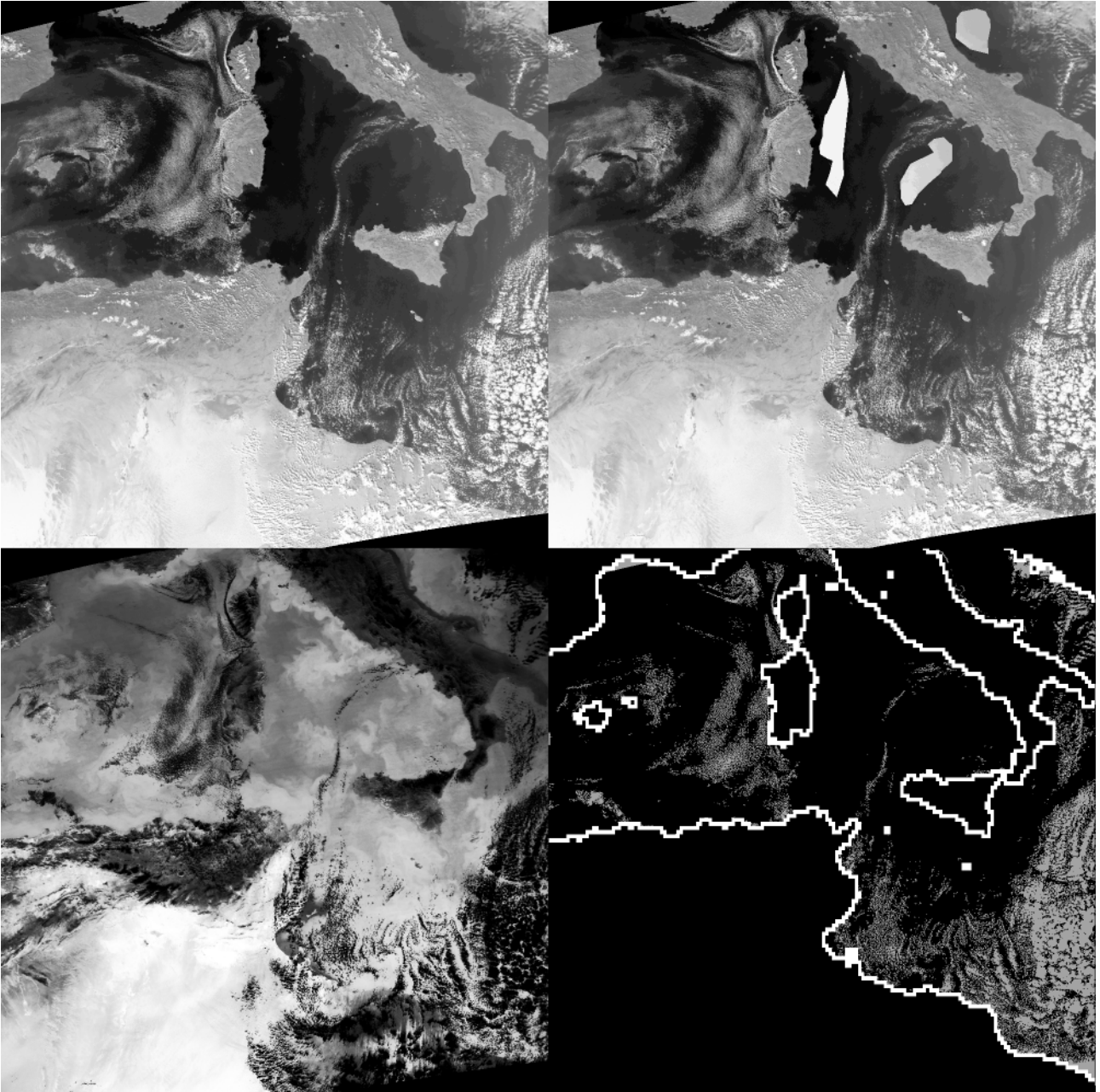
## Greenland Sea/ East Greenland



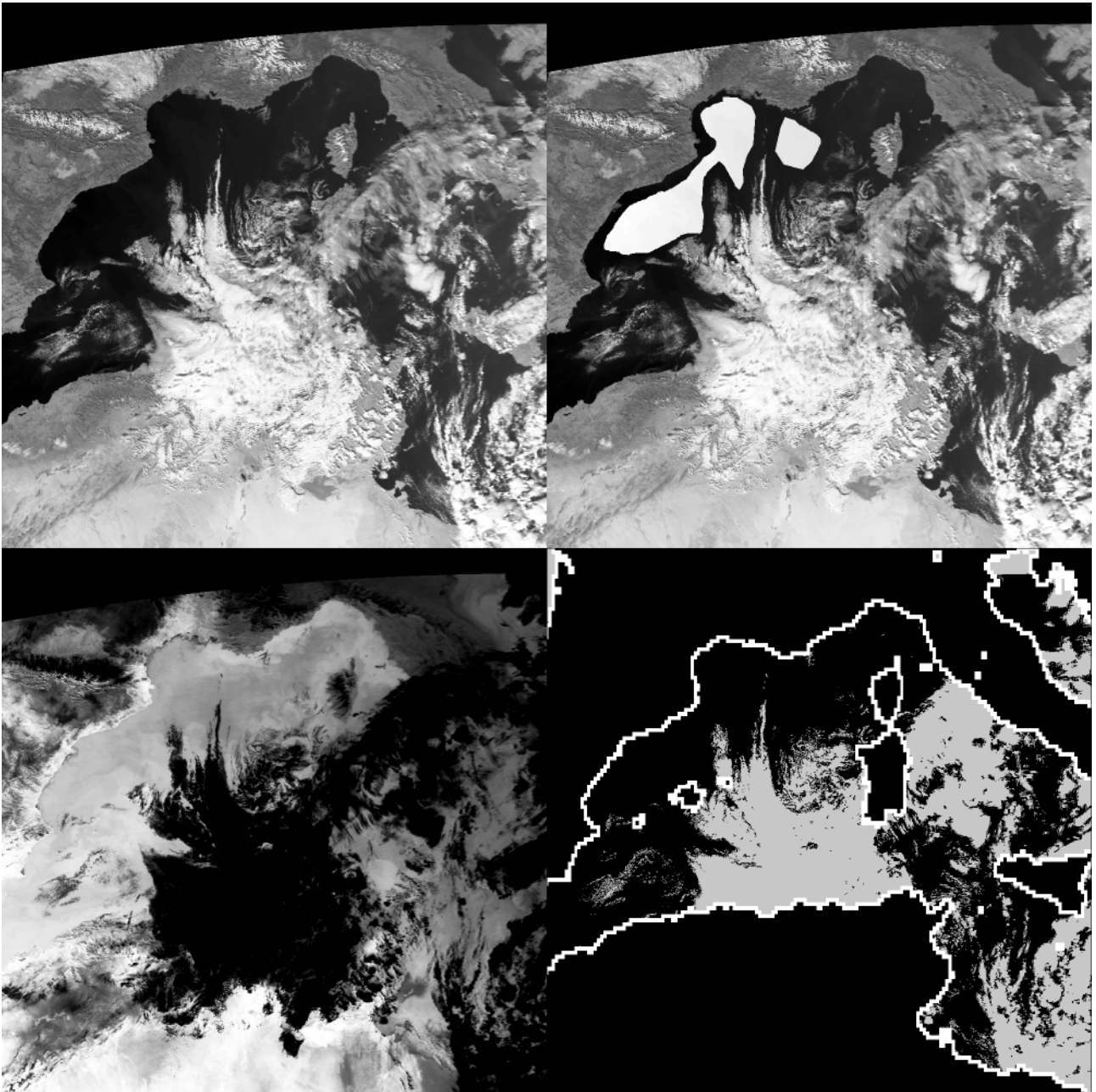




## Mediterranean



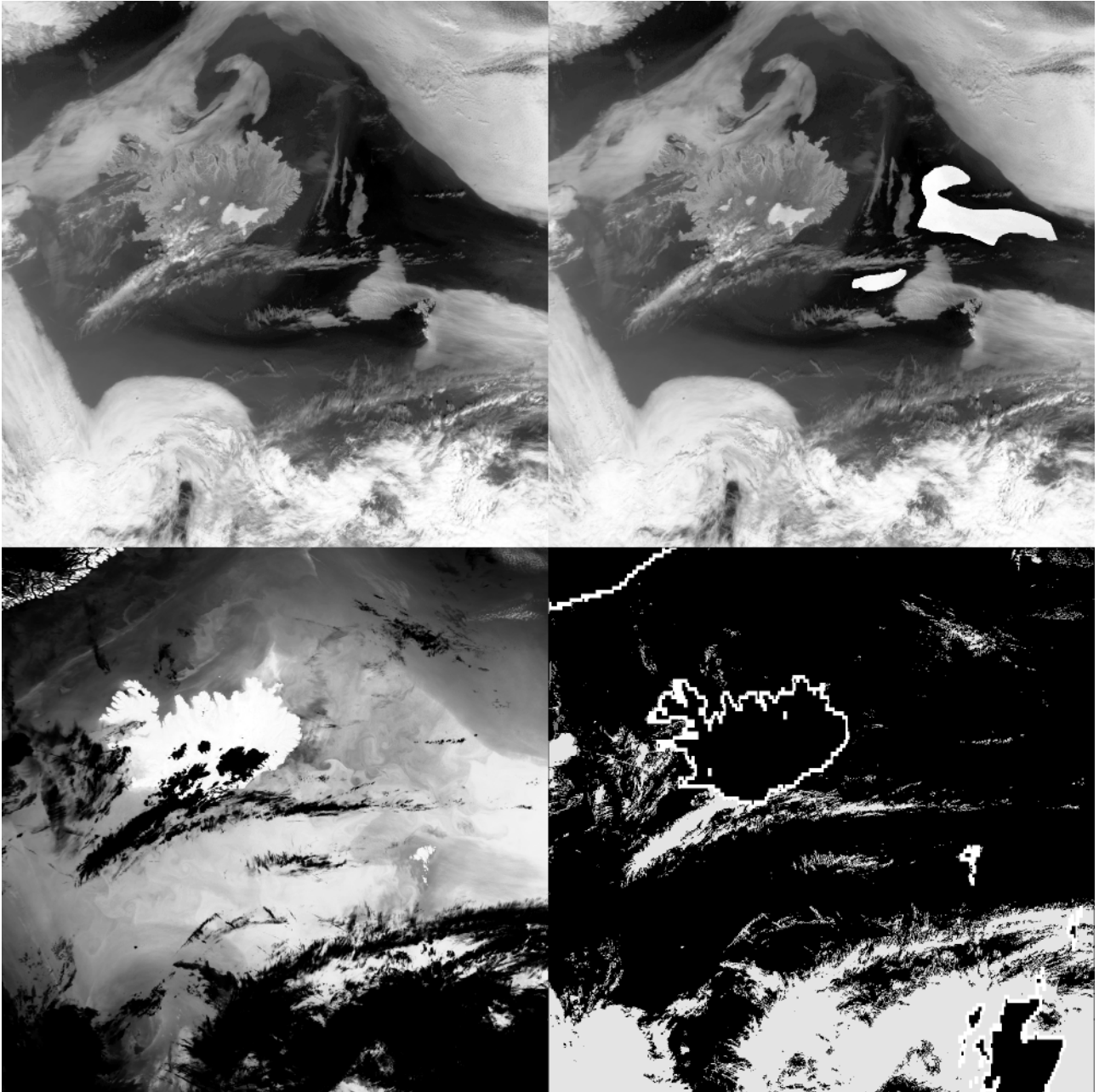
NSS.LHRR.NL.D05004.S1329.E1333.B2209797.GC.L0397191\_Wmed



NSS.LHRR.NL.D05001.S1404.E1408.B2205555.GC.L0397171\_Wmed



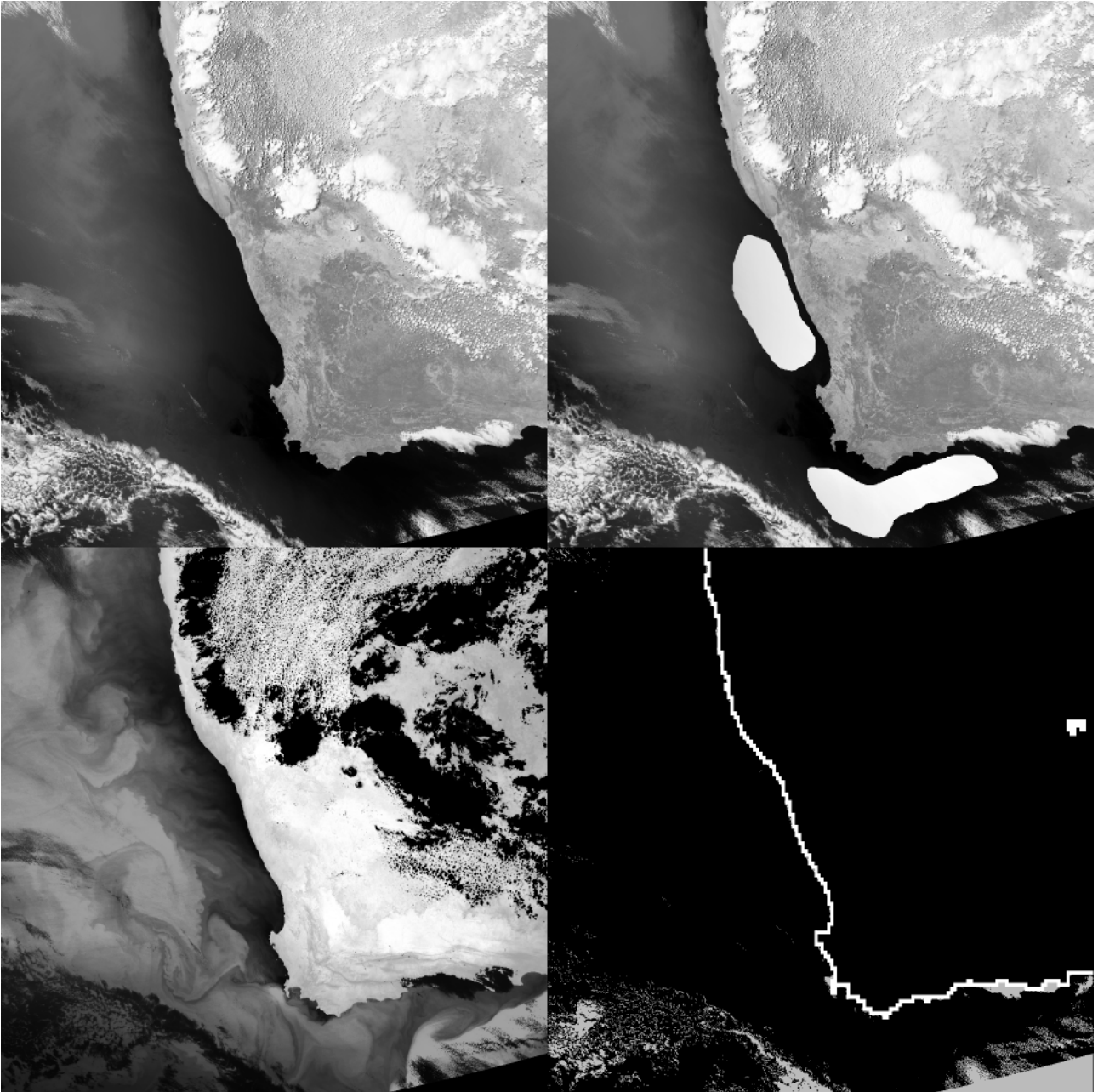
### Polar front area



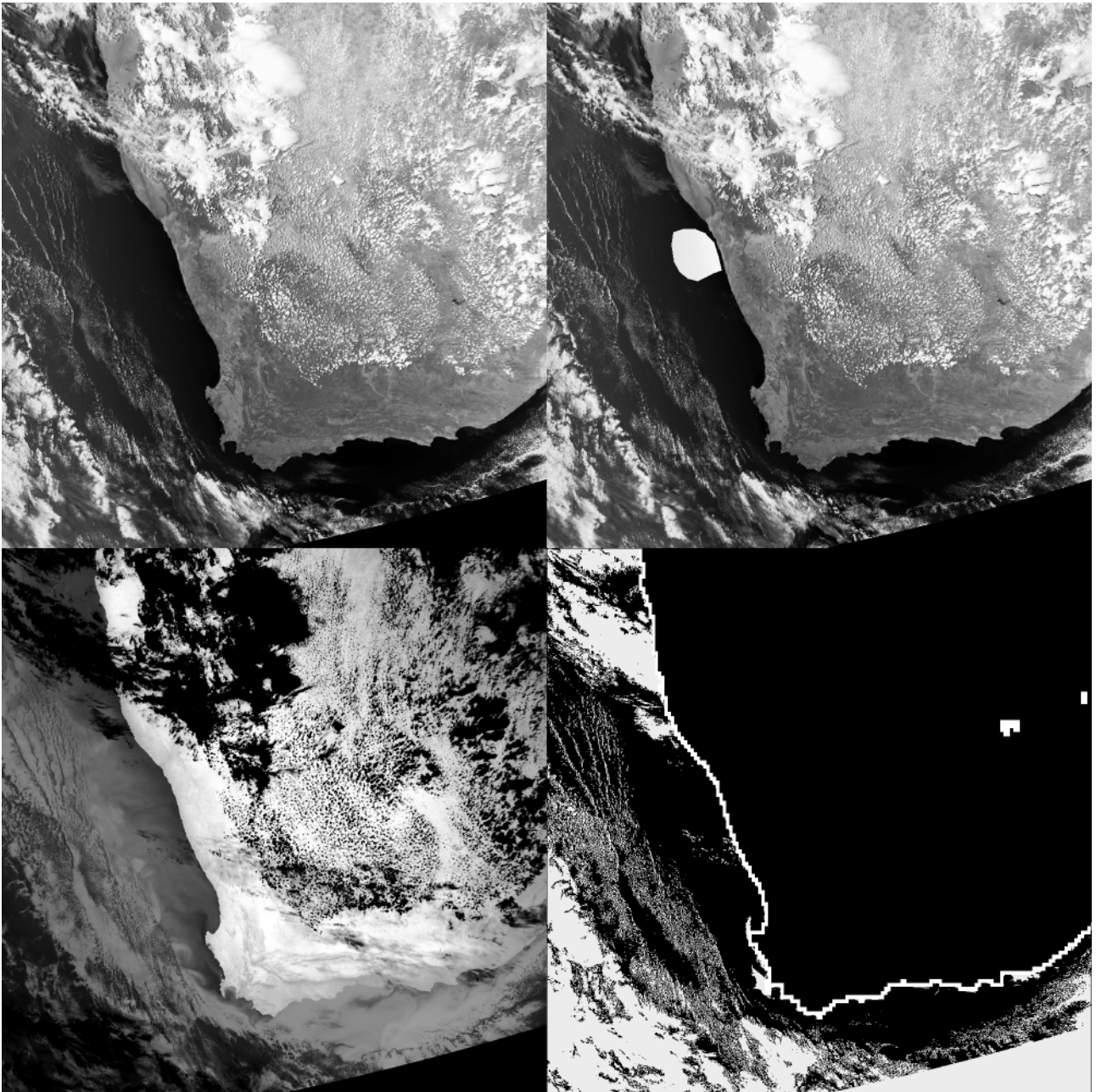
hrpt\_noaa17\_20040811\_1157\_11078.11b\_polfmnt



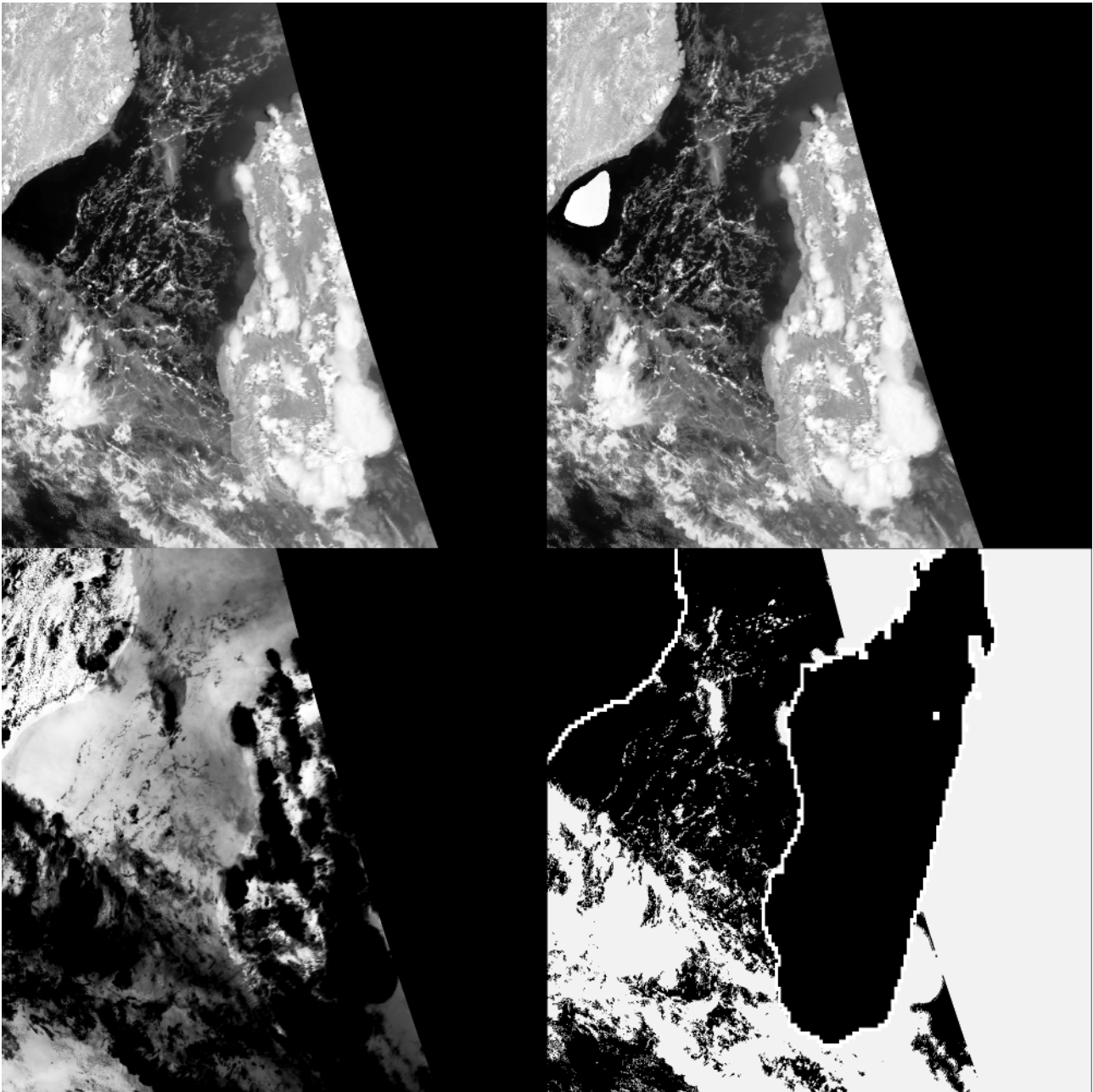
## South Africa



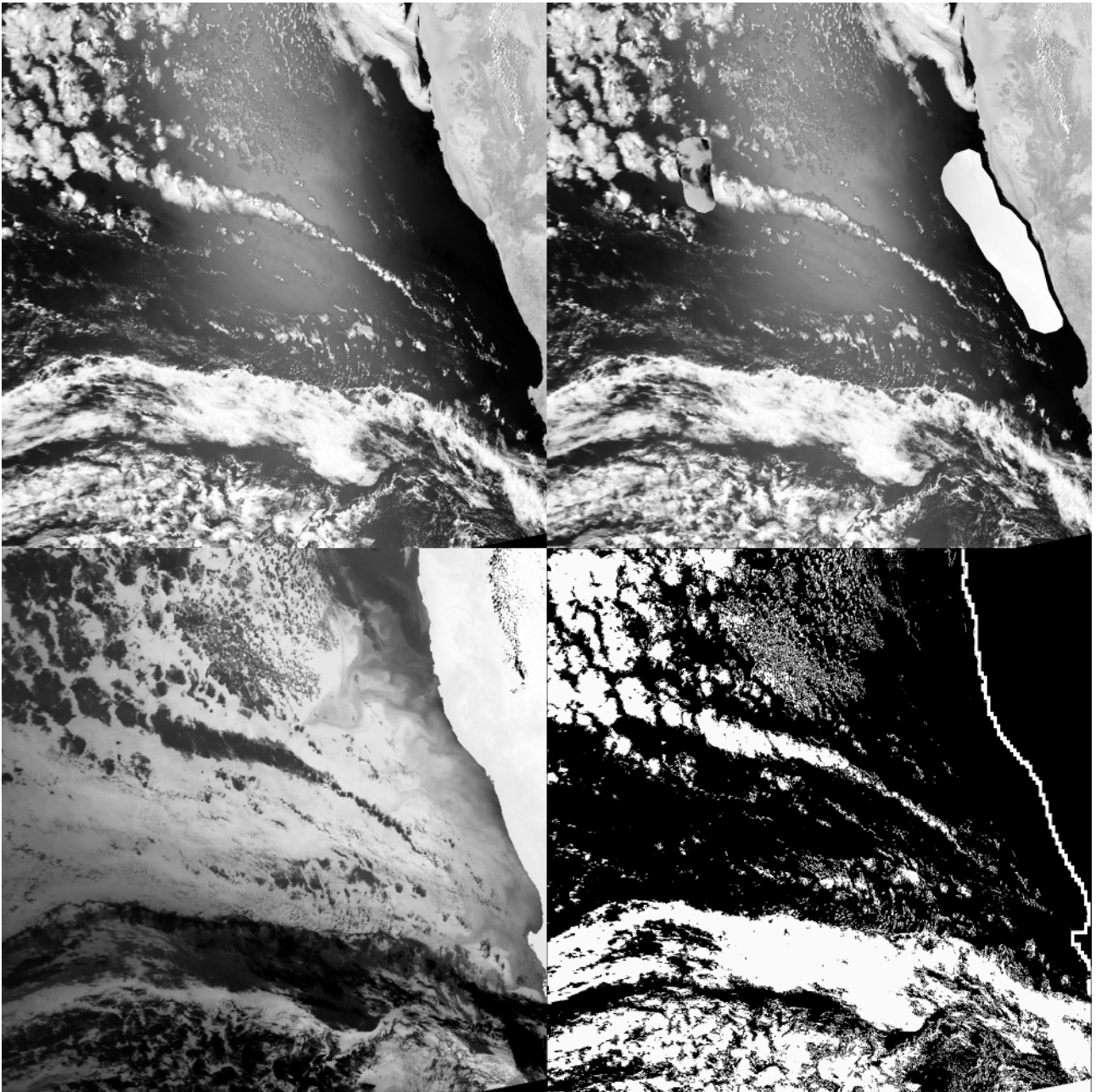
NSS.LHRR.NL.D05045.S1342.E1354.B2267576.GC.L0464351\_Wsaf



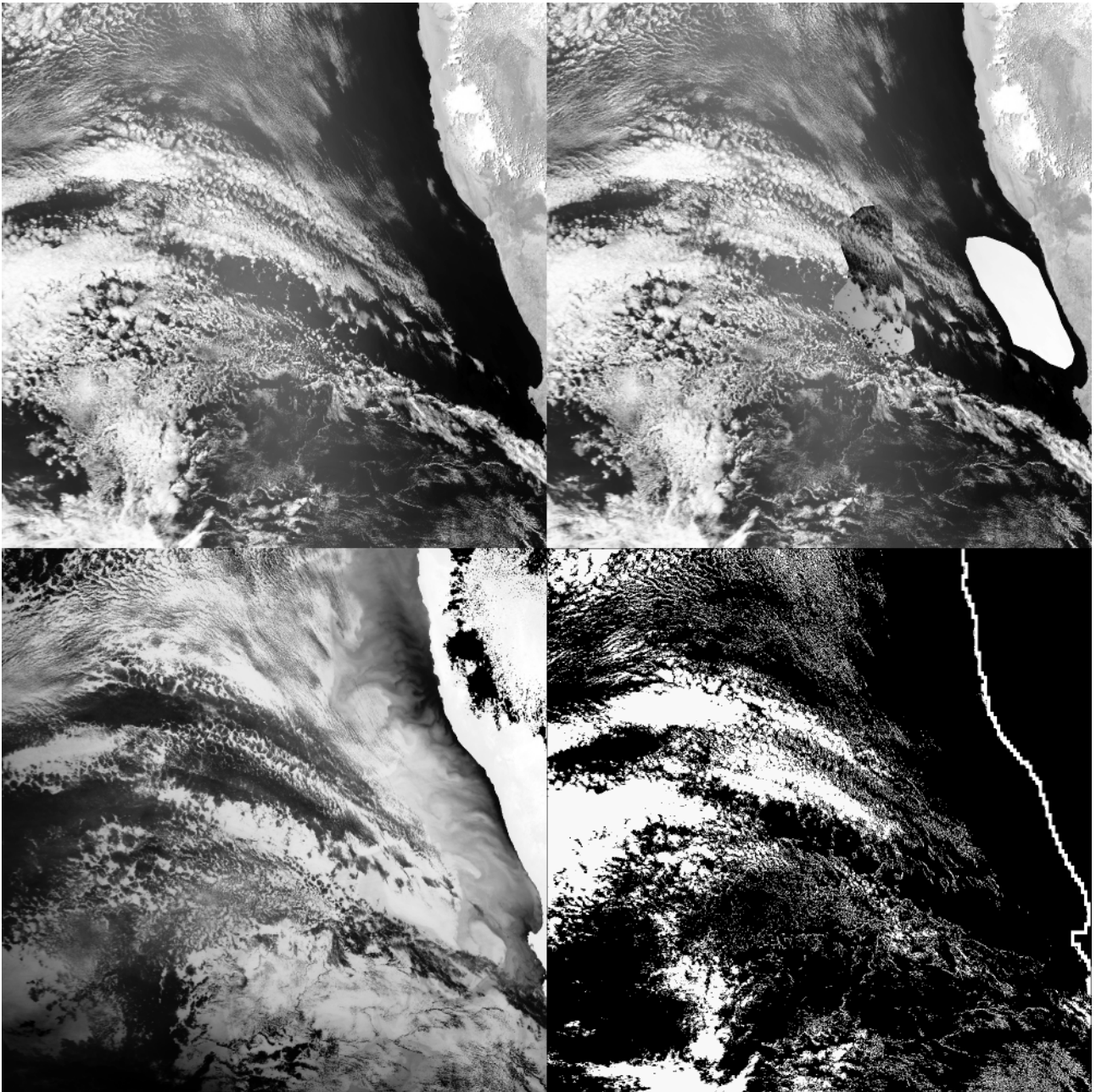
NSS.LHRR.NL.D05010.S1342.E1353.B2218182.GC.L0464311\_Wsaf



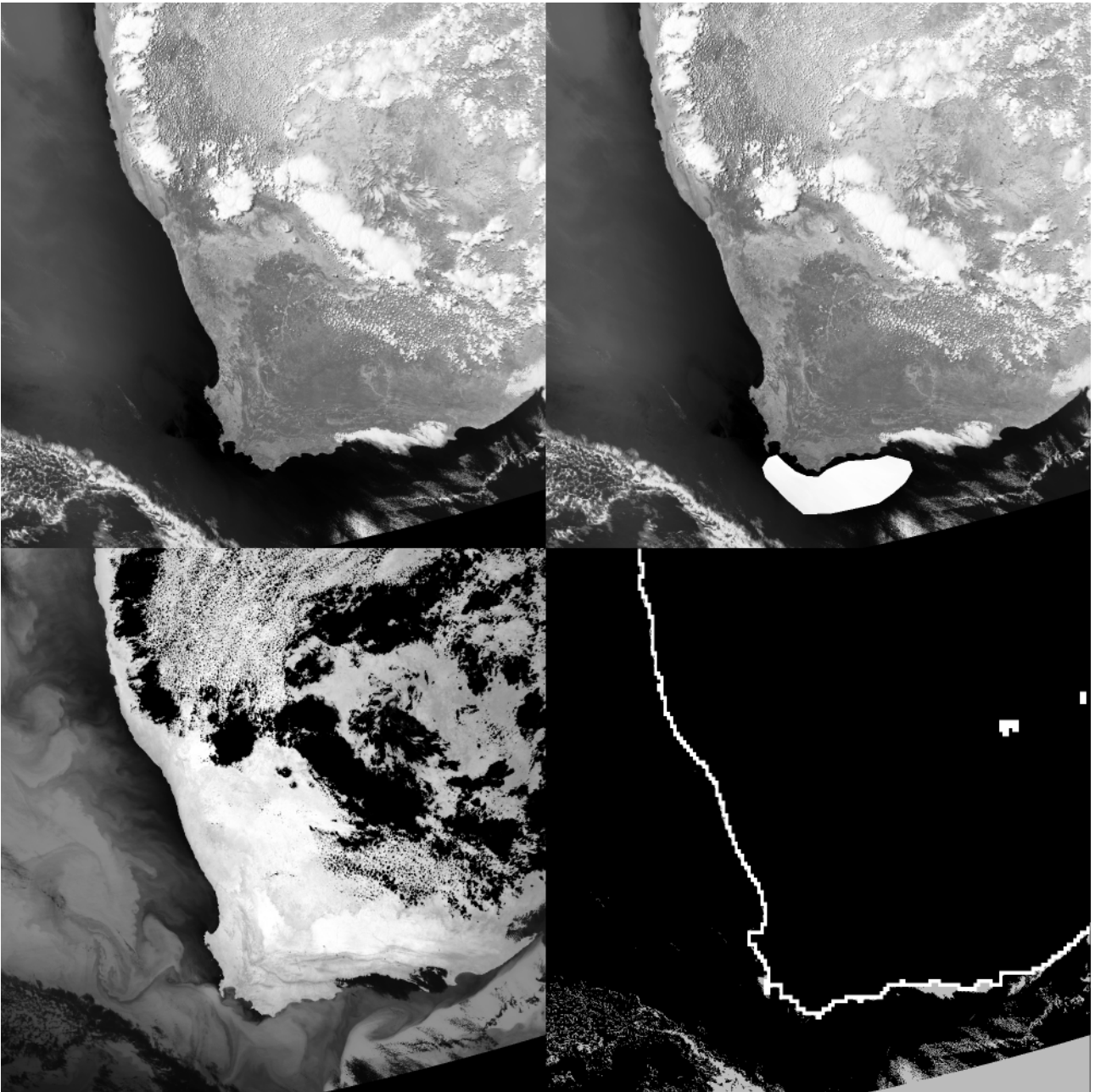
NSS.LHRR.NL.D05016.S1232.E1243.B2226566.GC.L0464321\_Esaf



NSS.LHRR.NL.D05027.S1348.E1359.B2242122.GC.L0464331\_Wsaf



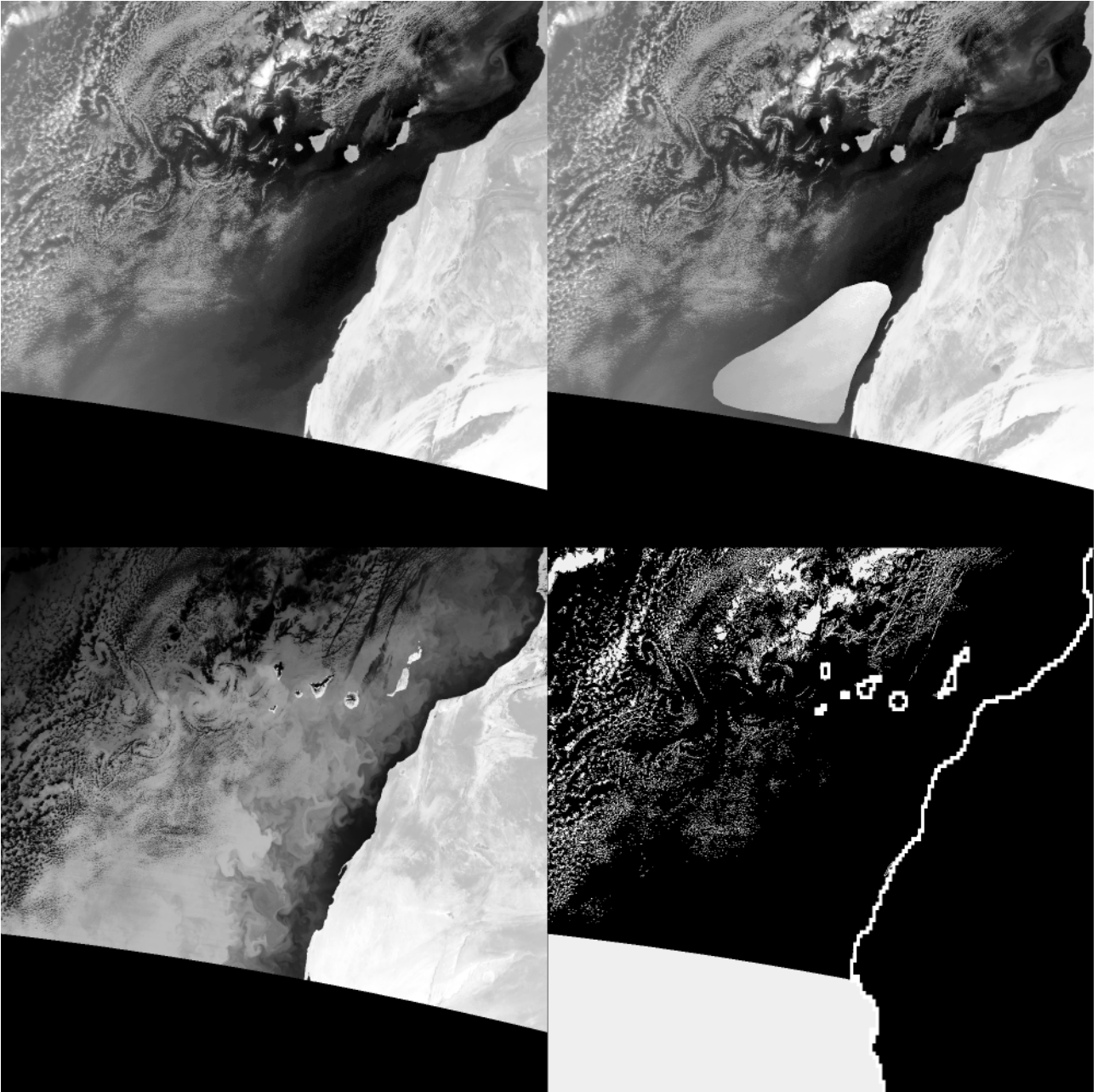
NSS.LHRR.NL.D05044.S1354.E1405.B2266162.GC.L0464341\_Wsaf



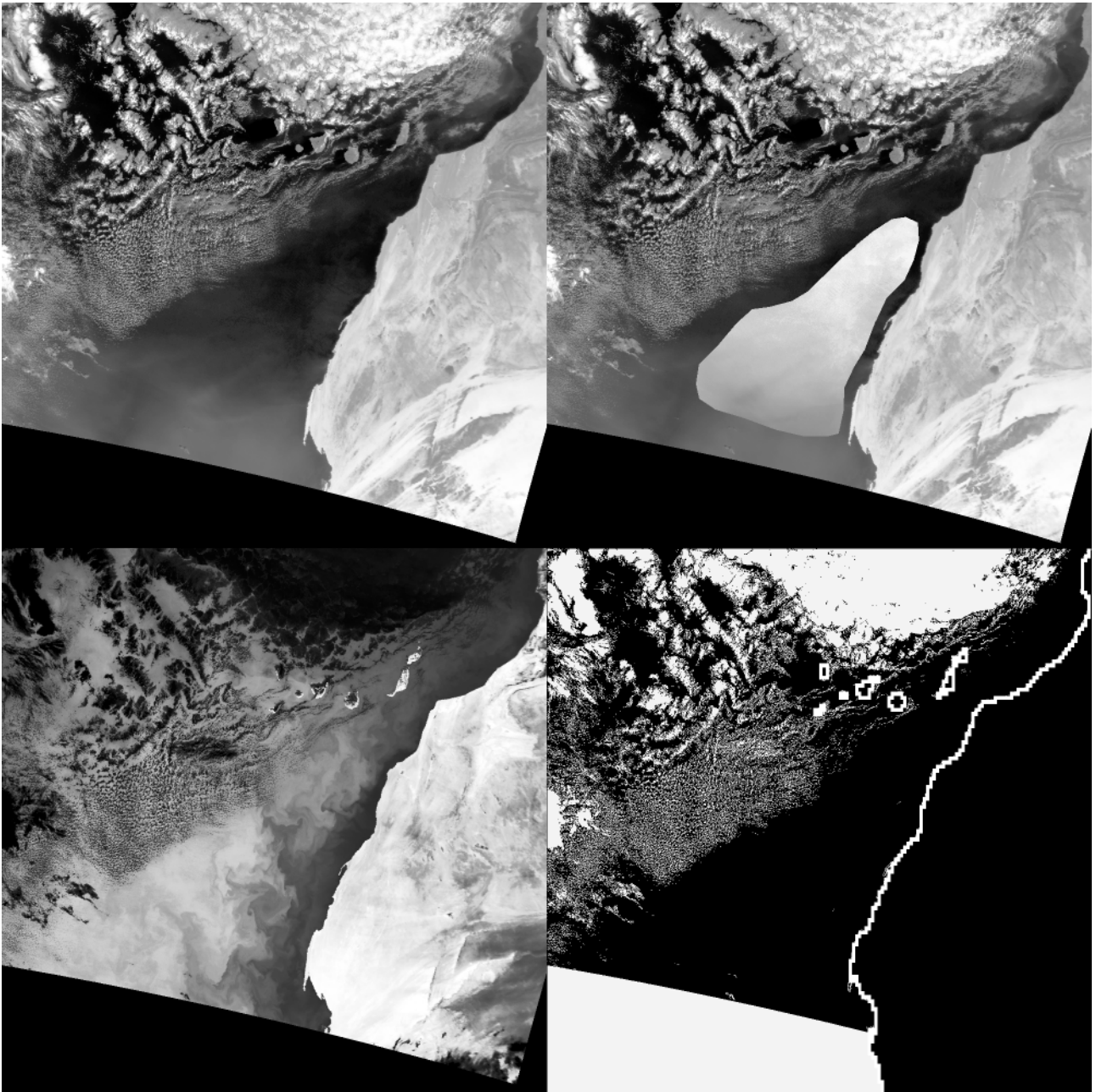
NSS.LHRR.NL.D05045.S1342.E1354.B2267576.GC.L0464351\_Ssaf



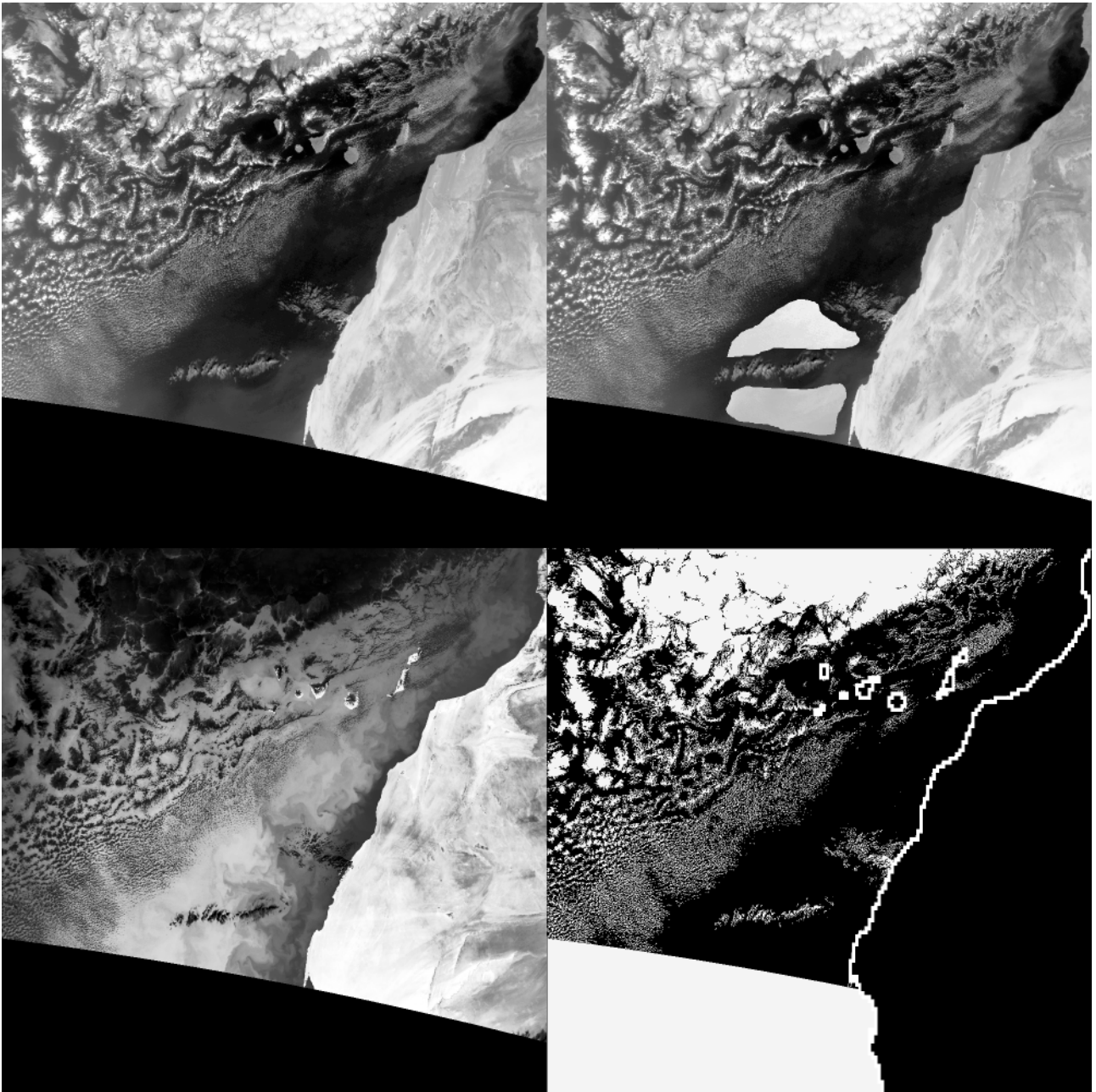
## West Africa



NSS.LHRR.NM.D05013.S1132.E1143.B1328383.WIL0397221\_Nwaf



NSS.LHRR.NM.D05003.S1200.E1212.B1314141.WIL0397181\_Nwaf



NSS.LHRR.NM.D05004.S1137.E1149.B1315555.WIL0397201\_Nwaf



## Previous reports

Previous reports from the Danish Meteorological Institute can be found on:

<http://www.dmi.dk/dmi/dmi-publikationer.htm>